INVESTIGATION ON PERFORMANCE OF COMBINED ANNULAR AND LONGITUDINAL RECTANGULAR FINS ON A HORIZONTAL CYLINDER IN FREE CONVECTION

A THESIS SUBMITTED TO
THE GRADUATE SCHOOL OF NATURAL AND APPLIED SCIENCES
OF
MIDDLE EAST TECHNICAL UNIVERSITY

BY

ELYAS SALAMATBAKHSH

IN PARTIAL FULFILLMENT OF THE REQUIREMENTS
FOR
THE DEGREE OF MASTER OF SCIENCE
IN
MECHANICAL ENGINEERING

JUNE 2024

Approval of the thesis:

INVESTIGATION ON PERFORMANCE OF COMBINED ANNULAR AND LONGITUDINAL RECTANGULAR FINS ON A HORIZONTAL CYLINDER IN FREE CONVECTION

submitted by **ELYAS SALAMATBAKHSH** in partial fulfillment of the requirements for the degree of **Master of Science in Mechanical Engineering, Middle East Technical University** by,

Prof. Dr. Naci Emre Altun
Dean, **Graduate School of Natural and Applied Sciences** _____

Prof. Dr. M. A. Sahir Arıkan
Head of the Department, **Mechanical Engineering** _____

Assoc. Prof. Dr. Özgür Bayer
Supervisor, **Mechanical Engineering, METU** _____

Examining Committee Members:

Prof. Dr. Zafer Dursunkaya
Mechanical Engineering, METU _____

Assoc. Prof. Dr. Özgür Bayer
Mechanical Engineering, METU _____

Prof. Dr. Almıla G. Yazıcıoğlu
Mechanical Engineering, METU _____

Assoc. Prof. Dr. Ali Karakuş
Mechanical Engineering, METU _____

Prof. Dr. Murat Köksal
Mechanical Engineering, Hacettepe University _____

Date: 13.06.2024

I hereby declare that all information in this document has been obtained and presented in accordance with academic rules and ethical conduct. I also declare that, as required by these rules and conduct, I have fully cited and referenced all material and results that are not original to this work.

Name Last name : Elyas Salamatbakhsh

Signature :

ABSTRACT

INVESTIGATION ON PERFORMANCE OF COMBINED ANNULAR AND LONGITUDINAL RECTANGULAR FINS ON A HORIZONTAL CYLINDER IN FREE CONVECTION

Salamatbakhsh, Elyas
Master of Science, Mechanical Engineering
Supervisor : Assoc. Prof. Dr. Özgür Bayer

June 2024, 96 pages

Natural convection has wide applications in various industries. However, it has a lower heat transfer rate compared to forced convection due to lower coolant velocity. To enhance heat exchanger performance under natural convection, surface extensions known as fins are commonly employed. While unconventional fin designs offer a significant surface area and effectively disrupt the thermal boundary layer, their usage is constrained by manufacturing complexities. On the other hand, annular and longitudinal fins have extensive usage due to ease of manufacturing, simplicity, rigidity, durability, and cost-effectiveness. In the conventional air-cooled annular fin and tube units, the airflow follows a relatively direct path between the fins, with thermal performance primarily reliant on surface area. In this study, a combined annular and longitudinal fin and tube design is proposed which aims to enhance the local air velocity at the vicinity of the unit and heat transfer by deflecting airflow. An experimental setup is constructed to investigate the effects of annular fin spacing and longitudinal fin inclination angle on thermal performance, with experimental data validating the numerical simulations. Furthermore, the performance of the proposed design in an array of fin and tube units is numerically

investigated. In the case of a single fin and tube unit, in the optimal annular fin spacing for maximizing the heat transfer, the heat transfer consistently decreases as the angle of the longitudinal fin increases from the vertical position, with the thermal performance always being lower than that of the conventional annular fin and tube design. However, when used in an array, the units with optimal fin spacing demonstrate up to 65% increase in heat transfer compared to an array of conventional annular fin and tube units.

Keywords: natural convection, heat exchanger, CFD, heat transfer

ÖZ

YATAY SİLİNDİR ÜZERİNDEKİ BÜTÜNLEŞİK DAİRESEL VE UZUNLAMASINA DİKDÖRTGEN KANATÇIKLARIN PERFORMANSININ DOĞAL TAŞINIMDA İNCELENMESİ

Salamatbakhsh, Elyas
Yüksek Lisans, Makina Mühendisliği
Tez Yöneticisi: Doç. Dr. Özgür Bayer

Haziran 2024, 96 sayfa

Doğal taşınımın farklı endüstrilerde çeşitli uygulamaları bulunmaktadır. Bununla birlikte, daha düşük soğutucu akışkan hızı nedeniyle zorlanmış taşınıma kıyasla daha düşük bir ısı transfer oranına sahiptir. Doğal taşınım altında ısı değiştirici performansını artırmak için, kanatçıklar olarak bilinen çıkıntıların kullanımı yaygındır. Geleneksel olmayan kanatçık tasarımları önemli bir yüzey alanı artışı sağlarken ve ısıl sınır tabakasını etkili bir şekilde bozarken, kullanımları üretim karmaşıklıkları nedeniyle kısıtlanmaktadır. Öte yandan, dairesel ve uzunlamasına kanatçıklar üretim kolaylığı, basitlik, sağlamlık, dayanıklılık ve maliyet etkinliği nedeniyle geniş bir kullanım alanına sahiptir. Geleneksel hava soğutmalı dairesel kanatçık ve boru ünitelerinde, hava akışı kanatçıklar arasında nispeten doğrusal bir yol izler ve termal performans öncelikle yüzey alanına bağlıdır. Bu çalışmada, ünitenin çevresindeki yerel hava hızını ve hava akışını saptırarak ısı transferini artırmayı amaçlayan yeni bir birleşik dairesel ve uzunlamasına kanatçık ve boru tasarımı önerilmektedir. Dairesel kanatçık aralığı ve uzunlamasına kanatçık eğim açısının termal performans üzerindeki etkilerini araştırmak için deneysel bir düzenek

oluşturulmuş ve deneysel veriler ile sayısal benzeşimler doğrulanmıştır. Ayrıca, önerilen tasarımın bir kanatçık ve boru dizisi ünitesindeki performansı sayısal olarak incelenmiştir. Tek bir kanatçık ve boru ünitesi durumunda, ısı transferini en üst düzeye çıkaran optimum dairesel kanatçık aralığında, boylamasına kanatçık açısı arttıkça ısı transferi sürekli olarak azalmakta ve termal performans geleneksel dairesel kanatçık ve boru tasarımından daha düşük olmaktadır. Bununla birlikte, optimum kanat aralığına sahip üniteler bir dizi halinde kullanıldığında, geleneksel dairesel kanatçık ve borulu ünitelerden oluşan bir diziye kıyasla ısı transferinde %65'e varan bir artış göstermektedir.

Anahtar Kelimeler: doğal taşınım, ısı değiştirici, HAD, ısı transferi

To my family and dear Nazanin

ACKNOWLEDGMENTS

I would like to thank my supervisor, Assoc. Prof. Dr. Özgür Bayer, for his continuous support. I would also like to express my gratitude to Mr. Mustafa Yalçın for his persistent assistance in the experimental procedure and I deeply appreciate the academic support of my friends Seyedmohsen Baghaei Oskouei and Deniz Alp Yılmaz. I am extremely grateful to my beloved Nazanin, for her endless kindness. I would like to show my most significant appreciation towards my family for their constant support throughout my academic life.

TABLE OF CONTENTS

ABSTRACT v

ÖZ vii

ACKNOWLEDGMENTS x

TABLE OF CONTENTS xi

LIST OF TABLES xiii

LIST OF FIGURES xiv

LIST OF ABBREVIATIONS xvii

LIST OF SYMBOLS xviii

1 INTRODUCTION 1

1.1 Natural Convection 1

1.2 Fin Designs for Natural Convection 2

1.2.1 Annular Fins 2

1.2.2 Longitudinal Fins 6

1.2.3 Pin Fins 10

1.2.4 Unconventional Fin Designs 12

1.3 Heated Units in an Array 13

1.4 Motivation and Problem Statement 14

2 METHODOLOGY 17

2.1 Experimental Work 17

2.1.1 Proposed Design, Parameters, and Manufactured Test Pieces 17

2.1.2 Experimental Setup 20

2.1.3 Experimental Procedure 24

2.2 Numerical Study 25
2.2.1 Computational Domains 25
2.2.2 Governing Equations 29
2.2.3 Boundary Conditions 33
2.2.4 Numerical Study Matrix 37
2.2.5 Mesh and Domain Independence Study 38
2.3 Data reduction 44
2.4 Uncertainty Analysis 45
3 RESULTS AND DISCUSSION 47
3.1 Validation 47
3.1.1 Experimental Procedure 47
3.1.2 Numerical Simulations 49
3.2 Numerical Results for a Single Fin and Tube Unit 51
3.3 Numerical Results for Fin and Tube Units in an Array 68
3.3.1 An Array with Two Rows 69
3.3.2 An Array with Several Rows 76
4 CONCLUSION 83
REFERENCES 87

LIST OF TABLES

TABLES

Table 2.1. Range of the important geometrical parameters in the relevant studies. 18
Table 2.2. Geometrical dimensions of the manufactured test pieces 20
Table 2.3. Under-relaxation factors used in the simulations..... 31
Table 2.4. The parameters in the study of the single fin and tube unit..... 37
Table 2.5. The parameters in the study of the fin and tube units in an array..... 38

LIST OF FIGURES

FIGURES

Figure 1.1. A typical annular fin design mounted on a tube 3
Figure 1.2. Typical longitudinal fin designs mounted on a (a) plate and a (b) tube.. 6
Figure 1.3. A typical pin fin design mounted on a plate 11
Figure 2.1. The proposed design with the geometrical parameters 17
Figure 2.2. Photographs of the manufactured test pieces 19
Figure 2.3. A photograph of the experimental setup. (1) fin and tube unit, (2) supporting frame, (3) DC power supply, (4) data logger, (5) computer 21
Figure 2.4. A photograph of the bare tube in the control experiment 22
Figure 2.5. Location of the thermocouples in the control experiment with the bare tube 23
Figure 2.6. Location of the thermocouples in the fin and tube experiments 24
Figure 2.7. The longitudinal fin inclination angle 25
Figure 2.8. The computational domain for a single fin and tube (not to scale) 26
Figure 2.9. The studied configurations of the fin and tube units in an array 27
Figure 2.10: The computational domain for an array of fin and tube units with two rows (not to scale) 28
Figure 2.11. The boundary conditions for a single fin and tube unit, (a) front view, and (b) side view 34
Figure 2.12. Boundary conditions for fin and tube units in an array, (a) front view, and (b) side view 36
Figure 2.13. The division pattern of the numerical domain 39
Figure 2.14. The mesh structure for the case with a fin spacing of 31.13 mm 40
Figure 2.15. Variation of Nu_s with the number of elements 41
Figure 2.16. Variation of Nu_s with (a) domain length, and (b) domain diameter 42
Figure 2.17. The mesh configuration for an array of fin and tube units 43
Figure 2.18. Variation of Nu_s with b for an array with $n = 5$ 43

Figure 3.1. Comparison of current experimental data with results obtained from correlations suggested in the literature for Nu_{d_o} of a bare tube..... 48
Figure 3.2. Variation of Nu_s with q_t 50
Figure 3.3. (a) Velocity contours and vectors, and (b) temperature contours and streamlines for conventional design, $s = 3$, 7.14, and 31.13 mm at $\Delta T = 60$℃ .. 52
Figure 3.4. Velocity contours and vectors for the proposed design, $s = 3$, 7.14, and 31.13 mm, and $\theta = 0°$, 30°, 60°, and 90° at $\Delta T = 60$℃..... 54
Figure 3.5. Temperature contours and streamlines for the proposed design, $s = 3$, 7.14, and 31.13 mm, and $\theta = 0°$, 30°, 60°, and 90° at $\Delta T = 60$℃ 56
Figure 3.6. Temperature contours of the solid domain for the proposed design, $s = 3$, 7.14, and 31.13 mm, and $\theta = 0°$, 30°, 60°, and 90° at $\Delta T = 60$℃ 59
Figure 3.7. Wall flux contours of the solid domain for the proposed design, $s = 3$, 7.14, and 31.13 mm, and $\theta = 0°$, 30°, 60°, and 90° at $\Delta T = 60$℃ 60
Figure 3.8. Temperature contours of the air plume for the proposed design, $s = 3$, 7.14, and 31.13 mm, and $\theta = 0°$, 30°, 60°, and 90° at $\Delta T = 60$℃ 61
Figure 3.9. Evolution of the convective heat transfer with s for different θ and ΔT values 63
Figure 3.10: Evolution of convective heat transfer with θ for different s and ΔT values 65
Figure 3.11 Evolution of Nu_s with ΔT for different θ and s values 67
Figure 3.12. Velocity contours embedded with streamlines, and temperature contours for $\psi_2 = 30°$, 60°, $-30°$, and $-60°$, $S_t = 3D/2$, and $S_l = 5D/2$, parallel configuration 70
Figure 3.13. Velocity contours embedded with streamlines, and temperature contours for $\psi_2 = 30°$, 60°, $-30°$, and $-60°$, $S_t = 3D/2$, and $S_l = 5D/2$, mirrored configuration 72
Figure 3.14. Velocity contours embedded with streamlines and the temperature contours for parallel configuration with $\psi_2 = 60°$ for different S_t and S_l values .. 74

Figure 3.15. Variation of $\mathrm{Nu}_{s,array}$ for an array with two rows at parallel and mirrored configurations and different ψ_2, S_t, and S_l values 75
Figure 3.16. Velocity contours embedded with streamlines for the cases without longitudinal fins 77
Figure 3.17. Temperature contours for the cases without longitudinal fins 78
Figure 3.18. Velocity contours embedded with streamlines for the cases with longitudinal fins 80
Figure 3.19. Temperature contours for the cases with longitudinal fins 81
Figure 3.20. The evolution of $\mathrm{Nu}_{s,array}$ with n for the parallel case, $\psi_n = 60°$, $S_t = 3D/2$, and $S_l = 5D/2$ 82

LIST OF ABBREVIATIONS

2D	2 dimensional
3D	3 dimensional
CFD	Computational fluid dynamics
FEM	Finite element method
FVM	Finite volume method

LIST OF SYMBOLS

A	Area, m^2
A_{array}	Total surface area of an array of fin and tube units, m^2
b	The vertical distances from the bottom and top boundaries of the computational domain to the centers of the tubes in the first and last rows of the array, respectively, mm
c_p	Specific heat capacity of air at constant pressure, J/kg°C
d_i	Tube inner diameter, mm
d_o	Tube outer diameter, mm
D	Annular fin outer diameter, mm
D_c	Computational domain diameter, mm
E	Emissive power, W/m^2
F	View factor, -
g	Gravitational acceleration, m/s^2
G	Irradiation, W/m^2
Gr	Grashof number, -
h	Convective heat transfer coefficient, $W/m^2°C$
h_{array}	Convective heat transfer coefficient for an array of fin and tube units, $W/m^2°C$
I	Current, A
J	Radiosity, W/m^2
k_f	Fluid thermal conductivity, W/m°C
k_s	Solid thermal conductivity, W/m°C
L	Tube length, mm
L_c	Computational domain length, mm
n	Number of rows in an array, -
Nu	Nusselt number, -

P	Pressure, Pa
Pr	Prandtl number, -
q_c	Convective heat transfer of the fin and tube unit, W
$q_{c,array}$	Convective heat transfer of an array of fin and tube units, W
q_r	Radiative heat transfer of the fin and tube unit, W
q_t	Total heat transfer of the fin and tube unit, W
q''	Heat flux, $\mathrm{W/m^2}$
Ra	Rayleigh number, -
s	Spacing between the annular fins, mm
S_l	Longitudinal spacing between the tubes, mm
S_t	Transverse spacing between the tubes, mm
t	Fin thickness, mm
T	Temperature, ℃
$\mathbf{U}$	Velocity vector, mm/s
V	Voltage, V
α	Thermal diffusivity, $\mathrm{m^2/s}$
β	Thermal expansion coefficient, $1/℃$
ε	Emissivity, -
θ	The inclination angle of the longitudinal fin, degrees
μ	Dynamic viscosity, $\mathrm{kg/m.s}$
ρ	Density, $\mathrm{kg/m^3}$
	Reflectivity, -
σ	Stefan-Boltzmann constant, $\mathrm{W/m^2K^4}$
υ	Kinematic viscosity, $\mathrm{m^2/s}$
ψ_1	The inclination angle of the longitudinal fin at the first row of the array, degrees
ψ_2	The inclination angle of the longitudinal fin at the second row of the array, degrees

CHAPTER 1

INTRODUCTION

Heat transfer enhancement is an essential factor in the design of energy conversion, recovery, deposit, and removal systems. Various branches of engineering including electronics cooling, air-conditioning, refrigeration, power plants, automobile industry, and aerospace technologies are dependent on sufficient heat transfer [1, 2]. To enable desirable heat transfer, researchers have proposed heat exchangers which are devices that facilitate heat transfer between two or more mediums and are used in both heating and cooling processes [3, 4]. The efficiency of heat exchangers critically affects the overall efficiency of systems. For instance, more than 50% of failures that occur in integrated circuits are related to overheating [5]. Therefore, the precise design of heat exchangers plays a crucial role in engineering.

The performance improvement of the heat exchangers designed for natural convection applications is majorly dependent on increasing surface area because the ambient temperature and heat transfer coefficient are constant in most applications [6]. However, recent studies on novel-shaped designs prove that the shape and orientation of the heat exchangers can significantly affect their performance [7–9].

In this thesis, a design of a fin and tube heat exchanger by combining the annular and longitudinal fins for natural convection applications is proposed. The proposed design maintains the simplicity of conventional designs while resulting in a greater heat transfer.

1.1 Natural Convection

The convective heat transfer, which is the main heat transfer mode heat exchangers benefit from, occurs when the fluid is in motion which can be forced or natural (free).

In forced convection, the fluid motion originates from an external force which can be a pump, fan, or the propulsion of a solid through the fluid [10]. In natural convection, the motion of the fluid is due to the body force caused by the density difference inside the fluid. Generally, the density difference in a fluid body is the result of temperature gradient and the body force is a result of the gravitational field.

Despite that forced convection has a greater heat transfer potential due to higher fluid velocity, natural convection is a popular mode in low heat flux applications because of its reliability, simplicity, low energy consumption and maintenance cost, and noise-free nature [11]. The major disadvantage of the natural convection systems is their low heat transfer rate compared with forced convection systems. Therefore, enhancing the performance of heat exchangers designed for natural convection applications is an important concern for researchers.

1.2 Fin Designs for Natural Convection

Surface extension is a method widely utilized to enhance the heat transfer from the heated surface to the surrounding medium. The extended surfaces, referred to as fins in the literature, are categorized into four main types: longitudinal fins, annular fins, pin fins, and unconventional fin designs. The following subsections provide a descriptive literature review of the mentioned fin configurations.

1.2.1 Annular Fins

Natural convection from an annularly finned horizontal tube is widely present in different applications such as electronics cooling, air conditioning, refrigeration, heatsinks, energy storage systems, gas turbines, compressors, etc. [12]. The annular fin's popularity stems from its simplicity, rigidity, and high durability [13]. Figure 1.1 depicts a typical annular fin design mounted on a cylindrical tube (hereafter referred to as tube). The geometrical dimensions of the fin and tube, their shape, and

the base tube inclination angle are the major parameters affecting the natural convection heat transfer.

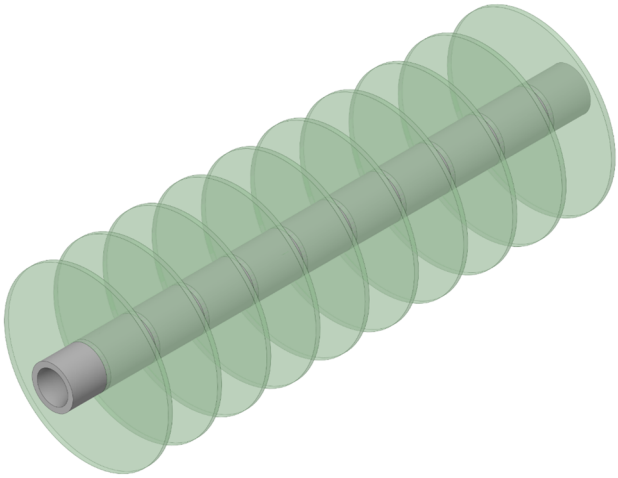


Figure 1.1. A typical annular fin design mounted on a tube

Fin and tube diameters, the spacing between the fins (s), and base-to-ambient temperature difference (ΔT) are the parameters extensively studied by scholars. Kayansayan and Karabacak [14] performed numerous experiments to assess the thermal performance of a horizontal tube with annular fins. It was found that the interaction between the thermal boundary layers formed by the fins and the tube diminishes the tube Nusselt number (Nu) compared with a heated bare tube. The reduction was determined to be realizable in the low Rayleigh numbers (Ra) nevertheless, in higher Ra numbers, Nu becomes insensitive to s and fin diameter. Yildiz and Yüncü [15] carried out experiments on 18 sets of annular fin and tube units where the variables were s, fin diameter, and ΔT. It was indicated that for a specific fin diameter and ΔT, there exists an optimum value for s in which the heat transfer is maximum. Furthermore, a scale analysis was performed to estimate the order of magnitude of s such that for the small and large s values the flow between the fins was assumed to be channel flow and external flow, respectively. Chen and colleagues studied annularly finned tubes with different configurations [16–23]. Using the finite difference method and least-squares scheme along with experimental

data, Chen and Hsu [17] calculated the average heat transfer coefficient on the annular fins of a fin and tube unit. It was seen that increasing s improves the heat transfer coefficient which reaches an asymptotic value as s goes to infinity.

Using a hybrid inverse method and computational fluid dynamics (CFD) commercial software along with experimental data, Chen *et al.* [21] investigated a horizontal finned tube unit in a chimney. It was reported that the heat transfer coefficient rises with a smaller fin diameter and greater s, while the fin efficiency declines with a larger fin diameter and s. The transient natural convection around an annular finned tube kept in a chimney was studied by Kumar *et al*. [24]. Besides finding the optimum s values with respect to the fin diameter and ΔT, the separation of the thermal boundary layer and its effect on the thermal behavior of the unit were discussed.

In a numerical investigation, Senapati *et al.* [12] optimized s for different fin diameters and ΔT. The motivation of the study was to visualize the plume structure and flow field around the fin and tube unit which gave a better understanding of the phenomenon. The effect of the eccentricity of the fins in an annular fin and tube unit was analyzed by Senapati *et al.* [25]. The obtained results suggested that the eccentricity of the fins marginally reduces the heat transfer however, the eccentric design can be used when there is a space restriction on one side of the unit. The heat transfer coefficient correlations for natural convection heat transfer were developed by Kang and Chang [26] through experiments on 16 annular fin and tube units with varying spacing-to-tube and fin-to-tube diameter ratios. It was stated that for the extremely short fins with finite s, the problem is similar to a heated tube however, when the fin diameter is increased and s is large, the physics becomes similar to that of flow between parallel plates. Wong and Lee [27] focused on the effect of fin material, s and diameter of the fins and the tube on the thermal performance of an annular fin and tube heat exchanger. It was concluded that for the fins with high thermal conductivity, the reduction of tube diameter improves heat transfer because of greater convective heat transfer surface area whereas, for the low thermal

conductivity fins, greater tube diameter results in a better performance due to the decrease in temperature gradient along the fins. Nemati *et al.* [28] proposed a modified definition for Ra where the fluid passes a circular path on the fins. The proposed correlation for the Nu based on the modified Ra proved to provide more accurate results compared with the results obtained by other correlations in the literature [12, 29].

The thermal performance of fin and tube units is significantly influenced by the shapes of the fins and tube. Variations in their shapes can alter flow pattern along the fins, impacting heat transfer. Nemati *et al.* [9] numerically analyzed the performance of a horizontal elliptically finned tube in natural convection. It was shown that there exists an optimal value for the ellipse diameter ratio where the heat flux is maximum. Moreover, the performance of elliptical fins is higher and lower than that of circular fins at small and large s values, respectively. Chen and Chou [16] applied the finite difference method along with the least-squares scheme on a vertical square fin of a horizontal fin and tube unit and validated the predictions with the experimental data. The results revealed that similar to the annular fin, increasing s enhances the heat transfer coefficient reaching an asymptotic value as s goes to infinity. The waviness of annular fins on a tube was studied by Siddhartha *et al.* [7], numerically. The outcomes disclosed that the wavy fins outperform straight circular fins at higher Ra and lower spacing-to-tube diameter ratios.

Usually, tubes are inclined to facilitate the drainage of the heat transfer fluid contained within or to minimize the footprint [30]. The tilt angle of the fin and tube unit can also substantially influence its thermal performance. Unger *et al.* [8] performed experimental investigations on oval fins mounted on a tube with inclination angles ranging from 0° to 40°. The tilt angle was found to be essential at higher s values whereas, at low s values the tube tilt angle did not affect the heat transfer substantially.

Annular fins have also been studied when they are mounted on a vertical tube. Senapati *et al.* [31] investigated the effect of fin diameter and s on the laminar and

turbulent natural convection from a vertical tube with annular fins. The results suggested that in the laminar regime, the heat transfer continuously increases by the addition of fins however, an optimal s is present for the turbulent flow regime. Pradhan *et al.* [32] studied the combined effect of radiation and natural convection and their ratios for a vertical annularly finned tube in the laminar and turbulent regimes. It was found that radiation is significant in the laminar Ra range however, in the turbulent regime the effect of radiation diminishes and becomes negligible.

1.2.2 Longitudinal Fins

A common type of extended surface used in heat exchangers is the longitudinal fin. Figure 1.2a and 1.2b represent longitudinal fins mounted on a plate and a tube, respectively. Ease of manufacturing, cheaper cost, and effective cooling capacity make the longitudinal fins one of the most common designs for cooling purposes [33]. The thermal performance of the longitudinal fins depends on their geometrical dimensions, arrangement, and orientation.

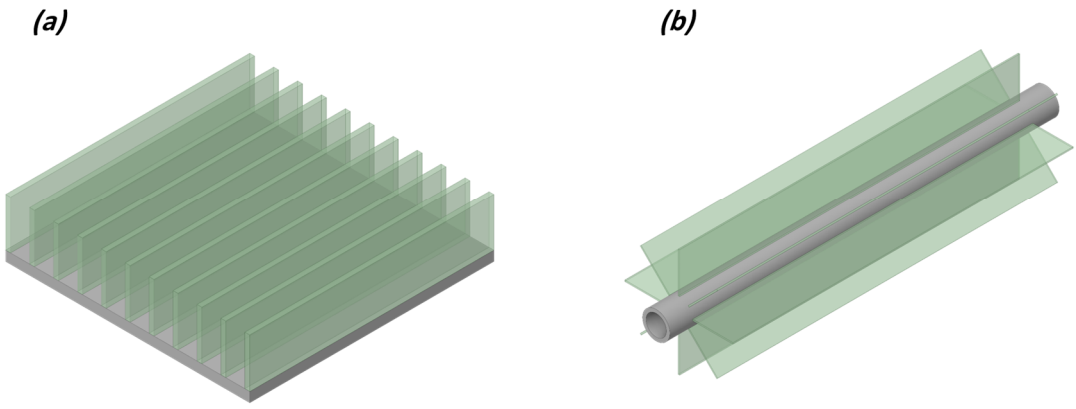


Figure 1.2. Typical longitudinal fin designs mounted on a (a) plate and a (b) tube

The fin height, length, s, and ΔT are the important parameters investigated in the literature. A set of experiments was performed by Yüncü and Anbar [34] to investigate the thermal performance of longitudinal aluminum fins mounted on a

horizontal heated plate in which the cases differed by fin height and s. The findings indicated that there is an optimum spacing-to-fin-height ratio value for a specific ΔT. Furthermore, the optimum s proved to decrease by increasing the fin height. Dayan *et al.* [35] conducted experimental, analytical, and numerical investigations to find the thermal performance of a downward-facing heated plate mounted with longitudinal rectangular fins. Plate base temperature, fin length, and s were found to be the main parameters affecting the heat transfer coefficient while the fin height had minimal effect. In an experimental study, Yazicioğlu and Yüncü [33] investigated the thermal performance of vertical rectangular fins mounted on a vertical heated plate. It was found that the optimum s is primarily dependent on fin height and length and ΔT; however, the mentioned variables did not affect the optimum s by more than 1.5 mm.

Natural convection from a heated plate with horizontal rectangular fins with a short length was examined by Dialameh *et al.* [36]. It was concluded that for low spacing-to-fin-length and high fin-height-to-length ratios, the flow only enters from the sides of the base plate however, for high spacing-to-fin-length and low fin-height-to-length ratios, the flow can also enter the spacings between the fins from the middle section of the heat sink. This critically affected the heat transfer coefficient such that for the second type of flow pattern, the heat transfer coefficient was found to be lower than the first flow type. Adhikari *et al.* [37] optimized the geometrical dimensions of rectangular fin arrays perpendicular to a horizontal heated surface utilizing dynamic-Q algorithm. It was indicated that the parameters affecting the air inlet area of the fin channel including fin height and s are the dominant factors affecting the heat transfer. Moreover, excessive reduction of s impedes the fluid flow and reduces its velocity resulting in a thicker thermal boundary layer and lower heat transfer rate.

The inclination angle of the longitudinal fins is a main factor affecting the heat transfer. Mittelman *et al.* [38] scrutinized natural convection underneath an inclined heated longitudinal fin array on a plate. It was established that the inclination angle

induces a stagnation point between the fins in which the flow splits. The heat transfer coefficient did not change significantly for small tilt angles however, after a certain angle the heat transfer increased substantially. Moreover, the tilt angle and fin height did not affect the optimum s. The effect of inclination angle for both downward and upward-facing longitudinal rectangular fin arrays was investigated by Tari and Mehrtash [39]. It was observed that small inclination angles from the vertical position slightly improve the heat transfer due to the thinner boundary layer compared with the vertical case. Moreover, the flow separation angle differed for the downward and upward-facing cases which affected the heat transfer. The natural convection heat transfer phenomenon from an inclined finned channel was scrutinized by Roy *et al.* [40]. The main findings indicated that an increase in the higher inclination angles, due to the chimney effect the flow velocity and consequently the heat transfer were greater compared with the lower inclination angles.

The heat transfer from longitudinal fins mounted on a heated tube is primarily dependent on fin height and number. Haldar [41] numerically investigated the natural convection phenomenon around a horizontal tube with longitudinal fins. It was observed that the air flows toward the tube and between the fins from various angles, rises along the finned tube, and leaves through a small passage at the top of the tube. The fins induce a zig-zag flow pattern to the airflow around the unit and the heat transfer is improved by increasing the fin height and number mainly due to heat transfer surface area augmentation. Moreover, the fins proved to have a negligible effect on heat transfer when the Grashof number (Gr) is below 10^3. The effect of longitudinal fin number and height on the natural convection heat transfer performance of a horizontal finned tube was analyzed by Wu and Tao [42]. The obtained results suggested that for a specific fin number, there exists an optimum fin height and vice versa in which the heat transfer is maximum. Furthermore, positioning a pair of fins in the vertical symmetry plane reduces the overall heat transfer as a result of obstructing the development of natural convection.

Kim *et al*. [43] conducted a series of experimental studies on longitudinally finned horizontal tubes to evaluate the effect of fin number and height and ΔT on natural convection. It was shown that although at small s values, the heat transfer surface area increases by increasing the fin number, the heat transfer coefficient diminishes as the formed thermal boundary layers from the longitudinal fins overlap. Moreover, increasing the fin height continuously reduces the overall thermal resistance however, it converges to a constant value. Konar *et al.* [44] performed numerical analyses on a horizontal finned tube and analyzed the fin height and number to find an optimum value. The results illustrated that increasing the fin height improves the overall heat transfer while decreasing the heat transfer from the tube. Furthermore, the increase of fin number enhances the overall heat transfer up to the point that the small s does not obstruct flow passage. The natural convection of a vertical tube mounted with vertical fins was elaborated by Sajedi *et al.* [45]. It was concluded that although the addition of fins augments the heat transfer surface area, it diminishes the flow velocity and natural convection between the fins. There are several other studies in the literature examining the natural convection heat transfer from longitudinal fins on a horizontal [46–48] or vertical [49–51] tube.

The inclination angles of the tube and longitudinal fins are important parameters affecting the heat transfer. Tolpadi and Kuehn [52] performed an experimental study where a single longitudinal fin was mounted on a horizontal isothermal tube, and they investigated the effect of the angle of the longitudinal fin on the natural convection heat transfer. It was stated that the plume separation location is displaced from above the heated tube when the fin is positioned within $50°$ from the upward vertical position. The thermal performance of one or more longitudinal fins mounted on a heated tube was examined by Abu-Hijleh [53]. Locating two long fins, one at the bottom within $15–45°$ and the other fin located above the tube within $135–165°$ resulted in the highest Nu.

In a combined experimental and numerical investigation, Jang *et al.* [54] analyzed the effect of tube inclination angle on the natural convection heat transfer of a

longitudinally finned tube. Increasing the inclination angle, blocked the upward movement of air resulting in drag coefficient growth and Nu decline. Li and Byon [55] analyzed the thermal performance of longitudinal fins on a tube mounted on a circular heated plate and found that the fin number and length are critical in the orientation effect whereas the impact of fin height is insignificant. Moreover, the horizontally oriented radial heatsink depicted better thermal performance compared with the vertically oriented radial heatsink. The angle of longitudinal fins with respect to the tube can also alter the heat transfer performance of longitudinal fin-tube heat exchangers. A longitudinally finned horizontal tube design with tilted fins was proposed by Lee *et al.* [56]. At the optimal fin inclination angle of 60°, the proposed design resulted in 6% better cooling performance compared with the conventional design.

1.2.3 Pin Fins

Pin fins are desirable in natural convection applications because of the significant surface area that they provide. Moreover, pin fins have the advantage of continuously interrupting the thermal boundary layer which can mix the cold regions of the fluid with the hotter regions in the vicinity of the heated surfaces. In the literature, the use of pin fins for natural convective heat transfer applications is confined to their installation on flat plates. Figure 1.3 represents an array of pin fins mounted on a plate. The optimal design of pin fin heatsinks has been extensively studied in the literature.

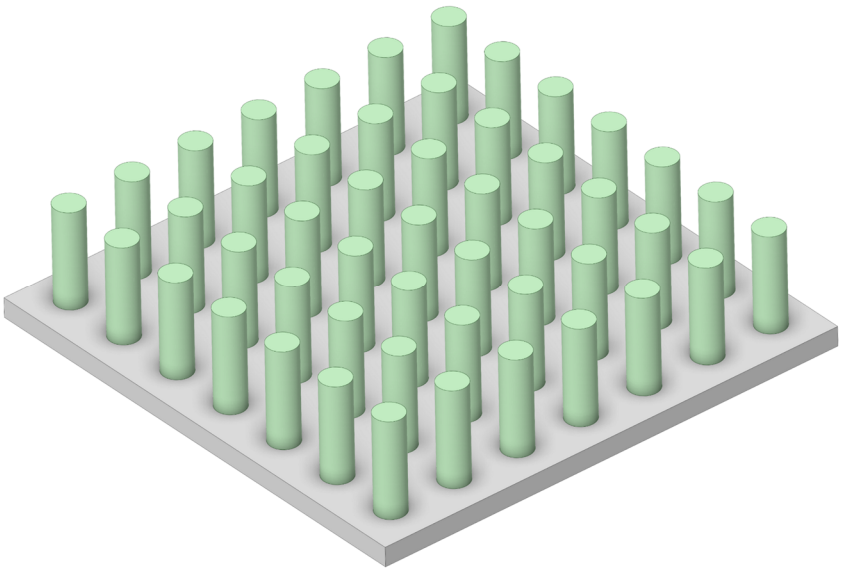


Figure 1.3. A typical pin fin design mounted on a plate

Joo and Kim [57] analytically compared the optimized vertical plate fin and pin fin heatsinks and validated the results with experiments. It was noted that plate fins can dissipate more heat however, the heat dissipation for unit mass is greater for pin fin heat sinks at equal base temperatures. Micheli *et al.* [58] compared the thermal performance of micro-fin arrays with pin micro-fin with equal heat transfer surface areas. Pin micro-fin design depicted a greater heat transfer enhancement because of the higher heat transfer coefficient provided. The pin fin density along the flow direction in a pin fin heatsink was optimized by Lee and Kim [59]. It was established that a variable density pin fin heatsink has higher heat transfer performance and lower mass compared with a uniformly distributed pin fin heatsink. In an experimental investigation, Ding *et al.* [60] elaborated on natural convection around an externally finned vertical tube. The outcomes illustrated that the thermal performance was enhanced by fin height and width while it was diminished by increasing the axial and circumferential fin pitch.

Orientation of the pin fin heatsinks has also a substantial effect on heat transfer. Huang and Wu [61] performed experimental and numerical investigations on a pin fin heatsink considering pin height and diameter and the orientation of the base plate. It was indicated that the tapered pin fin heatsink with a 66° inclination angle provides the lowest thermal resistance among the studied cases. Sertkaya *et al.* [62] experimentally scrutinized pin fin heatsinks with different fin numbers and heights and base plate orientations of 0, 90, and 180 degrees. The highest and lowest heat transfer rates were achieved for the upward and downward-facing heatsinks, respectively.

1.2.4 Unconventional Fin Designs

Recently, unconventional fin designs have gained popularity among scholars because of their heat transfer enhancement potential, reduced weight, and compactness [63]. The unconventional designs include serrated, interrupted, crimped, delta winglet, etc. configurations.

Kim and Kim [64] experimentally investigated the performance of a vertical tube with branched fins in natural convection. It was observed that the thermal resistance of the tube with branched fins was 20% lower than that of the tube with plate fins. Sundar *et al.* [65] analyzed the natural convection in a radial heatsink with perforated staggered fins. The thermal performance was increased by about 7–12% for different fin orientation angles compared with a similar heatsink with non-perforated fins. Park *et al.* [66] examined the natural convection heat transfer performance of an inclined cross-cut cylindrical heatsink. The minimum thermal resistance was achieved at a fin inclination angle of 25–30° while the cooling performance diminished for the inclination angles greater than 50°. Abbas and Wang [67] performed parametric studies to optimize the natural convection heat transfer of a plate fin heatsink using fin displacement. The maximum heat transfer performance was improved by 30% compared with the conventional plate fin heatsink and the proposed design was found to be appropriate for small s.

1.3 Heated Units in an Array

Natural convective flows in an array of heated units are encountered in various applications such as heat exchangers for air conditioning, refrigeration, vapor condensation, electronics cooling, nuclear power plant safety systems, thermal energy storage systems, heaters for high viscosity fuel oils, heating elements of drying plants, cooling of fluids in process plants, etc. [68–73]. In an array, the heated flow by a single unit affects adjacent units by disrupting the flow upstream. The boundary layers interact, and the arrangement of the units affects the local flow velocities and therefore, heat transfer. Therefore, the distance between adjacent units and their arrangement are critical factors.

Most studies in the current literature investigating natural convection from arrays concentrate on arrays of bare tubes. Marsters [74] experimentally investigated the heat transfer of an array of heated horizontal tubes with a single column. It was concluded that for small tube spacings, the average Nu is smaller than that of a single unit. However, when the distance between the tubes increases, the average Nu of the array is greater than that of a single tube. In an experimental study, Ashjaee and Yousefi [73] examined the natural convection from horizontal isothermal tubes arranged in vertical and inclined arrays. The results indicated that the heat transfer from an individual tube in an array critically depends on its positioning relative to other tubes. However, the heat transfer from the bottom tube regardless of position and Ra is identical to the natural convection from a single tube. Kitamura *et al.* [69] performed experiments to investigate the hydrothermal characteristics of a single-column tube bundle in natural convection. The assessed parameters included tube diameter and vertical distances between the tubes. The results indicated that the flow stays within the laminar regime when the gap distance is small and transitions to the turbulent regime by increasing the gap distances. Furthermore, in the laminar regime, the heat transfer coefficient decreases consistently toward downstream however, in the turbulent regime, it increases downstream.

Kang *et al.* [70] experimentally scrutinized the condensation heat transfer of an array of heated tubes. It was observed that the heat transfer coefficient is low for the tubes in the middle of the bundle due to the shadow effect of previous upstream tubes. Furthermore, compared with a single tube, the flow rate around the tubes in a bundle is greater because of the suction effect. Bian *et al.* [71] numerically investigated the condensation heat transfer of a tube bundle in natural convection. The results suggested that the bundle thickens the near-wall high-concentration air layer which decreases heat transfer. However, the bundle enhances the natural circulation of air, improving heat transfer. The bundle displays greater thermal performance by increasing the row and column numbers such that with triple rows, the average heat transfer coefficient shows a 14% improvement compared with a single tube.

The natural convection from arrays of conventional circular fin and tube units and units with novel fin designs were experimentally investigated by Unger *et al.* [75]. The results revealed that Nu is greater when there is a single row and decreases by increasing the number of rows, regardless of fin configuration.

1.4 Motivation and Problem Statement

The offered literature review illustrates the numerous efforts by the researchers to push the limits of natural convective heat transfer of various-shaped heatsinks by proposing novel designs and optimizing the geometrical parameters. Despite the fact that the unconventional designs and pin fins provide a desirable heat transfer performance, their manufacturing hardship attenuates their usage in the industry. Plate fins and annular fins, however, are extensively used in practical applications because of their uncomplicated manufacturing process, simplicity, and durability.

In conventional annular fin and tube designs, the heat transfer and flow pattern are majorly dependent on s. The addition of longitudinal fins to the conventional annular fin design can deflect the flow direction and the thermal footprint, enhance mixing, and affect heat transfer. The literature also emphasizes the critical effect of the

inclination angle of longitudinal fins on the performance of the heatsinks. Therefore, the positioning of the adjoined longitudinal fins to the conventional annular fin and tube design is a decisive parameter. Furthermore, in an array of heated units, the thermal performance of each unit differs from the unit's performance when it is used individually.

In the present work, a fin design is suggested based on the combination of annular and longitudinal fins which are mounted on a heated tube. The proposed design aims to maintain the simplicity of conventional annular and longitudinal fin designs while enhancing mixing and heat transfer. Experimental and numerical investigations are performed to analyze the heat transfer of the proposed design and the effects of s, longitudinal fin inclination angle, and ΔT. Furthermore, a set of numerical simulations is performed to investigate the heat transfer of an array with the proposed fin and tube design. In an array, the impact of varying unit distances in different columns and rows, as well as the inclination angles of the longitudinal fins on heat transfer is scrutinized.

CHAPTER 2

METHODOLOGY

2.1 Experimental Work

This section illustrates the proposed design along with a description of the details of the experimental study.

2.1.1 Proposed Design, Parameters, and Manufactured Test Pieces

The configuration consists of a tube on which the annular fins, and two planar longitudinal fins along each other on a single plane are placed. The longitudinal fins reach up to the annular fin's outer diameter (D). Figure 2.1 represents the proposed design along with the geometrical parameters.

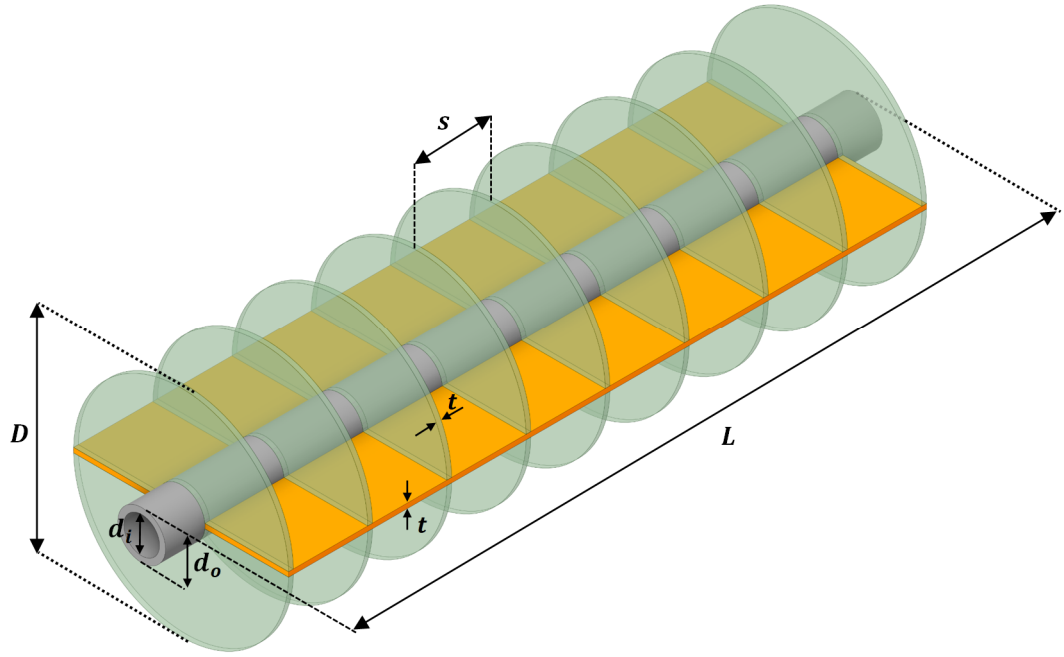


Figure 2.1. The proposed design with the geometrical parameters

According to the scale analysis performed by Yildiz and Yüncü [15] on a conventional annular fin and tube unit, two flow types are expected between the fins based on s:

- Fully developed channel flow in the limiting case of very small fin spacing
- External flow on a vertical heated plane in the limiting case of very large fin spacing which is significantly greater than the boundary layer thickness

Therefore, fin spacing impacts the hydrothermal performance of the fin and tube unit and must be considered in the current analyses.

The study of Tolpadi and Kuehn [52] suggested that in the case of a horizontal tube finned by a single longitudinal plate, the inclination angle of the plate is a critical factor regarding the plume separation location and heat transfer. As a result, in the present study, the inclination angle of the longitudinal fins is one of the considered parameters.

The tube's outer diameter (d_o), fin diameter (D), and fin spacing (s) are the main parameters investigated in the literature. The range of the mentioned essential geometrical parameters in the relevant studies is given in Table 2.1. In the current study, d_o, D, and s are chosen such that they fall in the range of those studied in the literature. It must be noted that the first and last fins have equal distances from the sides of the tube.

Table 2.1. Range of the important geometrical parameters in the relevant studies

$\boldsymbol{d_o}$ (mm)	$\boldsymbol{D}$ (mm)	$\boldsymbol{s}$ (mm)	**Reference**
25	50–125	3.75–150	[12]
24.9	35–125	3.6–146	[15]
24.9	35–50	2–12	[24]
10–50	55–120	4–9	[27]
1–120	57.15–140	3.22–24.24	[28]



Figure 2.2. Photographs of the manufactured test pieces

Figure 2.2 and Table 2.2 represent the photographs of the manufactured test pieces and the geometrical dimensions, respectively. The test pieces are manufactured from aluminum 6061 blocks with a thermal conductivity of 153 W/m°C using CNC machining with an accuracy of 0.01 mm which is an appropriate tolerance for the macro dimensions of the present study. Manufacturing from a single block prevents thermal contact resistances between the fins and the tube. The samples are polished after the manufacturing process to reduce emissivity and radiation. The emissivity of the manufactured pieces is $\varepsilon = 0.1$ which is measured using a FLIR E63900 thermal imaging camera.

Table 2.2. Geometrical dimensions of the manufactured test pieces

Dimension	**Value** (mm)
Tube inner diameter (d_i)	15
Tube outer diameter (d_o)	20
Fin diameter (D)	90
Fin spacing (s)	3, 5.16, 10.05, 15.67, 31.13
Fin thickness (t)	2
Tube length (L)	300

2.1.2 Experimental Setup

An experimental apparatus has been designed and constructed to investigate the heat transfer of the manufactured test pieces. Figure 2.3 depicts the experimental setup and the utilized instruments. The setup consists of the fin and tube unit, a nichrome heater wire, a DC power supply (Keysight N5771A), a Keysight 34972A data logger equipped with a Keysight 34901A switch card, T-type thermocouples, a computer, and the supporting frame. The thermocouples are put into the small grooves drilled on the tube surface and are attached using a thermal paste and an extra T-type thermocouple is used to measure the ambient temperature. The fin and tube unit is mounted on two wooden plates secured onto the supporting frame, ensuring that the unit's distance from the ground remains at 130 cm, mitigating any ground effects. The wooden plates are selected for their low thermal conductivity (0.1 W/m℃) to minimize the heat conduction from the tube's sides to the structure. This facilitates a uniform temperature distribution along the tube. The sides of the tube are effectively insulated to block the entry of ambient air into the tube. Natural convection is an extremely delicate phenomenon susceptible to disruption by external flows or objects. Thus, the experiments are performed in a windowless, insulated room to prevent external flows and maintain a stable air temperature throughout the experiments.

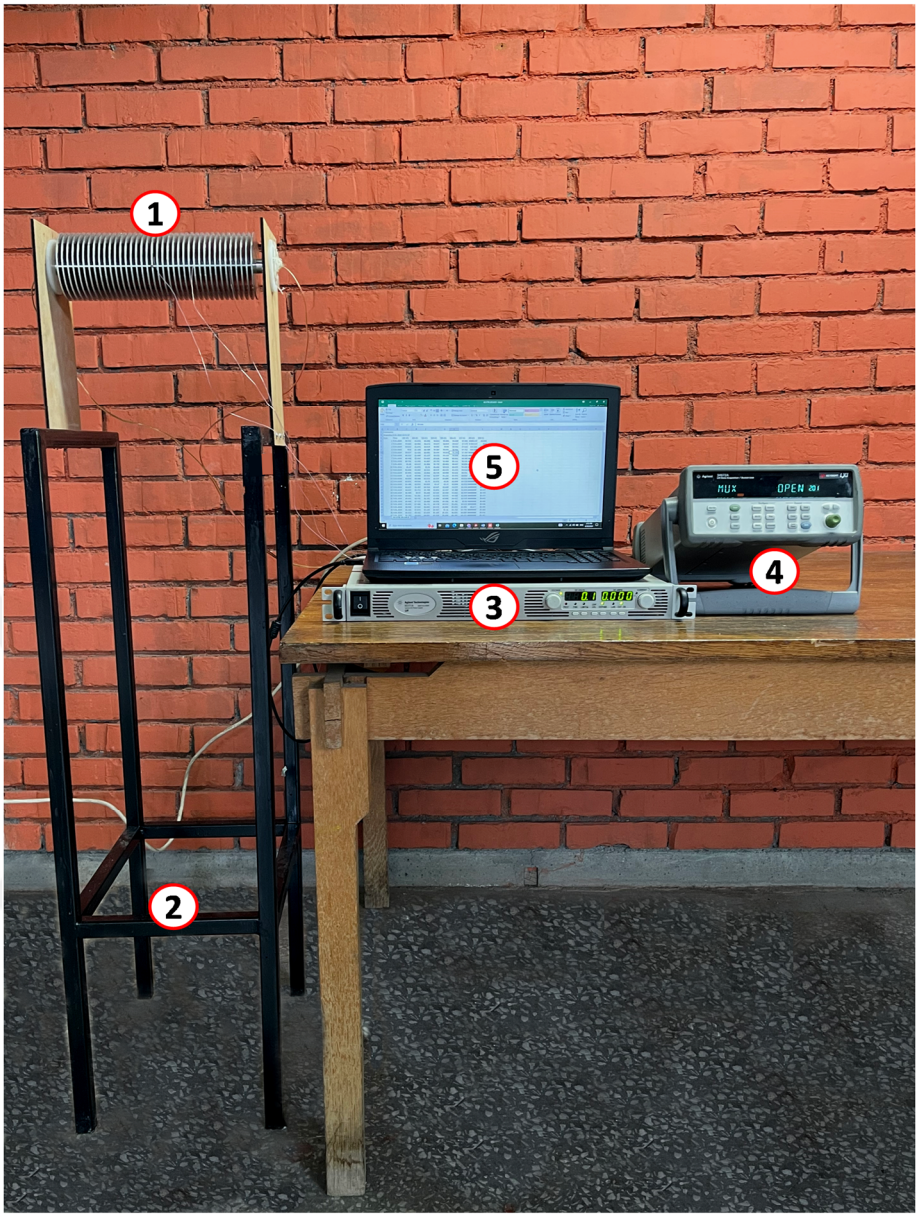


Figure 2.3. A photograph of the experimental setup. (1) fin and tube unit, (2) supporting frame, (3) DC power supply, (4) data logger, (5) computer

An experiment using a bare tube is carried out as a control experiment (Figure 2.4) to validate the experimental procedure, ensure the uniformity of the nichrome wire heater and insulation of the sides of the tube, and minimize the number of thermocouples. The sensitivity of the natural convection necessitates minimal usage

of thermocouples to prevent the disruption of the flow pattern. The optimal configuration is positioning the thermocouples from the interior of the tube to its surface. However, despite conducting several experiments on the bare tube using this method, the temperatures recorded by the thermocouples differ significantly from those obtained directly from the tube surface using a Fluke 724 temperature calibrator. This discrepancy arises from the insulation of the thermocouples. The temperature within the tube is significantly higher than the temperature at the surface of the tube, reaching up to 300℃. This damages the insulation of the thermocouples, leading to inaccurate temperature readings. In order to ensure accurate temperature measurements without disturbing the flow, thin T-type 36 AWG thermocouples with a diameter of 0.13 mm are attached to the bare tube surface.



Figure 2.4. A photograph of the bare tube in the control experiment

Figure 2.5 depicts the positioning of the thermocouples on the bare tube. The results of the experiments conducted on the bare tube indicate that for the maximum investigated ΔT, the temperatures on the tube are symmetric with respect to the

middle plane of the tube ($z = 0$). This symmetry is evident from the temperatures observed at locations *I*, *II*, and *VI*, mirroring those at locations *V*, *IV*, and *VII*, respectively, proving that the heater is symmetric. Moreover, the thermocouples at locations *II*, and *IV* represent equal values with locations *VI* and *VII*, respectively, indicating that the temperature on the tube is constant along the circular perimeter at a constant z. The maximum temperature is observed at location *III*, and the minimum temperatures are located at locations *I* and *V*. However, for the maximum studied ΔT in the current study (100°C), the maximum temperature difference along the tube is about 3°C. This value can probably be the result of the minor non-uniformity of the heater along the z-axis or the negligible heat conduction from the sides of the tube to the supporting frame.

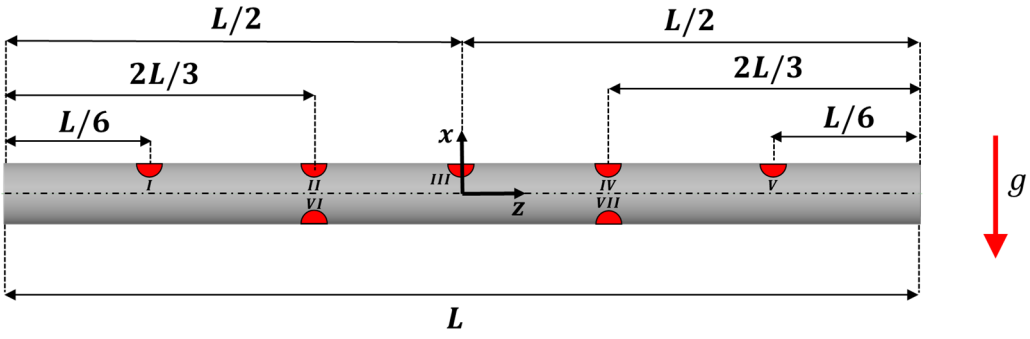


Figure 2.5. Location of the thermocouples in the control experiment with the bare tube

According to the control experiment and the necessity to minimize the number of thermocouples, 3 thermocouples are utilized in the experiments of the manufactured fin and tube units. Figure 2.6 depicts the location of the thermocouples in the fin and tube experiments. To prevent the concentration of thermocouples on one side and minimize the flow disruption, the thermocouples are distributed along the tube instead of being clustered on a single side. Similar to the experiment conducted on the bare tube, the maximum temperature difference at the base is found to be 3°C, with the base temperature assumed to be the average of the measured temperatures.

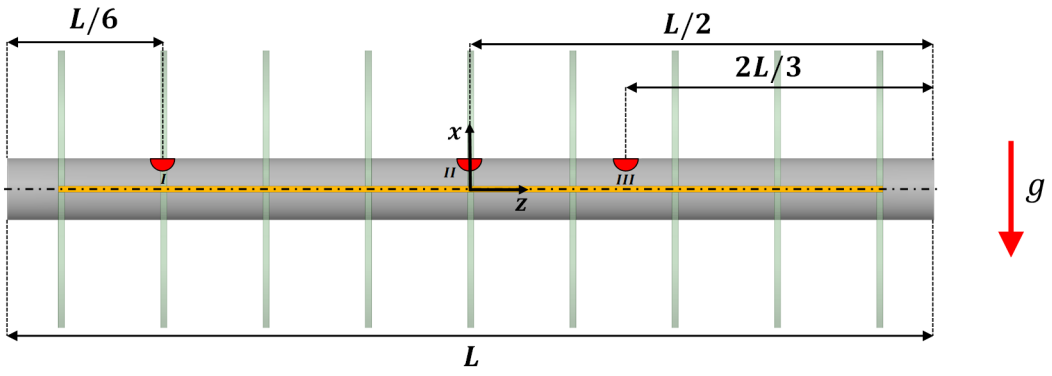


Figure 2.6. Location of the thermocouples in the fin and tube experiments

2.1.3 Experimental Procedure

To ensure reliable results, the proper function of the thermocouples is confirmed by calibrating them in a water bath of constant temperature utilizing a mercury-in-glass thermometer. In the current work, the ΔT range from 20°C to 100°C is studied. The applied heat is manually regulated using the DC power supply. Initially, a ΔT of 20°C is established through iterative adjustments, then the temperature difference is increased by 20°C increments, again by trial and error. It is important to emphasize that the accepted tolerance for the adjustments is within $\pm$1°C. The chosen tolerance aligns well with the uncertainty of the thermocouples ($\pm$1°C) and is manageable within the present experimental setup constraints. The tube temperatures are recorded at 10-second time intervals by the data logger with the steady-state conditions confirmed when ΔT remains stable within 0.2°C for 15 minutes [76]. The total heat transfer of the fin and tube unit (q_t) is evaluated by multiplying the current (I) with the voltage (V) read from the DC power supply and it is recorded for each experiment. Figure 2.7 represents the inclination angle of the longitudinal fin (θ). During the experiments, θ is manually adjusted to 0°, 45°, and 90°.

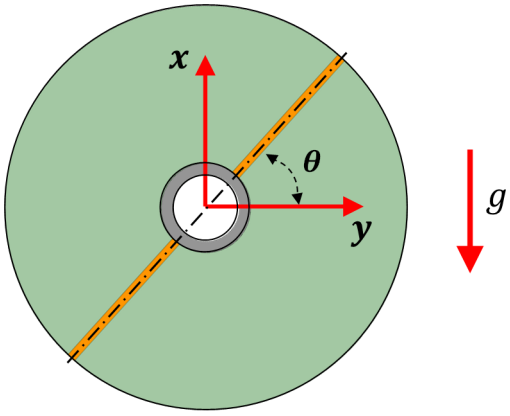


Figure 2.7. The longitudinal fin inclination angle

2.2 Numerical Study

Numerical simulations are conducted on the proposed design to deepen the understanding of its hydrothermal characteristics and to assess its performance in an array configuration. This section outlines the details of the performed numerical simulations.

2.2.1 Computational Domains

2.2.1.1 Single Fin and Tube Unit

A series of numerical simulations are performed to understand the hydrothermal behavior of the proposed design, obtain the convective heat transfer of a single fin and tube unit (q_c) for different ΔT, and comprehensively investigate the effects of s and θ values on q_c. The computational domain for a single fin and tube unit is given in Figure 2.8.

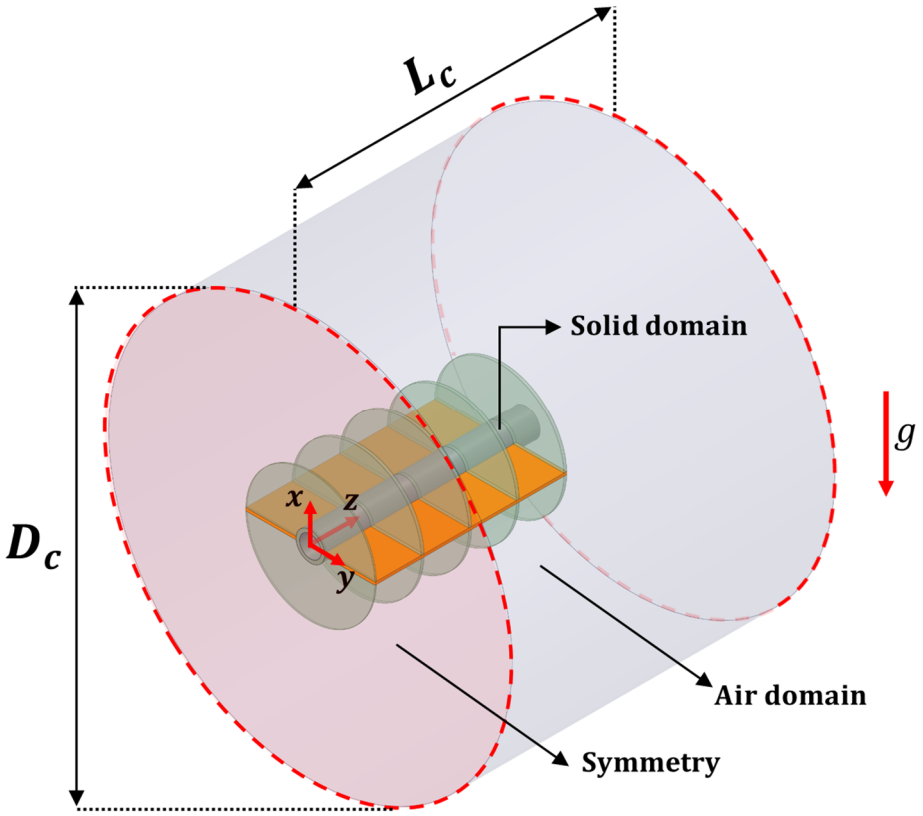


Figure 2.8. The computational domain for a single fin and tube (not to scale)

The domain consists of half the length of the fin and tube unit due to symmetry on the plane $z = 0$, along with a cylindrical domain around the fin and tube unit representing the air. The domain is cylindrical to replicate the shape of the annular fins which facilitates applying constructed radial mesh elements. Moreover, a cylindrical domain enables changing θ by altering the direction of gravity.

2.2.1.2 Fin and Tube Units in an Array

A set of parametric numerical simulations is conducted to investigate the performance of the proposed design in an array of fin and tube units. The key parameters include the inclination angles of longitudinal fins within different rows and columns of the array, and the transverse (S_t) and longitudinal (S_l) distances

between the centers of the tubes of adjacent fin and tube units. These parameters have a substantial role in influencing the collective heat transfer of the array.

Figure 2.9 represents the investigated configurations for the fin and tube units in an array. It is assumed that the number of columns within the array is large. This assumption suggests that the hydrothermal performance of the units is independent of their respective column, and simulating a single column is sufficient. The centers of the tubes are located on the same line in each row and column so that the heated air plume above the units can be deflected in the y-direction without directly entering the annular fin spacing of the unit above. The angles between the longitudinal fins of the units at the first and second rows and the y-axis are denoted as ψ_1 and ψ_2, respectively, where, $\psi_1 = |\psi_2|$. When $\psi_2 > 0°$, the longitudinal fins within a column are parallel, and when $\psi_2 < 0°$, the adjacent longitudinal fins within a column have opposite angles with respect to the y-axis.

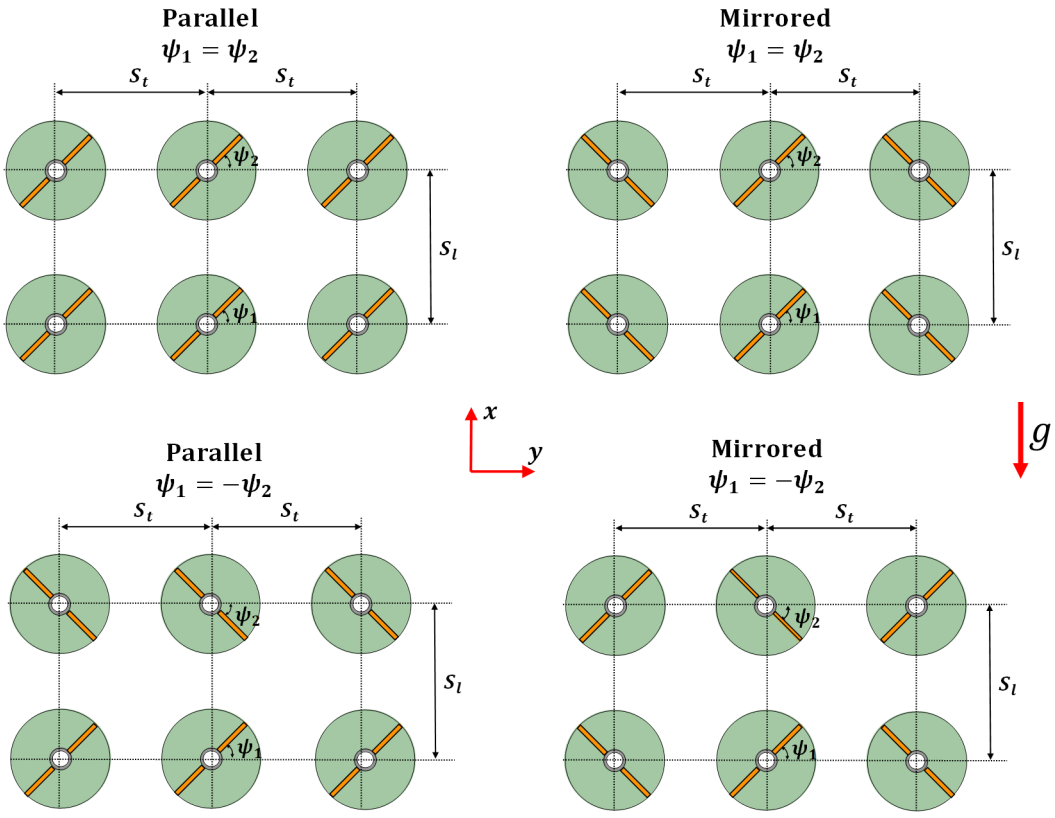


Figure 2.9. The studied configurations of the fin and tube units in an array

The studied cases are categorized into parallel and mirrored configurations. In the parallel configuration, the longitudinal fins within a row are parallel, while in the mirrored configuration, the angles between the longitudinal fins and the y-axis within a column are opposite to that of longitudinal fins at the adjacent columns.

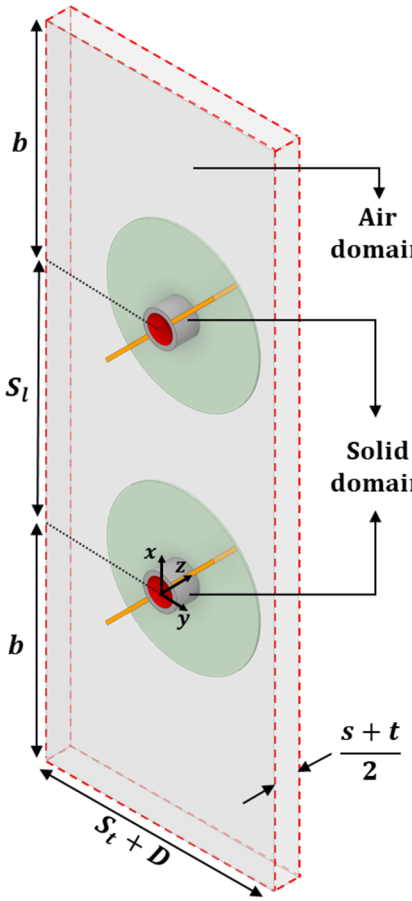


Figure 2.10: The computational domain for an array of fin and tube units with two rows (not to scale)

Figure 2.10 demonstrates the computational domain considered for an array of fin and tube units with two rows ($n = 2$). To reduce the computational cost, only a single column is considered, along with half of s and thickness of the annular fins, resulting in a domain thickness of $(s + t)/2$. The domain width is $S_t + D$ and domain length equals $S_l + 2b$, where b is the vertical distance from the bottom and top boundaries

of the computational domain to the centers of the tubes in the first and last rows of the array, respectively.

2.2.2 Governing Equations

In the numerical simulations, the natural convection phenomenon is based on the following assumptions:

- The system is at a steady state
- The air flow is laminar (explained in Section 3.1.1) and air is incompressible [7, 24, 25, 27]
- The thermophysical properties of the air are constant and calculated at $(T_{base} + T_{amb})/2$
- Boussinesq approximation can be used to simulate the buoyancy-driven flow and the density difference is only effective in the generation of the buoyant forces
- Radiation is significant and considered in the simulations of the validation study; however, in the rest of the numerical simulations radiation is disregarded as the focus is on convective heat transfer
- Viscous dissipation is negligible

The governing equations for 3D steady natural convection are continuity, momentum, and energy, denoted by Eqns. 2.1, 2.2, and 2.3, respectively.

Continuity:

$$\nabla \cdot \mathbf{U} = 0 \tag{2.1}$$

where **U** stands for the fluid velocity vector.

Momentum:

$$\rho(\mathbf{U}\cdot\nabla)\mathbf{U} = -\nabla P + \mu\nabla^2\mathbf{U} + \rho\beta\left(T_f - T_{amb}\right)g \tag{2.2}$$

here, ρ, P, μ, β, T_f, T_{amb}, and g are the fluid density, pressure, dynamic viscosity, thermal expansion coefficient, fluid temperature, ambient temperature, and the gravitational acceleration, respectively. The last term in Eqn. 2.2 stands for the Boussinesq approximation which incorporates density variation only due to temperature.

Energy:

$$\rho c_p\mathbf{U}\cdot\nabla T_f = k_f\nabla^2 T_f \tag{2.3}$$

In the above equation, c_p and k_f represent fluid's specific heat at constant pressure, and thermal conductivity, respectively.

The heat conduction in the solid domain complies with the following energy equation:

$$\nabla^2 T_s = 0 \tag{2.4}$$

where T_s is the solid temperature.

The governing equations are solved using ANSYS FLUENT 2021 R2, a finite-volume-method-based commercial software. The least square cell based method is used to discretize the convection and diffusion terms in the conservation equations. The momentum and energy equations are discretized employing a second-order

upwind scheme, while the second-order method is utilized for discretizing the pressure field. In the simulations involving a single fin and tube unit, the SIMPLE algorithm is adopted for coupling the velocity and pressure [77]. Convergence is achieved when residuals for all variables except energy reach 10^{-5}, and for energy, the criterion is set to 10^{-7}. For the simulations of fin and tube units in an array, the coupled method is used for pressure-velocity coupling along with the pseudo-transient time method. For these simulations, convergence is achieved when residuals for all variables, except energy, reach 10^{-7}, while for energy, the criterion is set to 10^{-11}. The mentioned residual values are scaled residuals which means that the solution residual of each discretized governing equation at a specific iteration is divided by a reference value, which is the maximum residual value from the first five iterations [77].

The under-relaxation factors used for the convergence of the variables (relative whole field residuals) for the single unit and array configurations are shown in Table 2.3.

Table 2.3. Under-relaxation factors used in the simulations

Configuration	Pressure	Density	Body force	Momentum	Energy
Single unit	0.3	1	1	0.7	1
Array	0.5	1	1	0.5	0.75

In the experimental studies, the radiation heat transfer is a considerable portion of the total heat transfer. As a result, in the numerical simulations of the validation study, the radiation is considered. The surface-to-surface method is utilized for the radiation heat transfer analysis. This method is used to consider the radiation exchange within an enclosure containing gray-diffuse surfaces. Within this model, the exchange of energy between two surfaces is influenced by various factors including the surface dimensions, separation distance, and orientation, all of which

are accounted for through a geometric function known as a view factor. In the simulations, any absorption, emission, or scattering of radiation is disregarded. Furthermore, fin and tube surfaces are assumed to be diffusive-gray bodies and the outer boundaries of the computational domain are blackbodies at T_{amb}.

The radiosity of surface i is written as:

$$J_i = E_i + \rho_i G_i \tag{2.5}$$

In the above equation, E_i, ρ_i, and G_i are the emissive power, reflectivity, and irradiation of surface i, respectively.

E_i is expressed by the relation below:

$$E_i = \varepsilon_i \sigma T_i^4 \tag{2.6}$$

where ε_i, σ, and T_i are the emissivity of surface i, the Stefan-Boltzmann constant, and the temperature of surface i, respectively.

G_i is the irradiation on surface i originated from all j surfaces forming an enclosure and is written as below:

$$G_i = \sum_{j=1}^{N} F_{ij} J_j \tag{2.7}$$

here, F_{ij} represents the view factor and is given by the below relation:

$$F_{ij} = \frac{1}{A_i} \int_{A_i} \int_{A_j} \frac{\cos \zeta_i \cos \zeta_j}{\pi r^2} dA_i dA_j \tag{2.8}$$

In the above equation, A_i and A_j are the areas of the surfaces i and j, r is the distance between surfaces i and j, ζ is the angle between the normal and the vector from surface to surface for each respective surface i.

In order to obtain the convective heat transfer from the experimental results, the radiative heat transfer of the fin and tube unit (q_r) needs to be subtracted from q_t. To find q_r for the experiments, Finite Element Method (FEM) based ANSYS Mechanical commercial software is utilized. Again, the surface-to-surface radiation model is used for the simulations and the assumptions are the same as those mentioned above.

2.2.3 Boundary Conditions

This section outlines the applied boundary conditions, detailing the specific parameters for a single fin and tube unit as well as for the units arranged in an array.

2.2.3.1 Single Fin and Tube Unit

Since the investigated study is natural convection, the exterior boundaries of the domain, except for the symmetry plane, must be at atmospheric pressure. Figure 2.11 represents the front and side views of the simulated domain. The pressure outlet boundary condition is applied to the cylindrical outer wall and the circular wall at $z = L_c$. Furthermore, the symmetry boundary condition is applied to the circular boundary on $z = 0$.

In the numerical simulations, to simplify the model, the heater and the air between the heater and the inner wall of the tube are not simulated. Instead, the thermal boundary condition is directly applied to the inner wall of the tube. It must be noted

that in the validation study, the recorded q_t values from the experiments are utilized as the thermal input in the simulations. Subsequently, in the numerical simulations following the validation study, the constant temperature boundary condition is applied to facilitate a fair comparison between the cases. As observed in both the experiments and the validation study, the temperature variation along the tube of the fin and tube unit is insignificant. Hence, the constant temperature boundary condition effectively replicates the actual thermal input. Additionally, in all of the numerical simulations, the outlet temperature is set to a constant value of 20°C. The ambient temperatures recorded during the experiments fall within a range of $18 - 22$°C depending on the weather conditions and time of the day. Given that ΔT is being investigated, the constant temperature boundary condition does not impact the results.

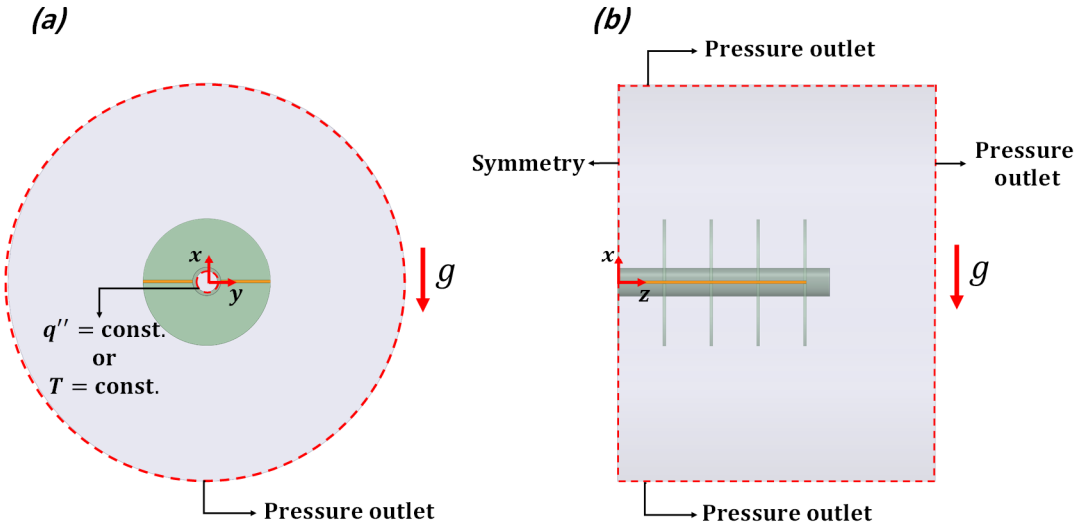


Figure 2.11. The boundary conditions for a single fin and tube unit, (a) front view, and (b) side view

Based on the above explanation, at the outer boundaries of the cylindrical domain except the symmetry wall ($z = 0$):

$$P = 1 \text{ atm and } T = T_{amb} \tag{2.9}$$

At the inner wall of the tube, in the validation study:

$$q'' = \text{constant} \tag{2.10}$$

here, q'' represents the heat flux.

At the inner wall of the tube, in the rest of the numerical simulations:

$$T = \text{constant} \tag{2.11}$$

At the symmetry wall ($z = 0$):

$$\mathrm{U_z} = 0, \partial \mathbf{U}/\partial z = 0, \text{ and } \partial T/\partial z = 0 \tag{2.12}$$

At the fluid-solid interface:

$$\mathbf{U} = 0, T_s = T_f, \text{ and } k_s(\partial T_s/\partial n) = k_f\left(\partial T_f/\partial n\right) \tag{2.13}$$

where k_s is the solid thermal conductivity.

In the radiation analyses using ANSYS Mechanical, due to the high thermal conductivity of the fin material and low fin diameters, the variation of temperature on the fins is assumed to be insignificant and the whole surface of the fin and tube unit is assumed to be at the base temperatures measured in the experiments [15]. The

open enclosure option with an ambient temperature of 20℃ is selected since the dimensions of the test pieces are significantly smaller compared to the experiment room and the emissivity of the fin and tube unit is set to $\varepsilon = 0.1$.

2.2.3.2 Fin and Tube Units in an Array

The applied boundary conditions in the simulations of the fin and tube units in an array are illustrated in Figure 2.12.

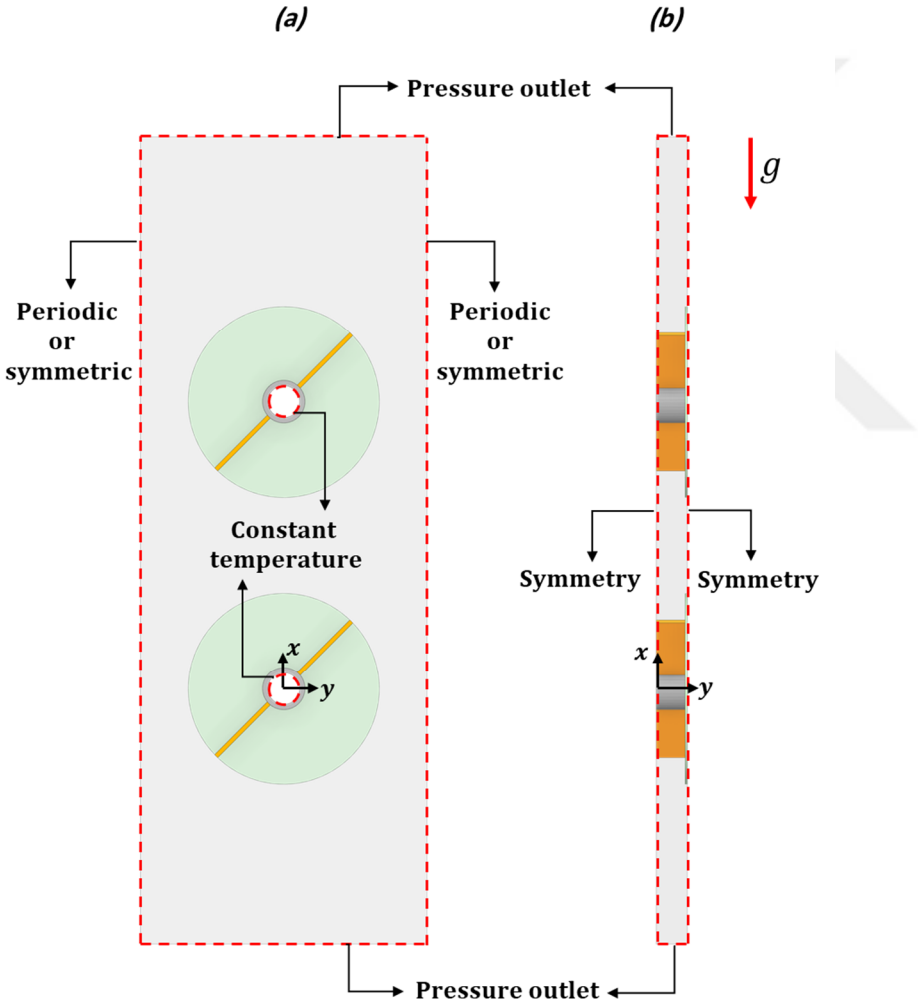


Figure 2.12. Boundary conditions for fin and tube units in an array, (a) front view, and (b) side view

The top and bottom boundaries are assumed to be in atmospheric pressure. In the parallel configuration, the left and right boundaries in the frontal view are periodic boundary conditions while in the mirrored configuration symmetric boundary conditions are applied to the mentioned boundaries. As for the side view, symmetric boundaries are applied to the left and right sides, with a constant temperature boundary condition applied to the inner surface of the tubes.

2.2.4 Numerical Study Matrix

Table 2.4 and Table 2.5 represent the parameters investigated in the numerical studies of the single fin and tube unit and units arranged in an array, respectively. In the numerical study of the single fin and tube unit, s, θ, and ΔT which are the essential parameters affecting the heat transfer are investigated. The parameter values written in bold text represent the values not studied in the experiments.

In the numerical simulations of the fin and tube units arranged in an array, s yielding the highest heat transfer from the study of a single fin and tube unit is adopted and the simulations are performed in the constant ΔT of 60℃. Here, the studied parameters include ψ_2, S_t, S_l, and the configuration of the longitudinal fins with respect to each other in adjacent columns.

Table 2.4. The parameters in the study of the single fin and tube unit

Parameter	Studied values
s (mm)	3, 5.16, **7.14**, 10.05, 15.67, **22.09**, 31.13
θ (degrees)	0, **15**, **30**, 45, **60**, **75**, 90
ΔT (℃)	20, 40, 60, 80, 100

Table 2.5. The parameters in the study of the fin and tube units in an array

Parameter	Studied values
ψ_2 (degrees)	$-60, -45, -30, 30, 45, 60$
S_t (in D)	$3D/2$, $2D$, $5D/2$
S_l (in D)	$3D/2$, $2D$, $5D/2$
Configuration of the longitudinal fins in adjacent columns	parallel, mirrored

2.2.5 Mesh and Domain Independence Study

The cylindrical shape of the domain in the simulations of a single fin and tube unit makes it suitable for structured elements. For this purpose, the domain is divided into several partitions. Figure 2.13 illustrates the division pattern of the domain to facilitate structured meshing. The cylindrical domain is divided into sections *I* and *II* using the $z = L/2$ plane to reduce the density of mesh in $z > L/2$. The air domain between the fins in section *I* (depicted in red) is separated from the rest of the domain and the rest of the air domain is divided into two semicircular rings by two planar elements perpendicular to the tips of the longitudinal fins (depicted in blue). The inner diameter of the semicircular air domains is equal to the annular fin diameter and their outer diameter is equal to the computational domain diameter (D_c). The semicircular and planar partitions in section *II* of the domain are similar to their counterparts in section *I*; however, there exists a cylindrical air domain at the central region of section *II* (depicted in green).

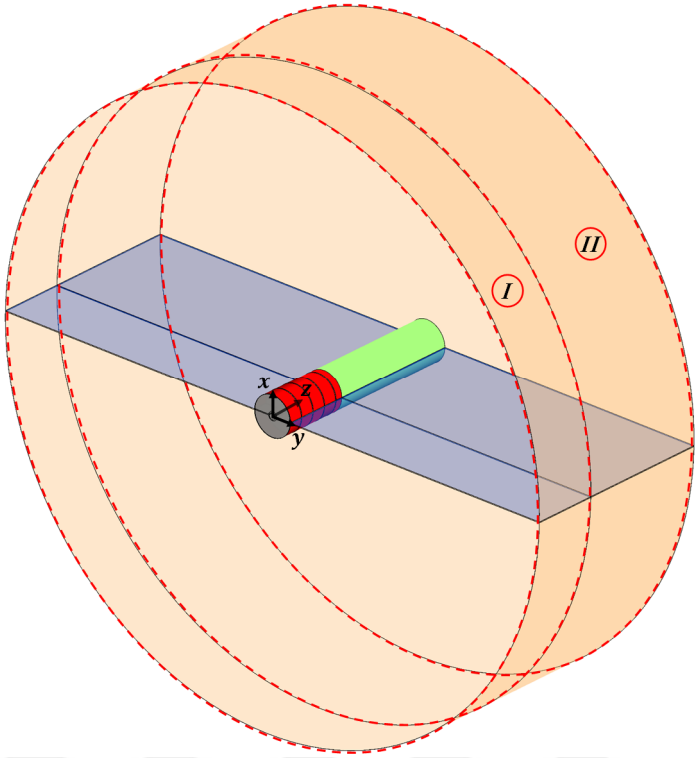


Figure 2.13. The division pattern of the numerical domain

Structured meshing is utilized across all sub-domains except for the fin and tube unit and the cylindrical air domain at the center of section *II* where unconstructed tetrahedrons are employed. Within the remaining portion of the air domain, the meshing technique involves sweeping a 2D mesh across a surface in the z-direction. The applied mesh configuration for the fin and tube unit with $s = 31.13$ mm is presented in Figure 2.14. Notably, the size of the elements is smaller in the proximity of the fin and tube unit and gradually increases towards the outer boundary of the domain. Furthermore, the element size in the z-direction is larger in section *II* compared to section *I* due to the absence of significant velocity and temperature gradients in section *II*.

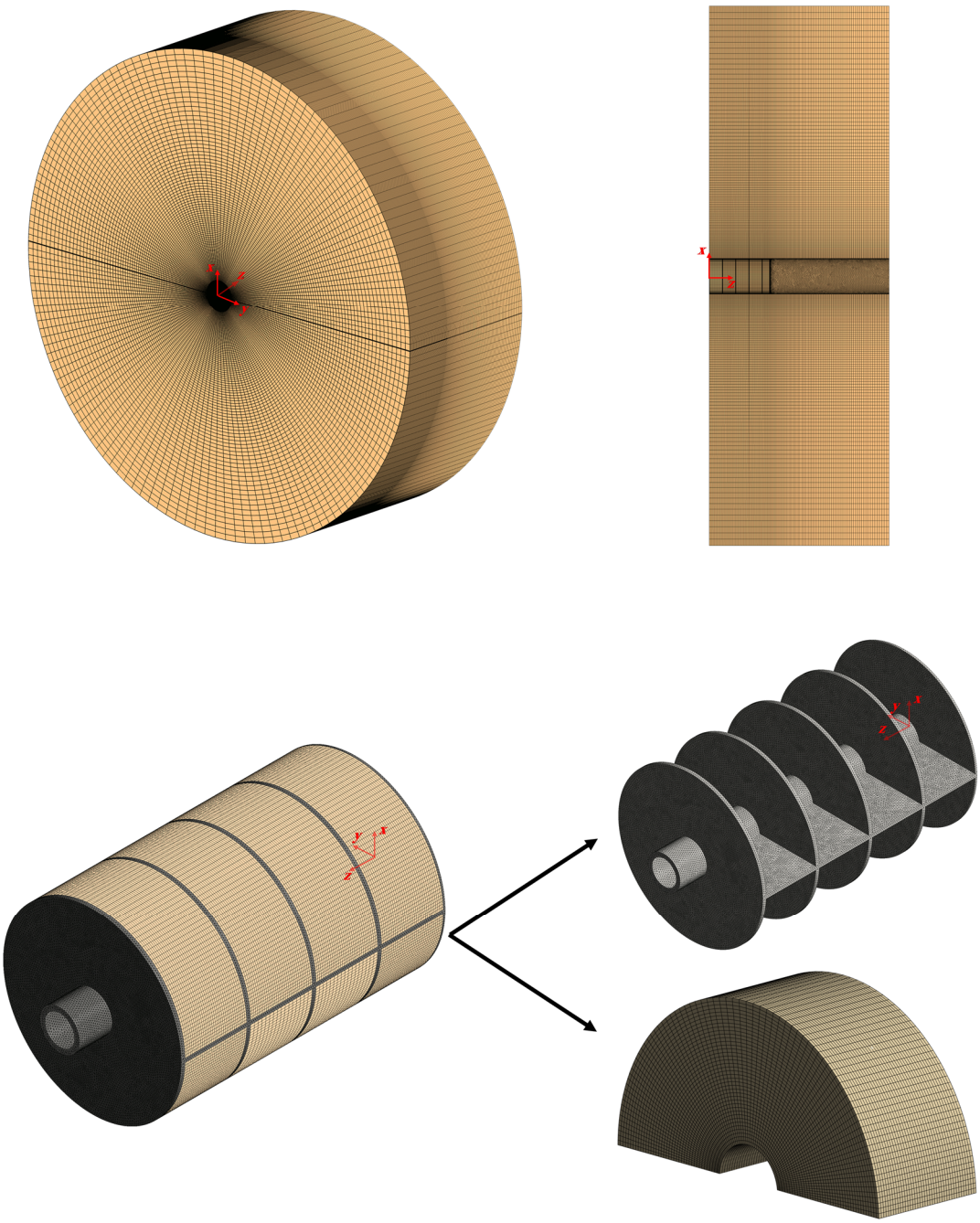


Figure 2.14. The mesh structure for the case with a fin spacing of 31.13 mm

Conducting a mesh independence analysis is essential to ensure the accuracy of numerical results. In this analysis, a fin and tube unit with $s = 31.13$ mm, and $\theta = 0°$ is selected. The heat input of $q_t = 119.92$ W, which resulted in

$\Delta T = 99.09$℃ in the experimental study, is applied to the fin and tube unit. For this particular case, the change in Nu_s with respect to the number of elements is depicted in Figure 2.15. A total of 5,887,367 computational cells provide acceptable accuracy for this specific case, with a deviation of approximately 0.05% in Nu_s from the Nu_s value obtained with 9,430,367 elements. Therefore, this mesh configuration is adopted for subsequent numerical simulations to ensure result accuracy and minimize computational costs. In the simulations of other s values, the mesh configuration remains unchanged, except for the adjustments made to the semicircular elements between the fins. As the s value decreases, fewer elements are required between the fins. However, the density of the elements between the fins is kept constant across all studied cases.

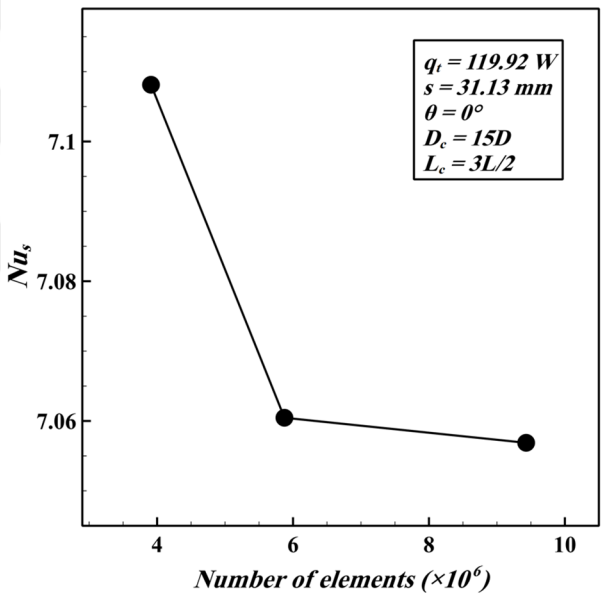


Figure 2.15. Variation of Nu_s with the number of elements

In the natural convection problems involving pressure boundaries, the domain size can affect the numerical results. To ensure the domain independence of the numerical results in the simulations of a single fin and tube unit, the effects of the diameter and length of the domain are investigated. Figure 2.16 illustrates the impact of domain

sizes on Nu_s. Increasing L_c from $1.5L$ to $2L$, results in 0.33% change in Nu_s, while increasing D_c from $15D$ to $20D$, yields a change of 0.23%. Thus, it is concluded that a domain with geometrical dimensions of $L_c = 1.5L$ and $D_c = 15D$ is sufficient for obtaining accurate results.

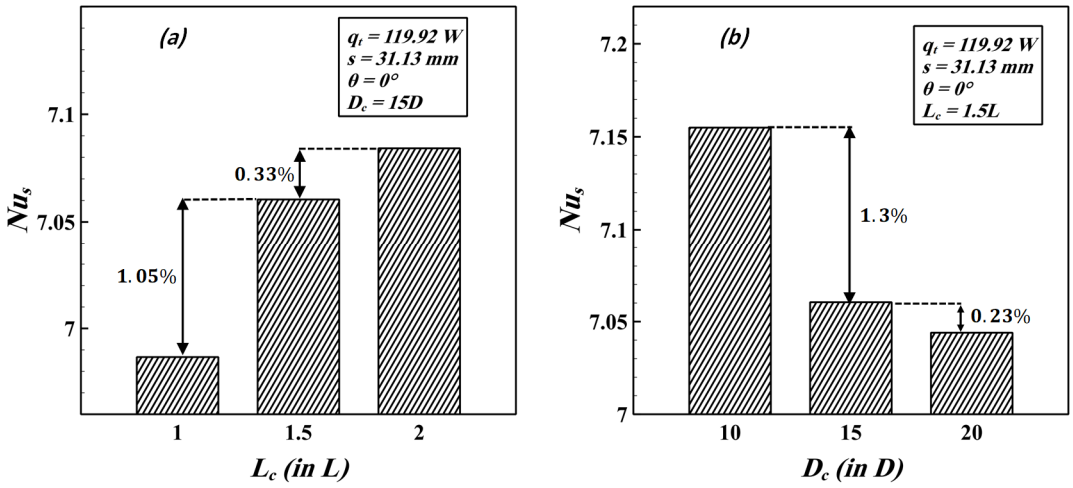


Figure 2.16. Variation of Nu_s with (a) domain length, and (b) domain diameter

Figure 2.17 depicts the adopted mesh for an array of fin and tube units. The arrangement and density of elements between the annular fins and within the solid domain are identical to those utilized in the simulations of the single fin and tube unit study. However, unconstructed elements are used for the remaining air domain, which are swept in the z-direction. To ensure that the domain is independent of the distances between the centers of the tubes of the first and last rows from the bottom and top boundaries (b), a domain independence study is performed for an array with $n = 5$, $\psi_n = 60°$, $S_t = 3D/2$, and $S_l = 5D/2$. According to Figure 2.18, $b = 15D$ provides an acceptable accuracy and is selected for further studies.

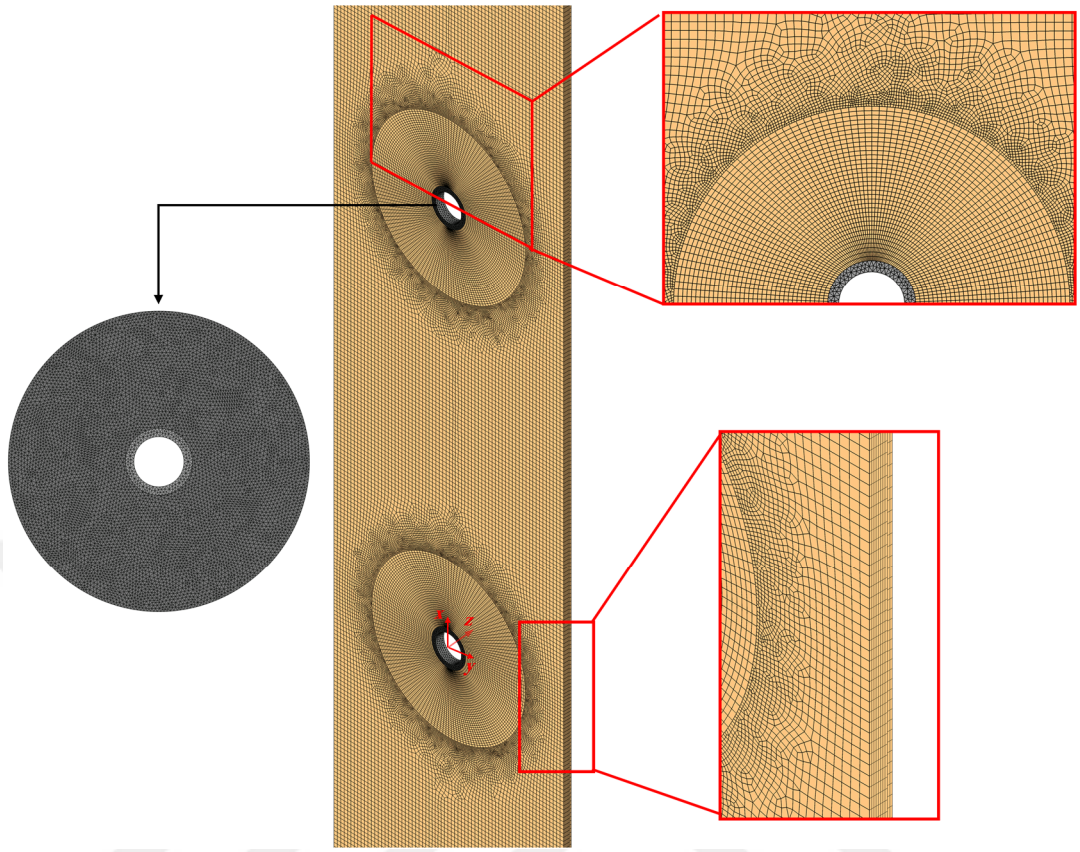


Figure 2.17. The mesh configuration for an array of fin and tube units

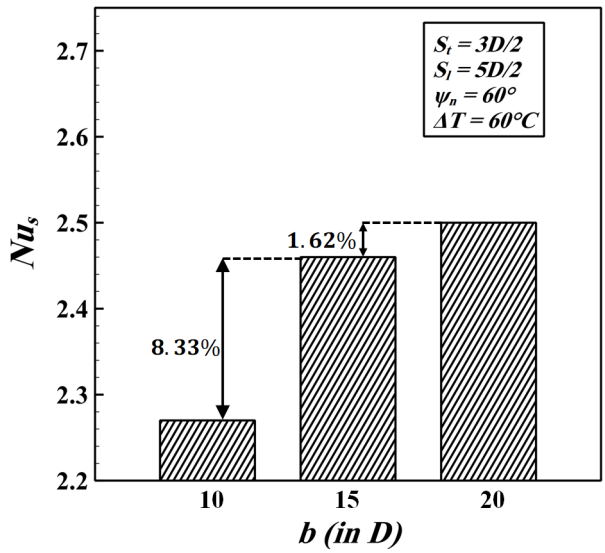


Figure 2.18. Variation of Nu_s with b for an array with $n = 5$

2.3 Data reduction

In this subsection, the important parameters defining the flow and thermal characteristics of the investigated configurations are listed.

The Ra based on the tube's outer diameter is written as follows:

$$\mathrm{Ra}_{d_o} = \frac{g\beta\Delta T {d_o}^3}{\nu\alpha} \tag{2.14}$$

where ν and α are the kinematic viscosity and thermal diffusivity of air, respectively.

The Ra based on s can be calculated using the following relation [12]:

$$\mathrm{Ra}_s = \frac{g\beta\Delta T s^3}{\nu\alpha}\left(\frac{s}{D}\right) \tag{2.15}$$

The convective heat transfer of a single fin and tube unit is calculated as follows:

$$q_c = q_t - q_r \tag{2.16}$$

The convective heat transfer coefficient for the fin and tube unit is given by:

$$h = \frac{q_c}{A\Delta T} \tag{2.17}$$

The Nu based on d_o for a bare tube can be derived using the below equation:

$$\mathrm{Nu}_{d_o} = \frac{h d_o}{k_f} \tag{2.18}$$

The Nu based on s is written as:

$$\mathrm{Nu}_s = \frac{hs}{k_f} \tag{2.19}$$

The convective heat transfer coefficient for an array of fin and tube units is calculated as follows:

$$h_{array} = \frac{q_{c,array}}{A_{array}\Delta T} \tag{2.20}$$

where $q_{c,array}$ and A_{array} are the convective heat transfer and total area of the units in the array, respectively.

Nu_s for an array of fin and tube units is:

$$\mathrm{Nu}_{s,array} = \frac{h_{array} s}{k_f} \tag{2.21}$$

2.4 Uncertainty Analysis

In the experiments, due to the errors of the measurement equipment, there are inevitable uncertainties in the measured and calculated quantities. These uncertainties can be estimated using the Guass error propagation law [78]:

$$w_R = \sqrt{\left(\frac{\partial R}{\partial x_1} w_1\right)^2 + \left(\frac{\partial R}{\partial x_2} w_2\right)^2 + \cdots + \left(\frac{\partial R}{\partial x_n} w_n\right)^2} \tag{2.22}$$

here, R is the measured value as a function of independent quantities x_1, x_1, ..., and x_n and w_n stands for the uncertainty of n_{th} measured quantity. The only measurement devices in the present study are the T-type thermocouples and their uncertainty is ± 1℃ or 0.75% of the measured temperatures, whichever is greater. The uncertainty values for the regulated voltage and current using the power supply are 0.1 V and 0.01 A, respectively.

The calculated variables from the experimental results are Nu_{d_o} for the bare tube and Nu_s for the fin and tube units. The maximum uncertainty values for Nu_{d_o} and Nu_s are determined as 6.8% and 6.5 %, respectively.

CHAPTER 3

RESULTS AND DISCUSSION

3.1 Validation

This section validates the experimental procedure and the proper function of the equipment used in the experimental setup along with the accuracy of the numerical results based on the details provided in Section 2.2.

3.1.1 Experimental Procedure

In order to validate the experimental procedure, the obtained experimental Nu_{d_o} values for the horizontal tube are compared with the Nu_{d_o} correlations from the existing literature for a horizontal tube.

For an isothermal horizontal tube, Morgan [79] suggests the following correlation:

$$\mathrm{Nu}_{d_o} = C\mathrm{Ra}_{d_o}{}^{n} \tag{3.1}$$

where $C = 0.48$ and $n = 0.25$ for the range of $10^4 \leq \mathrm{Ra}_{d_o} \leq 10^7$.

Churchill and Chu [80] have proposed the below expression for an isothermal horizontal tube when $\mathrm{Ra}_{d_o} \leq 10^{12}$:

$$\mathrm{Nu}_{d_o} = \left[0.60 + \frac{0.387\mathrm{Ra}_{d_o}{}^{1/6}}{[1 + (0.559/\mathrm{Pr})^{9/16}]^{8/27}}\right]^2 \tag{3.2}$$

here, Pr stands for the Prandtl number of air.

The results of the present experiment and the results obtained from Eqns. (3.1) and (3.2) are plotted in Figure 3.1. The relative errors of the experimental data for Nu_{d_o} compared to the results by Eqns. (3.1) and (3.2) are 9.35% and 1.48%, respectively. The experimental data align more closely with Morgan's results than with those of Churchill and Chu. The larger discrepancy in the Churchill and Chu correlation is due to its applicability to a broader range of Ra_{d_o} and the errors introduced by empirical fitting. The close agreement between the experimental data and the correlations affirms the validity of the experimental setup, procedure, and the utilized instruments.

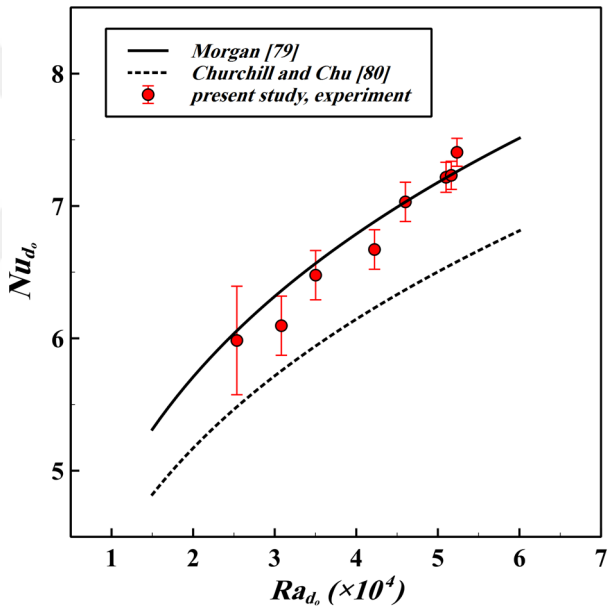


Figure 3.1. Comparison of current experimental data with results obtained from correlations suggested in the literature for Nu_{d_o} of a bare tube

3.1.2 Numerical Simulations

In this subsection, a validation study is carried out based on the experimental data acquired by the experiments conducted on the manufactured test pieces and the numerical simulations based on the governing equations and the relative boundary conditions mentioned in sections 2.2.2 and 2.2.3, respectively. Figure 3.2 represents the obtained experimental and numerical Nu_s values with respect to q_t for the manufactured test pieces.

The average difference between the experimental and numerical results is 3.6%. Taking into account the uncertainties and measurement errors inherent in the experiments, alongside the assumptions in the numerical simulations, the deviation between the experimental and numerical results falls within acceptable limits. Hence, the numerical models can be considered reliable for further investigations. It should be noted that radiation heat transfer accounts for 10–24% of q_t across the studied cases. The highest contribution, 24%, is observed in the case where $s = 31.13$ mm and $\theta = 0°$ at $\Delta T = 20$℃.

In the natural convection problems, the laminar flow regime is assumed to be valid when $\mathrm{Ra} \leq 10^9$ [10]. In the present study, the maximum Ra_{d_o} is at $\Delta T = 100$℃, with a value of $\mathrm{Ra}_{d_o} = 5.3 \times 10^4$. Similarly, the maximum Ra_s corresponds to the case with $s = 31.13$ mm at $\Delta T = 100$℃, yielding $\mathrm{Ra}_s = 3.1 \times 10^5$. Therefore, considering both Ra_{d_o} and Ra_s, the validity of the laminar flow assumption is confirmed.

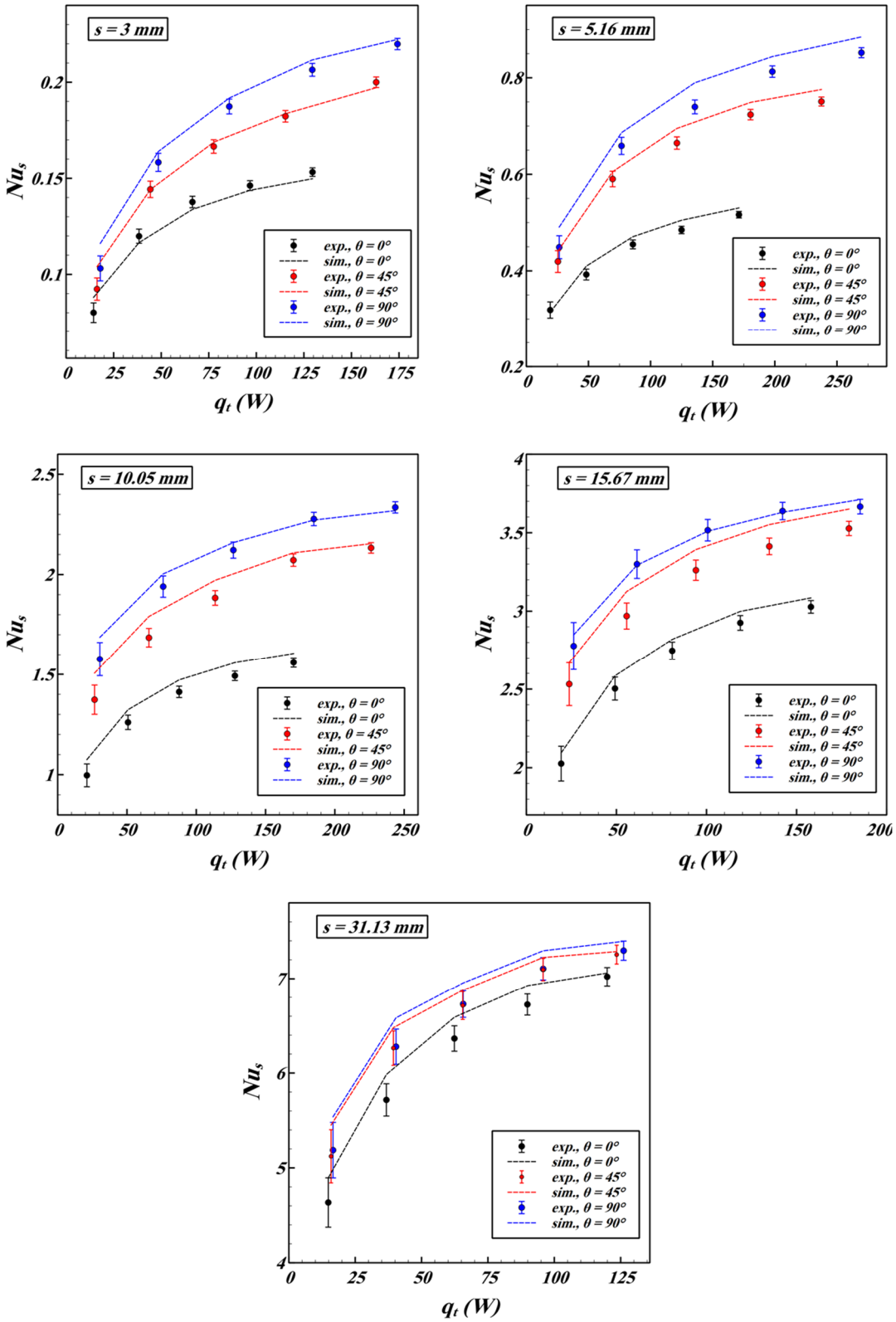


Figure 3.2. Variation of Nu_s with q_t

3.2 Numerical Results for a Single Fin and Tube Unit

In the natural convection phenomenon, the thermal and hydrodynamic characteristics of the flow are interconnected. Figure 3.3 illustrates the velocity contours with embedded velocity vectors, and temperature contours embedded with streamlines at $\Delta T = 60℃$ for the conventional design with $s = 3,\ 7.14$, and 31.13 mm. These specific values are chosen to represent flow characteristics for the narrowest, optimal, and widest s, respectively. It is worth noting that for the cases with $s = 3$, and 7.14 mm, where the number of fins is even (54 and 30, respectively), the contours, vectors, and streamlines are depicted on the symmetry plane between two middle fins ($z = 0$). For the case $s = 31.13$ mm, where the number of fins is odd (9) they are located between the middle fin and the fin adjacent to the middle fin ($z = 16.5$ mm). These locations are valid across all contours, vectors, and streamlines for the cases with the same s in this section.

Examining the velocity and temperature contours of the case $s = 31.13$ mm reveals that due to the large s value, the plane in the middle of the fins is distant from the heated surfaces, resulting in lower velocity and temperature compared with other cases. This indicates the dominance of convection heat transfer and the limited conduction of heat into the air at the middle of the fins. Decreasing s to 7.14 mm, increases the velocity and temperature on the plane between the fins, indicating a thicker boundary layer covering a greater portion of s. A comparison between the velocity contours of the cases $s = 3$, and 7.14 mm suggests that further reduction in s reduces the velocity between the fins. Furthermore, in the case with $s = 3$ mm, the velocity is evenly distributed between the fins which suggests that the boundary layer fully covers s and limits the air velocity as flow moves in x-direction. Moreover, at $s = 3$ mm, the air temperature between the fins is close to the tube temperature suggesting that the natural convection is obstructed and the conduction is dominant.

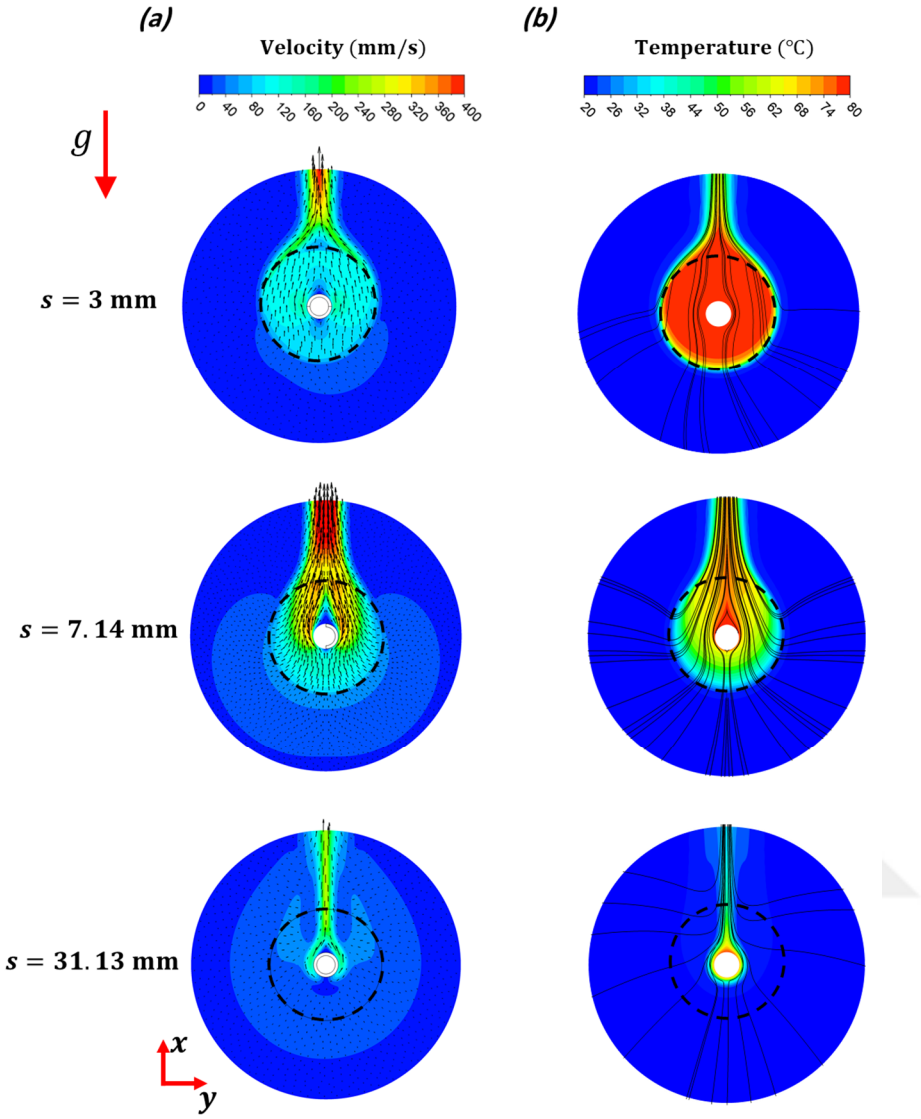


Figure 3.3. (a) Velocity contours and vectors, and (b) temperature contours and streamlines for the conventional design, $s = 3$, 7.14, and 31.13 mm at $\Delta T = 60$°C

An essential observation from the contours is the higher air velocity and temperature above the unit in $s = 7.14$ mm compared to other cases. The reason lies in the higher heat transfer in this case. As will be discussed later in this section, this case has the highest heat among the studied cases. This suggests that the air absorbs a greater amount of heat compared with other cases resulting in a greater temperature

difference between the ambient air and the heated air plume above the unit, strengthening the buoyant forces and increasing the momentum of the air.

Figure 3.4 shows the velocity contours embedded with velocity vectors for the proposed design with $s = 3, 7.14$, and 31.13 mm and $\theta = 0°$, $30°$, $60°$, and $90°$ at $\Delta T = 60℃$.

Comparing Figure 3.4 with Figure 3.3a indicates that at $\theta = 90°$, the hydrodynamic behavior of the air closely mirrors that of the conventional design. The only difference is the formation of a thin boundary layer along the sides of the longitudinal fin. Similar to the conventional design, the highest velocity above the fin and tube unit is observed when $s = 7.14$ mm in all θ values.

Similar to the velocity distribution observed in the conventional design, at $s = 31.13$ mm and $\theta = 90°$, the velocity at the middle plane of the fins is lower than other illustrated s values. However, decreasing θ enhances the velocity on a portion of the mentioned plane. For instance, at $\theta = 0°$, the air velocity at the top half of the air domain between the annular fins is approximately 120 mm/s, whereas at $\theta = 90°$, it decreases to about 40 mm/s.

For $s = 7.14$ mm, the velocity contours exhibit similarity between θ values of $90°$ and $60°$, with the primary difference being the rotation of the velocity vectors along the z-axis. However, decreasing θ to $30°$ leads to decreased velocity values between the annular fins, particularly at the bottom half of the air domain between the fins. Further decreasing θ to $0°$ results in a substantial decrease in velocity at the top half of the air domain between the fins, forming a stationary area above the longitudinal fin. This observation suggests that when the longitudinal fin is horizontal, it obstructs the flow passage toward the top half of the annular fins. Similarly, at $s = 3$ mm, reducing θ also diminishes the velocity between the annular fins.

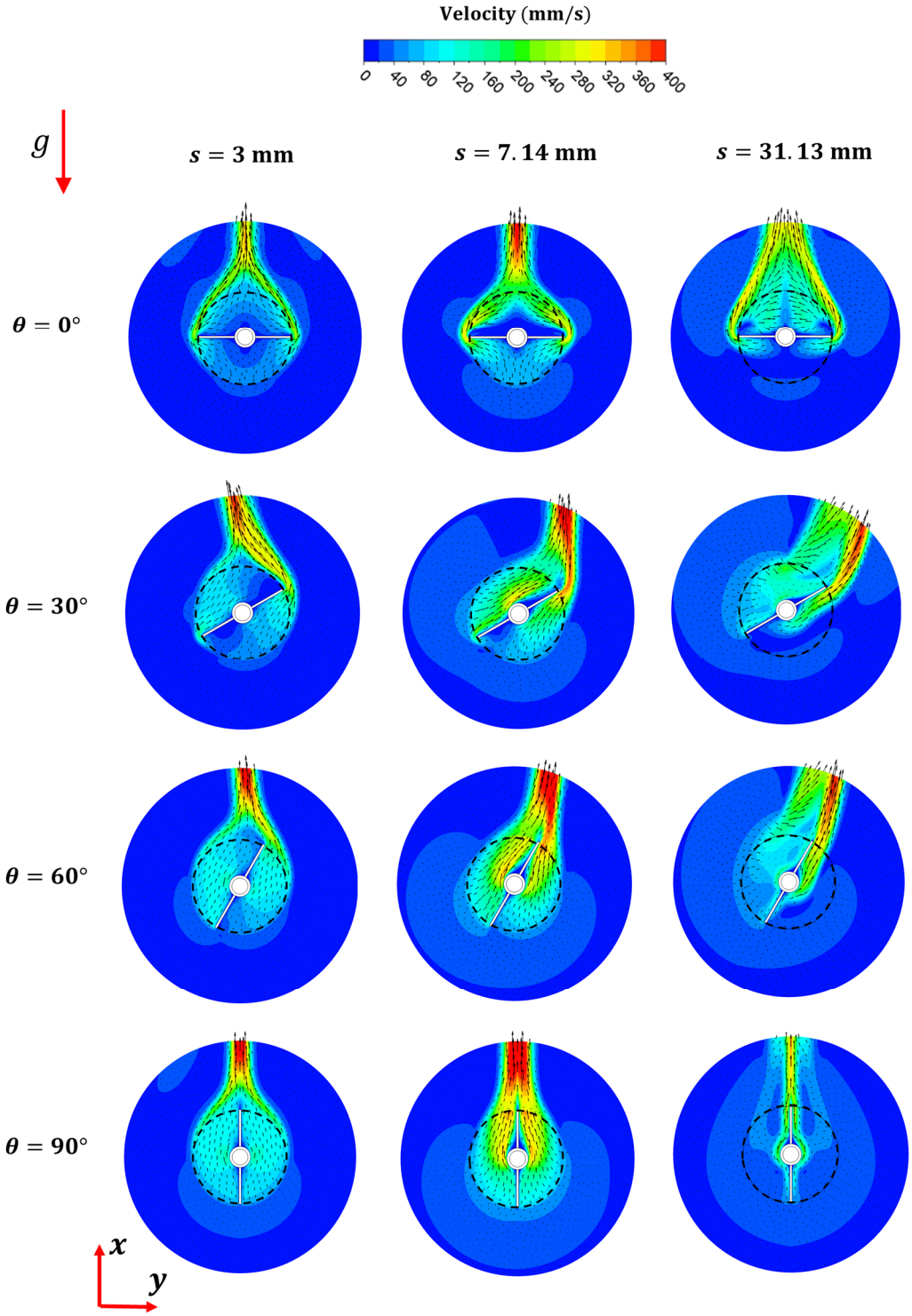


Figure 3.4. Velocity contours and vectors for proposed design, $s = 3$, 7.14, and 31.13 mm, and $\theta = 0°$, 30°, 60°, and 90° at $\Delta T = 60℃$

A noteworthy point in Figure 3.4 is the velocity magnitude and direction of the air after it exits the area between the annular fins. At all θ values, the highest velocity belongs to $s = 7.14$ mm. However, at $s = 31.13$ mm the air has the maximum deflection compared with other illustrated cases. In the case where $s = 3$ mm, regardless of the θ value, the highest air velocity leaving the area between the annular fins is positioned above the tube. This occurs because a significant portion of the air bypasses the area between the annular fins and instead flows outside the diameter of the annular fins. Changing θ value substantially affects the maximum air velocity above the unit. For $s = 31.13$ mm, decreasing θ from 90° to 60° and 30° enhances the maximum velocity of the air plume above the unit, while this velocity decreases at $\theta = 0°$. However, in the cases where $s = 3$ mm and 7.14 mm the maximum plume velocity decreases continuously by reducing θ.

The temperature contours embedded with streamlines for the proposed design with $s = 3$, 7.14, and 31.13 mm and $\theta = 0°$, 30°, 60°, and 90° at $\Delta T = 60$℃ are depicted in Figure 3.5.

A notable difference between the temperature contours of the cases with various s, regardless of θ, is the temperature rise due to the reduction in s and the boundary layer covering the spacing between the annular fins. With decreasing s, the dominance of conduction increases, resulting in higher air temperatures between the annular fins, reduced temperature gradients between the fins and air, and ultimately, lower convective heat transfer.

By decreasing θ, the temperature of air between the annular fins increases. In the case of $s = 31.13$ mm, when $\theta = 90°$, the temperature at the plane between the fins is close to the ambient temperature. However, decreasing θ to 60° and 30° leads to the formation of a layer of higher-temperature air at the air domain between the annular fins. Further reduction in θ to 0° increases the temperature of both the bottom and top halves of the air domain between the annular fins. Nevertheless, Figure 3.4 indicates that the velocity is also enhanced at the locations with high-temperature air between the annular fins.

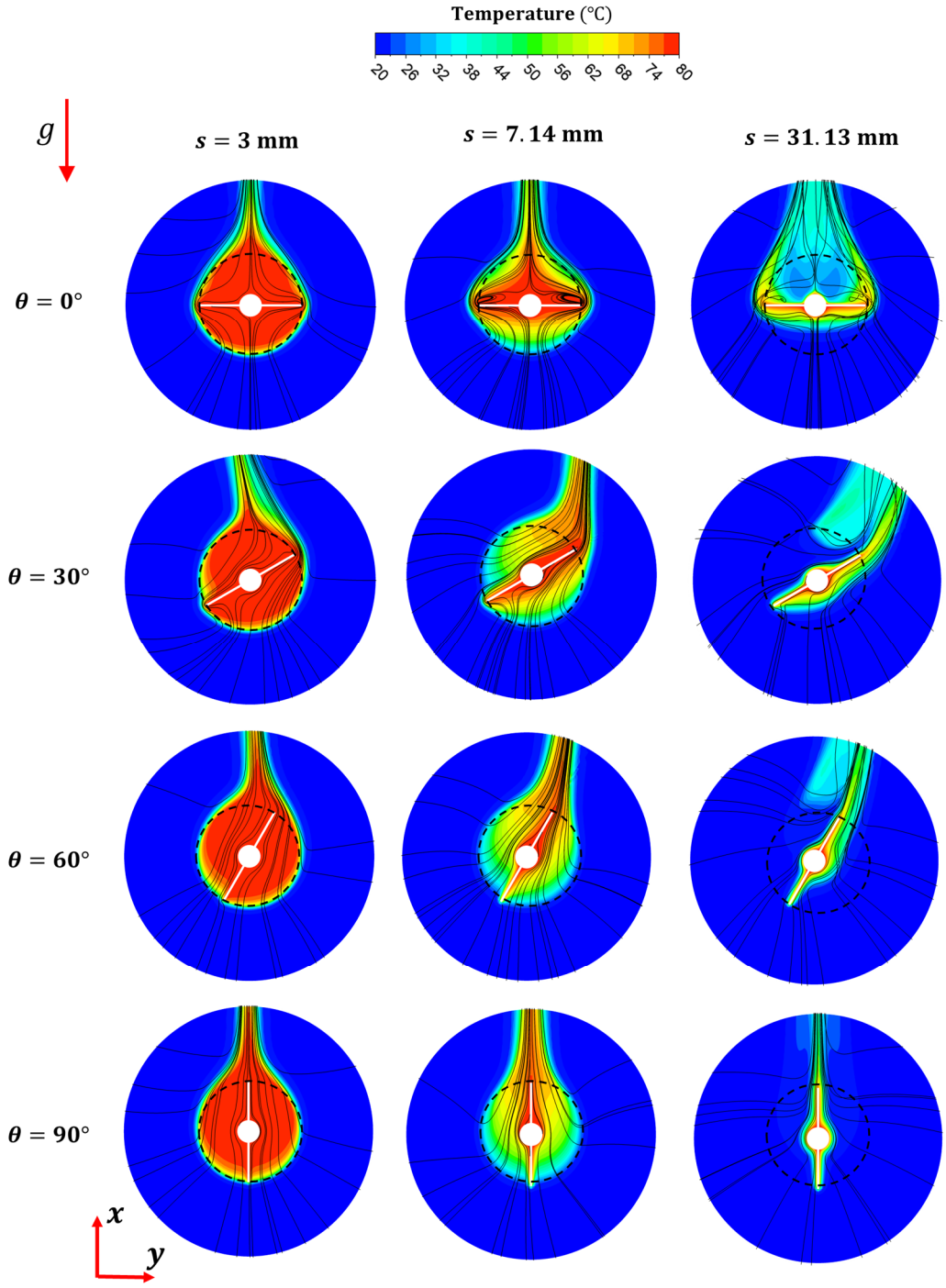


Figure 3.5. Temperature contours and streamlines for the proposed design, $s = 3$, 7.14, and 31.13 mm, and $\theta = 0°$, 30°, 60°, and 90° at $\Delta T = 60℃$

As s decreases to $7.14\ \text{mm}$, the temperature of the air between the annular fins becomes more dependent on θ. As will be mentioned later in this section, in this fin spacing, the rate of change of q_c increases as θ decreases (see Figure 3.10). This fact can be explained by an examination of temperature contours across $\theta = 0°, 30°, 60°,$ and $90°$. The temperature of the air between the annular fins does not vary considerably when θ is decreased from $90°$ to $60°$. However, a further decrease in θ results in higher temperatures observed in both the bottom and top halves of the air domain between the annular fins. An examination of the velocity magnitudes in Figure 3.4 suggests that in contrast with the case with $s = 31.13\ \text{mm}$, when $s = 7.14\ \text{mm}$, there is a significant reduction in velocity between the annular fins as θ decreases. This reduction explains the observed temperature rise.

For $s = 3\ \text{mm}$, the air temperature between the annular fins closely aligns with the temperature of the solid domain, suggesting minimal convection heat transfer. Moreover, the trend of increase in the air temperature with decreasing θ matches with the trend observed in the $s = 7.14\ \text{mm}$ case, a result of the air velocity reduction between the annular fins as shown in Figure 3.4.

A noteworthy observation regarding the temperature of the air plume above the fin and tube units is its correlation with the direction of the streamlines. For instance, in the case with $s = 7.14\ \text{mm}$ and $\theta = 90°$, similar to the longitudinal fin direction, the streamlines follow a vertical path as they exit the region between the annular fins, with the highest air temperature positioned precisely above the tube. As θ decreases to $60°$ and $30°$, the streamlines above the unit deflect rightward, similar to the maximum plume temperature. However, a further decrease in θ does not deflect the streamlines' direction, and the maximum plume temperature above the unit remains similar to that in the $\theta = 90°$ case, positioned exactly above the tube.

Figure 3.6 and Figure 3.7 present the temperature and wall flux distribution on the fin and tube unit for $s = 3$, 7.14, and $31.13\ \text{mm}$ and $\theta = 0°, 30°, 60°,$ and $90°$ at $\Delta T = 60℃$.

When $s = 31.13$ mm, the unit exhibits the lowest temperature and highest heat flux, contrasting with $s = 3$ mm case, where it demonstrates the highest temperature and lowest heat flux. For $s = 7.14\ mm$, both temperature and heat flux fall between the extremes observed in the other illustrated cases. However, the temperature rise and heat flux reduction are more noticeable when decreasing s from 7.14 mm to 3 mm compared to the transition from 31.13 mm to 7.14 mm.

When $s = 31.13$ mm, the temperature distribution across the fins shows minimal variation with decreasing θ. However, when $s = 3$ and 7.14 mm, when θ decreases from 90° to 0°, there is a notable temperature rise along the top half of the annular fins. Throughout all θ values, the lowest temperature is consistently observed at the bottom of the annular fins, gradually increasing toward the tube and longitudinal fin.

Regarding the heat flux, there are discernible changes by decreasing θ. Across all θ values, the maximum heat flux, similar to the lowest temperature, is concentrated at the bottom of the annular fins. A comparison of heat flux contours of the case $s = 31.13$ mm with $\theta = 90°$ and 0° indicates that decreasing θ has a limited impact on the heat flux at the bottom half of the annular fins while noticeable changes occur in the top half. There, some areas exhibit lower heat flux values, while others show an increase.

At the decreased s values of 3 and 7.14 mm, the change in the fin temperature and heat flux is more remarkable compared with $s = 31.13$ mm case. At $s = 7.14$ mm, the temperature and heat flux distribution are fairly similar for the θ values of 90° and 60°. However, a further decrease in θ results in an increase in temperature and a decrease in wall heat flux above the longitudinal fin which is the result of low air velocity at the mentioned location, as depicted in Figure 3.4. The temperature and heat flux variation by θ at $s = 3$ mm shows a similar trend with $s = 7.14$ mm. A decrease in θ enlarges the temperature across the annular fins and reduces the heat flux.

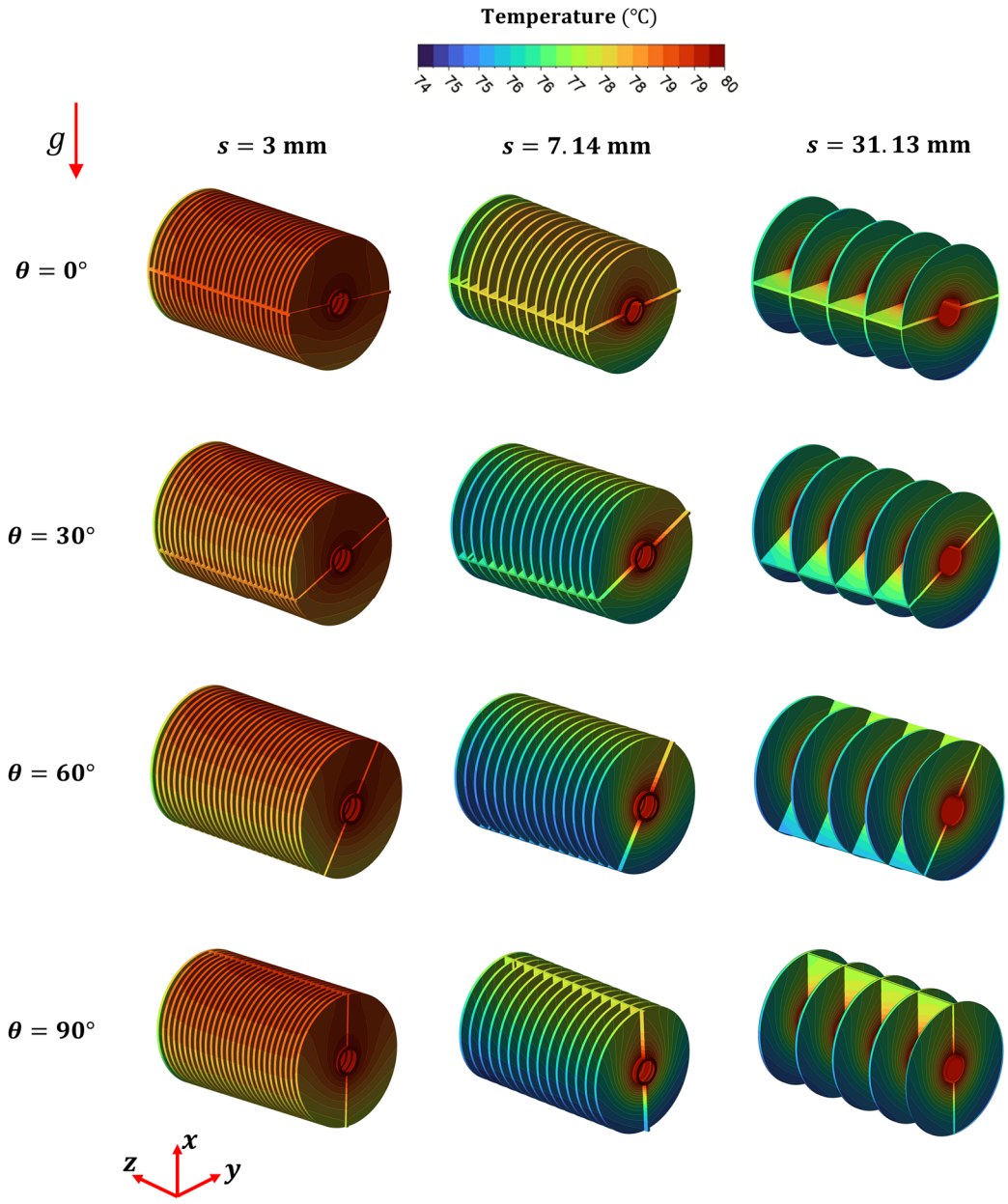


Figure 3.6. Temperature contours of the solid domain for the proposed design, $s =$ 3, 7.14, and 31.13 mm, and $\theta = 0°$, 30°, 60°, and 90° at $\Delta T = 60℃$

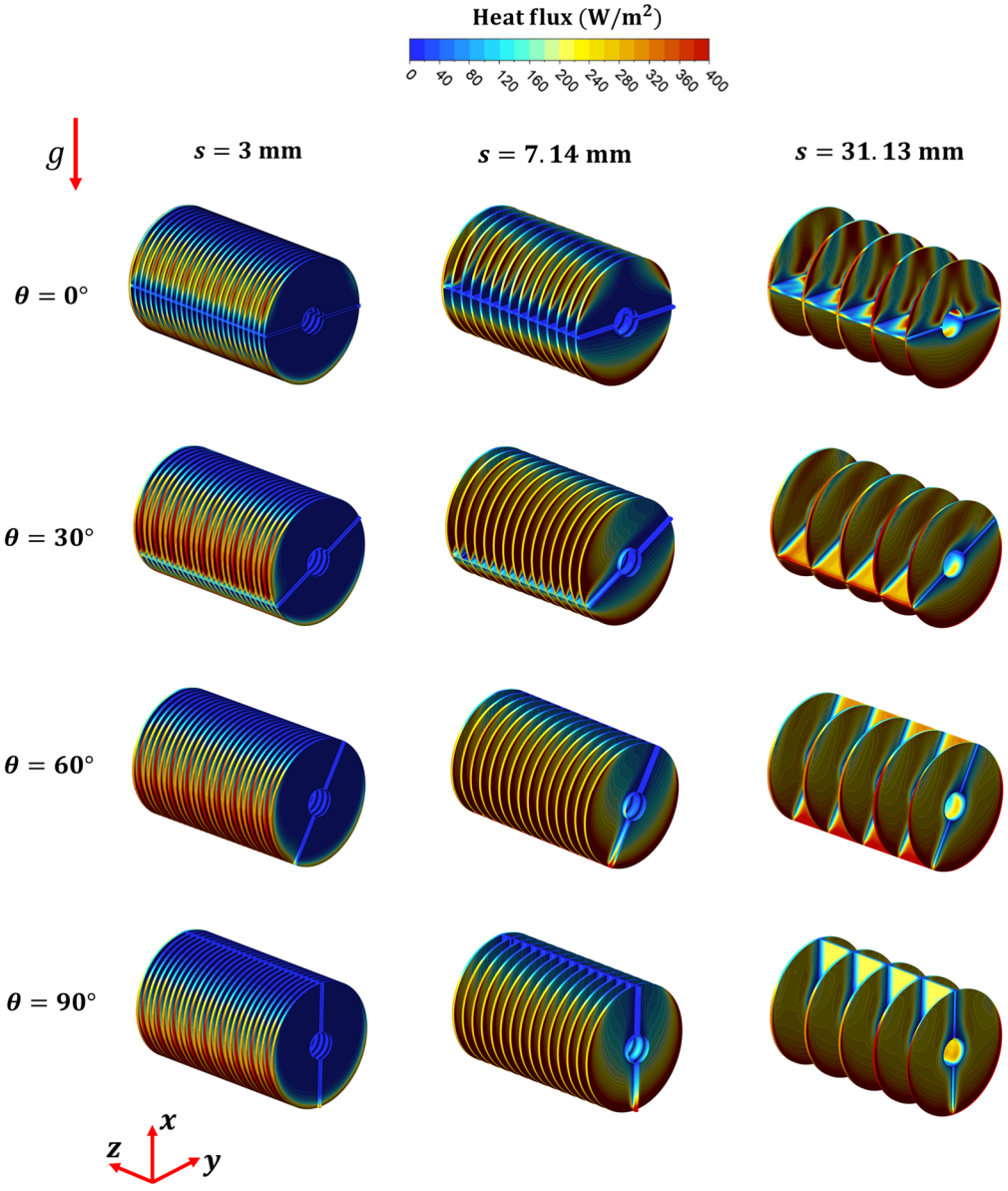


Figure 3.7. Wall flux contours of the solid domain for the proposed design, $s =$ 3, 7.14, and 31.13 mm, and $\theta = 0°$, 30°, 60°, and 90° at $\Delta T = 60℃$

The temperature contours of the air plume between the fins and above the unit for the cases with $s = 3$, 7.14, and 31.13 mm and $\theta = 0°$, 30°, 60°, and 90°, at $\Delta T =$ 60℃ are demonstrated in Figure 3.8.

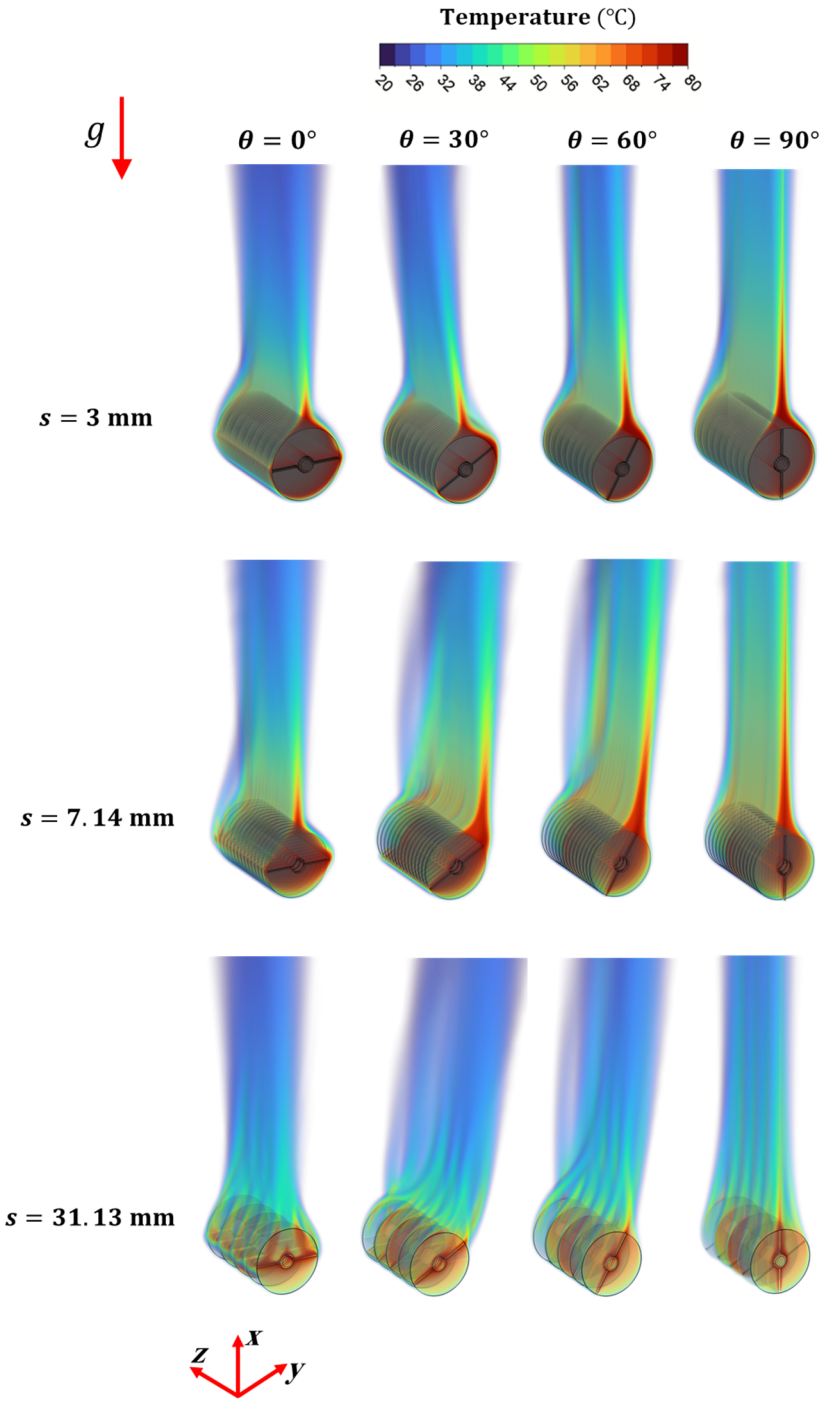


Figure 3.8. Temperature contours of the air plume for the proposed design, $s = 3$, 7.14, and 31.13 mm, and $\theta = 0°$, 30°, 60°, and 90° at $\Delta T = 60℃$

The air plume above the $s = 31.13$ mm case exhibits the lowest temperature among those depicted. For $s = 7.14\ mm$, the temperature of the air plume far from the fin and tube unit is notably higher compared to other illustrated cases. This is due to the substantially larger heat transfer surface area compared to the $s = 31.13$ mm case, resulting in a greater convective heat transfer. Furthermore, as depicted in Figure 3.8, reducing θ results in a temperature decrease in the air plume, indicating a reduction in convective heat transfer and decreased heat absorption by the airflow.

The air plume precisely above the $s = 3$ mm case exhibits the highest temperature among the depicted cases. This is attributed to the presence of high-temperature, low-velocity fluid between the annular fins in which the conduction heat transfer is dominant. However, as the distance from the fin and tube unit increases, the temperature gradually decreases and becomes lower than the temperature of the plume in the $s = 7.14$ mm case. The temperature variation of the air plume by θ in the $s = 3$ mm case follows a similar pattern to that of $s = 7.14$ mm case and significantly diminishes by decreasing θ.

Figure 3.9 depicts the variation of q_c with s for different θ values within the studied ΔT range. The inclination angles of $\theta = 15°$, $45°$, and $75°$ are not depicted in the charts to avoid overcrowding. It is evident that similar to the design without longitudinal fins, q_c critically depends on s at all θ values. For all of the studied θ and ΔT values, there exists an optimal s at which q_c reaches its maximum. Starting from $s = 31.13$ mm, the addition of fins to the tube increases q_c due to the increased heat transfer surface area. For all θ values, the q_c enhances up to a maximum value by adding fins. However, beyond a certain point, the addition of fins causes q_c to decrease sharply. This is because, at very small s values, the airflow between the fins is obstructed due to narrow passages, leading to lower flow velocity between the annular fins.

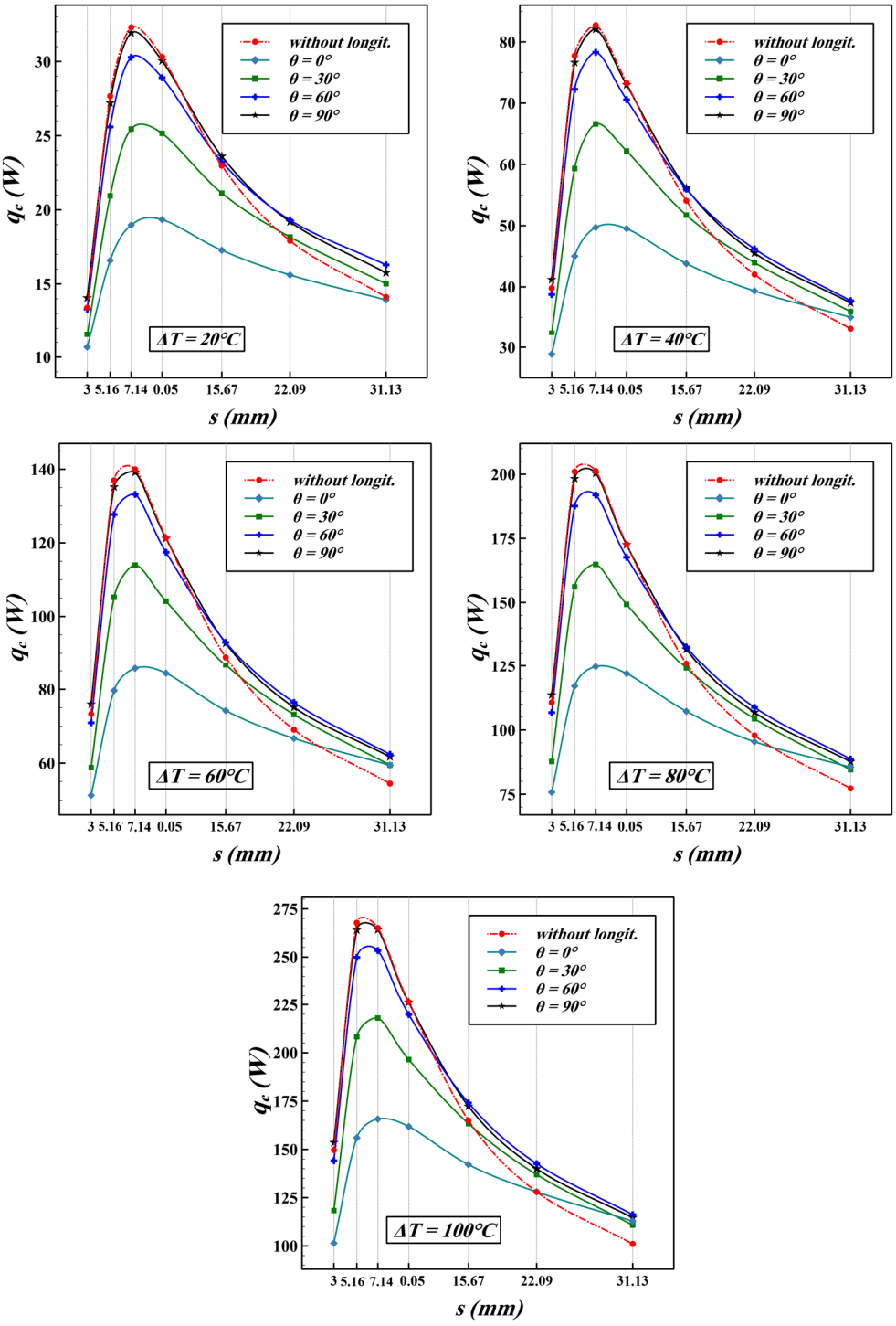


Figure 3.9. Evolution of the convective heat transfer with s for different θ and ΔT values

At all θ values, the highest convective heat transfer belongs to the case with $s = 7.14$ mm, except when $\Delta T = 20$℃ and $\theta = 0°$ where $s = 10.05$ mm performs slightly better. Nevertheless, an examination of the progression of q_c with the increase of ΔT indicates that the difference in q_c between the cases $s = 5.16$ mm and 7.14 mm decreases as ΔT increases. For instance, at $\Delta T = 20$℃ when $\theta = 90°$, q_c at $s = 7.14$ mm surpasses q_c at $s = 5.16$ mm by 17.4%. However, this difference drops to 0.1% at $\Delta T = 100$℃. This suggests that the optimal s tends to shift toward smaller s values as ΔT increases.

Furthermore, the heat transfer of the design with the longitudinal fin diminishes as θ decreases across all s values, with the highest convective heat transfer observed in cases where $\theta = 90°$ and the longitudinal fin is parallel to g. An important aspect of Figure 3.9 is the convective heat transfer difference between the proposed and conventional designs. It is evident that at the s values where q_c reaches its maximum, the heat transfer of the proposed design is slightly lower than that of the conventional design. For instance, at $\Delta T = 60$℃ where $\theta = 90°$, the q_c value of the proposed design with $s = 7.14$ mm is 0.5% lower than that of the conventional design at the same s value. However, at both small and large s values, q_c values of the cases with longitudinal fin when $\theta = 90°$ exceed that of the conventional design. For example, at $s = 31.13$ mm and $\Delta T = 60$℃, the proposed design with $\theta = 90°$ performs 13.3% better than the conventional case.

Another noteworthy point regarding the optimal s for maximizing the heat transfer is that the addition of the longitudinal fin does not significantly alter the optimal s compared to the conventional design. However, decreasing θ slightly increases the optimal s value. For instance, at $\Delta T = 20$℃, when $\theta = 90°$, the unit has the highest heat transfer when $s = 7.14$ mm. Conversely, when $\theta = 0°$, the unit achieves the highest heat transfer when $s = 10.05$ mm.

Figure 3.10 displays the convective heat transfer evolution of the proposed design with θ.

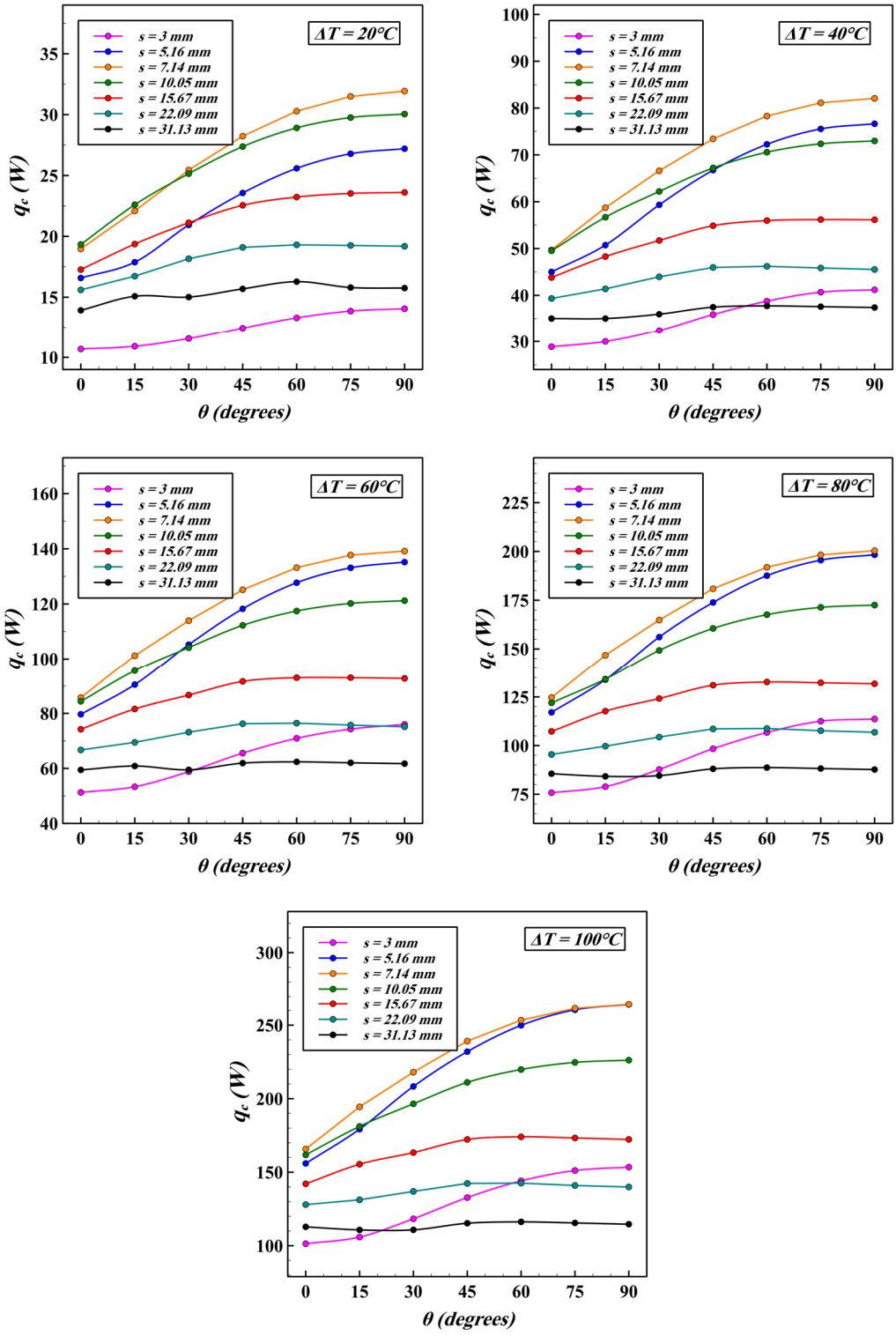


Figure 3.10: Evolution of convective heat transfer with θ for different s and ΔT values

An assessment reveals that q_c is significantly dependent on θ except when s is large. For example, q_c does not change significantly by altering θ for the cases with $s = 31.13$ mm and 22.09 mm by changing θ. However, when $s = 7.14\,mm$, q_c falls significantly as θ is decreased from 90° to 0°. For instance, at $\Delta T = 60$℃ when $s = 7.14$ mm, q_c drops by approximately 38.4% as θ decreases from 90° to 0°.

An important observation is the rate of change in q_c when rotating the longitudinal fin. As it appears from Figure 3.10, for the cases that are significantly affected by θ, the change in q_c is subtle as θ decreases from 90° to 75° and further to 60°. Nevertheless, the rate of change in q_c rises with a further decline in θ. For example, at $\Delta T = 60$℃, when $s = 7.14$ mm, the decrease in q_c is approximately 1% and 4% as θ decreases from 90° to 75° and 60°, respectively. However, at $\theta = 45°$ and 30°, the reduction is approximately 10% and 18%, respectively, compared to when $\theta = 90°$.

The impact of increasing ΔT on the optimal s value is evident in Figure 3.10. At $\Delta T = 20$℃, the top performers are $s = 7.14$ and 10.05 mm. Nevertheless, when $\Delta T = 100$℃, the curve representing q_c for the case with $s = 5.16$ mm surpasses that of $s = 10.05$ mm across all θ values except for $\theta = 0°$ and 15°.

Studying Nu_s can provide insights into convective heat transfer characteristics. Figure 3.11 represents the variation of Nu_s as a function of ΔT for the studied s values and θ values of 0°, 30°, 60°, and 90°. Increasing ΔT significantly enhances Nu_s primarily because of the greater temperature gradient between the heated surface and the surrounding air which increases the fluid velocity and thus improves the convective heat transfer. At lower ΔT, the buoyant forces are weak, resulting in lower flow momentum compared to higher ΔT. This restricts the fluid flow between the fins and results in lower convective heat transfer.

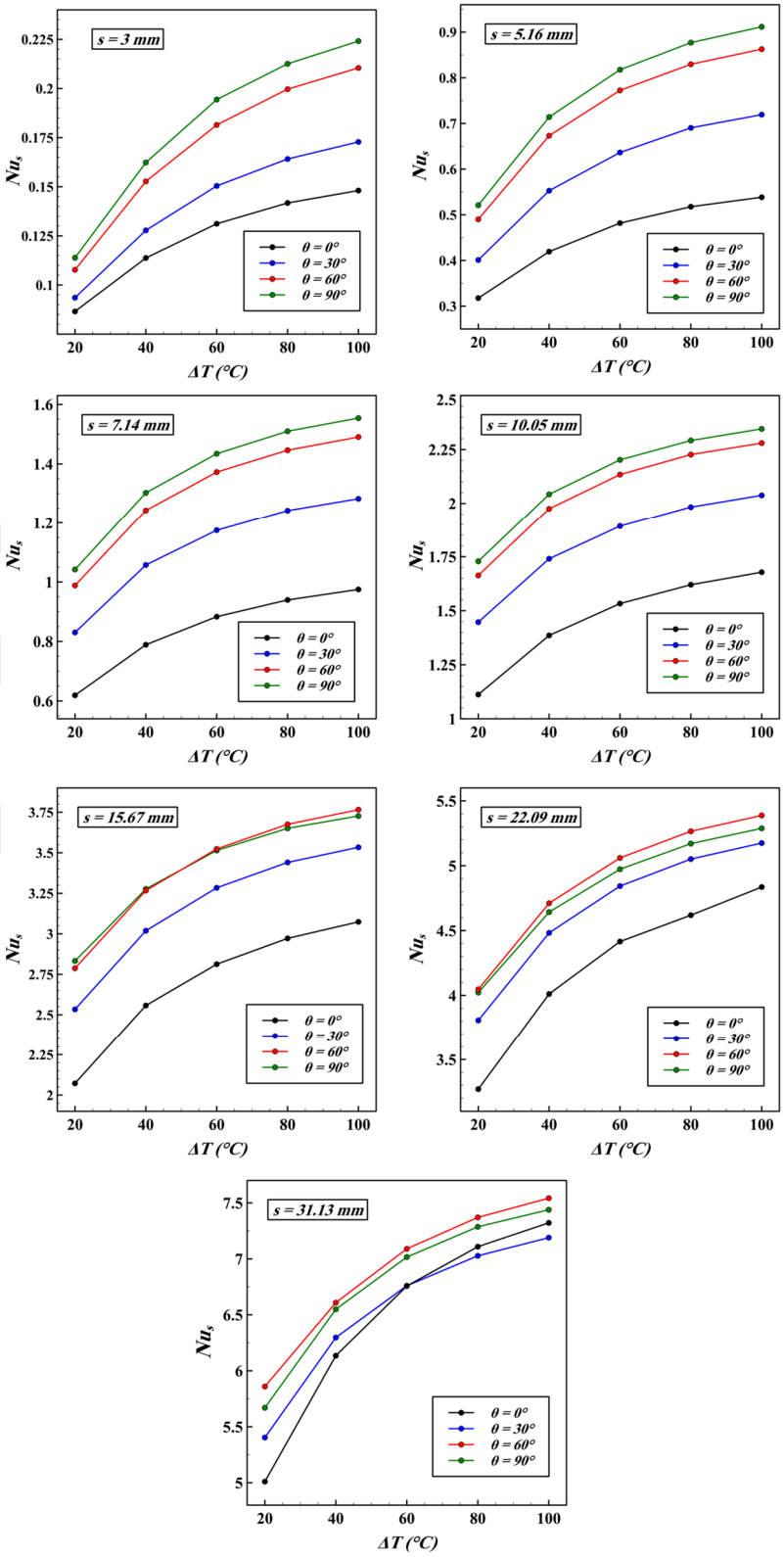


Figure 3.11 Evolution of Nu_s with ΔT for different θ and values s

An examination of Figure 3.11 reveals that Nu_s is the highest when $s = 31.13$ mm, decreasing gradually with the addition of more fins to the tube. The addition of fins increases the heat transfer surface area, promoting the interaction between the fluid and the heated surface. This increased interaction results in a thicker hydrodynamic and thermal boundary layer near the heated surfaces, decreasing the fluid velocity and heat transfer coefficient, thereby resulting in lower Nu_s values.

When $s = 31.13$ mm, Nu_s is the highest when $\theta = 60°$, followed by $\theta = 90°$. At $\Delta T = 20$℃ and 40℃, $\theta = 30°$ outperforms $\theta = 0°$, but at $\Delta T = 60$℃, the latter surpasses the former, with this difference increasing with a further increase in ΔT. When $s = 22.09$ mm, the peak heat transfer is again achieved at $\theta = 60°$, followed by $\theta = 90°$ while the case with $\theta = 30°$ consistently exhibits superior Nu_s compared to $\theta = 0°$. Decreasing s to 15.67 mm narrows the gap between q_c values of the cases with $\theta = 60°$ and 90°, with further s reduction resulting in greater heat transfer of $\theta = 90°$, followed by 60°, 30°, and 0°.

An important observation regarding the difference in Nu_s lies in its greater reliance on θ at smaller s values. For instance, when $s = 31.13$ mm and $\Delta T = 60$℃, the minimum Nu_s is 3.6% smaller than the maximum Nu_s. However, this difference increases to 41% when s decreases to 5.16 mm.

3.3 Numerical Results for Fin and Tube Units in an Array

In the previous section, it was indicated that the heat transfer of the proposed design at the optimal s is always lower than that of the design without longitudinal fins. However, the proposed design can perform differently when used in an array compared to when used individually. Therefore, in the current section, the array heat transfer of the proposed design with $s = 7.14$ mm which performed the best among the studied s values is investigated at $\Delta T = 60$℃.

The parameters achieving the highest heat transfer in a two-row configuration are determined and the multi-row configuration based on the determined parameters is assessed and compared to the cases without longitudinal fins.

3.3.1 An Array with Two Rows

The thermal characteristics of the array are significantly dependent on the arrangement of the units within the array. Figure 3.12 presents the velocity contours embedded with streamlines and the temperature contours for $S_t = 3D/2$, and $S_l = 5D/2$, respectively, in the parallel configuration with ψ_2 values of 30°, 60°, −30°, and −60°. These specific spacings are chosen because the case with $\psi_2 = 60°$ within these spacings exhibits the highest heat transfer among the studied cases. It must be stated that all contours in the current and next section are depicted on the symmetry plane at $z = 0$.

A notable fact is regarding the velocity below the fin and tube unit in the first row. For the $\psi_2 = 60°$ case, the velocity is maximum below the first fin and tube unit, suggesting a larger volume of air entering the domain from the bottom boundary. The increased airflow results in enhanced convection, leading to higher heat transfer. In contrast, $\psi_2 = -30°$ exhibits the lowest airflow velocity, indicating lower heat transfer.

Although higher local velocities are observed at the vicinity of the fin and tube units in the cases with $\psi_2 = 30°$ and $-30°$, the velocity above both units is lower compared to cases with $\psi_2 = 60°$ and $-60°$, respectively. These regions have less contribution to the heat transfer and diminish the heat transfer. The discernible high-temperature areas above the fin and tube units in cases $\psi_2 = 30°$ and $-30°$ support this observation.

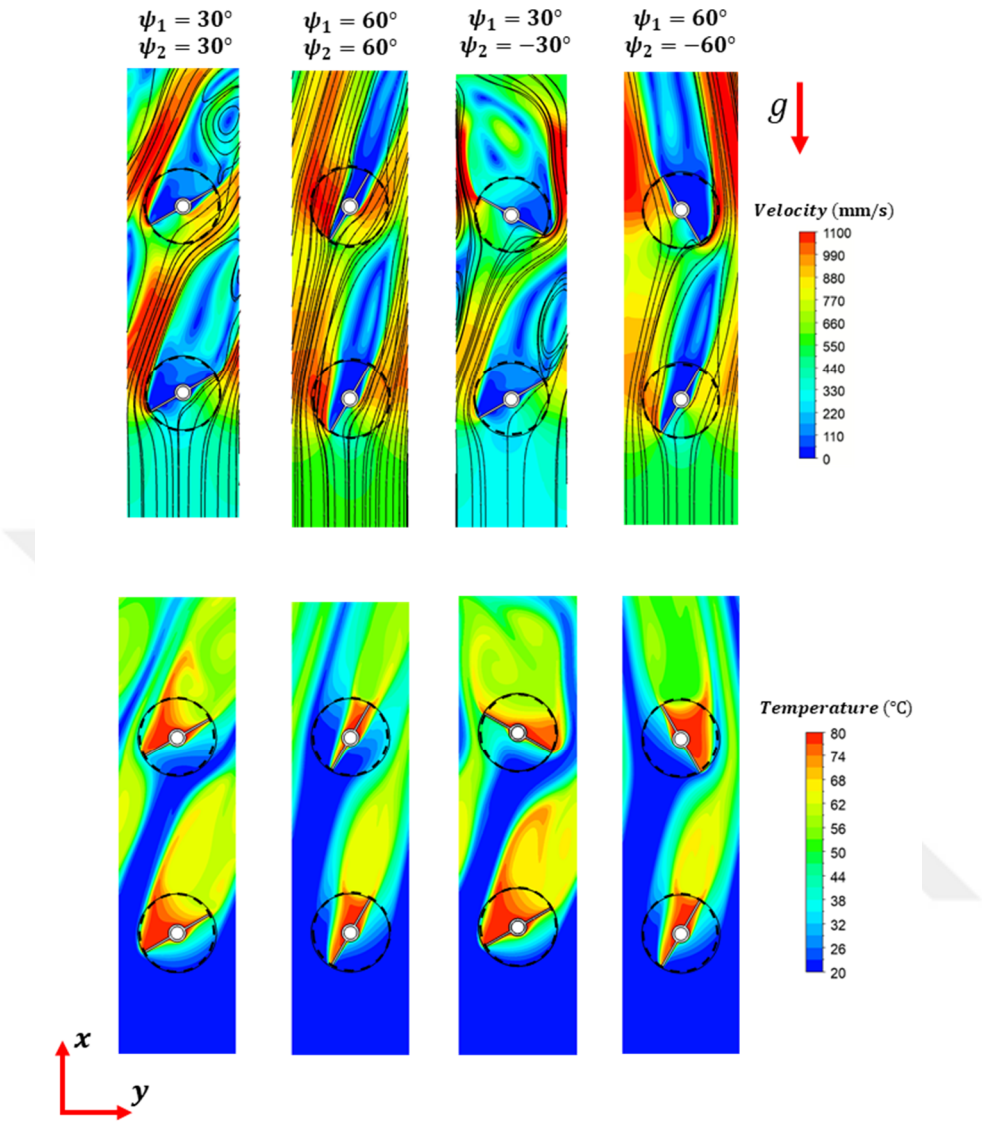


Figure 3.12. Velocity contours embedded with streamlines, and temperature contours for $\psi_2 = 30°$, $60°$, $-30°$, and $-60°$, $S_t = 3D/2$, and $S_l = 5D/2$, parallel configuration

In cases where $\psi_2 > 0°$, the bottom unit deflects the airflow toward the top unit in the subsequent column, thereby increasing velocity and mixing the hot and colder fluid regions, leading to enhanced heat transfer at the top fin and tube unit. For instance, examining the temperature contour of the case $\psi_2 = 60°$ reveals a smaller

area with high-temperature air above the second unit, indicating greater heat transfer. Conversely, in the cases where $\psi_2 < 0°$, a low-velocity and high-temperature area forms above the second unit. The air deflected by the first row of fin and tube units is obstructed by the longitudinal fins at the second row, which oppose the flow direction. This results in lower heat transfer in the second row and diminishes overall heat transfer.

Figure 3.13 represents the velocity contours embedded with streamlines and temperature contours for $\psi_2 = 30°$, $60°$, $-30°$, and $-60°$, with $S_t = 3D/2$, and $S_l = 5D/2$, respectively, in the mirrored configuration.

A remarkable difference from the parallel configuration is the low velocity of air beneath the first row, indicating weaker buoyant forces in the mirrored configuration. However, in contrast with the parallel configuration where the velocities at the bottom of the first row are higher when $\psi_2 > 0°$, in the mirrored configuration, higher velocities are observed when $\psi_2 < 0°$.

In the mirrored configuration, the velocity of the flow deflected by the longitudinal fin diminishes as it approaches the side walls of the computational domain. Additionally, the air deflected by the lower unit fails to reach the above row in the adjacent column. This results in reduced velocities across the entire domain, thereby limiting the heat transfer potential of the fin and tube units.

Similar to the parallel configuration, a low-velocity, high-temperature region forms above the longitudinal fins when $\psi_2 = 30°$ and $-30°$. In this scenario, the air fails to effectively absorb heat from the fin and tube units, resulting in lower heat transfer compared to when $\psi_2 = 60°$ and $-60°$.

In contrast with the parallel configuration where the velocities in the vicinity of the fin and tube units are higher when $\psi_2 > 0°$, in the mirrored configuration the velocities are greater when $\psi_2 < 0°$. Consequently, due to lower air velocities, the temperature of the air above the fin and tube units is lower when $\psi_2 < 0°$ in the mirrored configuration.

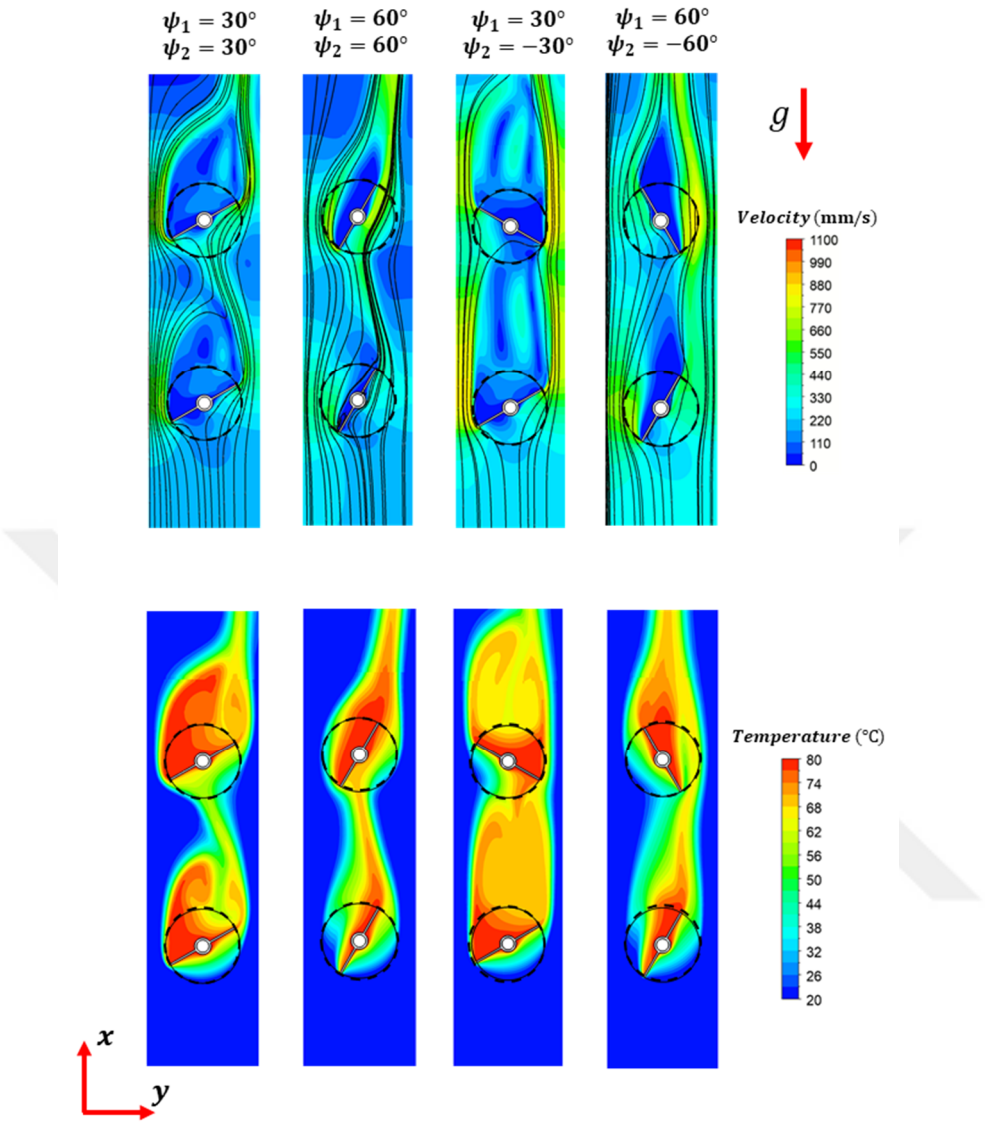


Figure 3.13. Velocity contours embedded with streamlines, and temperature contours for $\psi_2 = 30°$, $60°$, $-30°$, and $-60°$, $S_t = 3D/2$, and $S_l = 5D/2$, mirrored configuration

Figure 3.14 demonstrates the velocity and temperature contours for the parallel configuration with $\psi_2 = 60°$ which depicted the highest heat transfer among the studied S_t and S_l values. The selected values for illustration in Figure 3.14 for the S_t and S_l are either the maximum or minimum within the studied range. It is seen that

the velocity of the air entering the domain and at the vicinity of the fin and tube units decreases by either increasing S_t or decreasing S_l.

In the low S_t value, the high-velocity air accelerated by the longitudinal fins possesses enough momentum to cross the lateral boundaries and enter the adjacent domain, thereby affecting the units in other columns. Conversely, with a high S_t value, the large distance between columns prevents the accelerated air from entering the adjacent domain. The temperature contours of the depicted cases with $S_t = 5D/2$ support this observation, illustrating that the air temperature between the annular fins is significantly higher than that when $S_t = 3D/2$.

The temperature contours in the cases where $S_t = 5D/2$ reveal that the colder air at the sides of the domain remains unmixed with the higher temperature air plume above the fin and tube units. This increases the local air temperature at the fluid-solid interface and diminishes the temperature gradient. With low S_t value, the high-temperature air plume exerted by the unit at the first row crosses the second row of units without fully infiltrating the space between its annular fins. However, at the high S_t value, the high-temperature plume from the first row directly enters the fin spacing of the units at the second row. This results in a reduced temperature gradient between the heated surfaces and the air in the second row, leading to diminished heat transfer.

Increasing S_l enhances heat transfer by elevating the velocity near the fin and tube units. At lower S_l value, the unit in the second row is close to the dead region behind the first unit, characterized by low velocity and high temperature. With an increase in S_l, this dead region merges with the high-velocity, low-temperature air. As a result, the velocity of the air entering the space between the annular fins of the unit in the second row is higher and its temperature is lower compared to the case with low S_l.

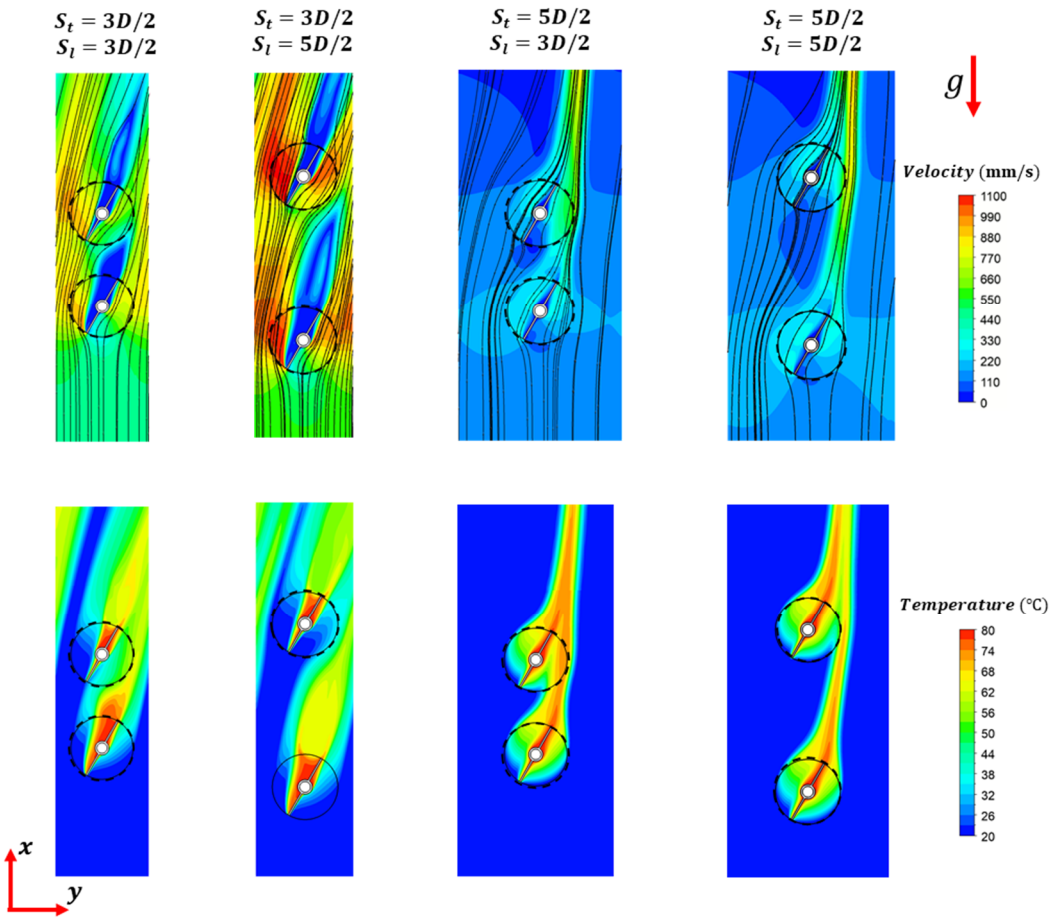


Figure 3.14. Velocity contours embedded with streamlines and the temperature contours for parallel configuration with $\psi_2 = 60°$ for different S_t and S_l values

Figure 3.15 demonstrates the variation of $\mathrm{Nu}_{s,array}$ for an array of fin and tube units with two rows and different longitudinal fin configurations. Changing the parameters such as ψ_2, S_t, S_l, as well as employing the units in parallel or mirrored configurations, notably impacts the heat transfer of the proposed design. Firstly, the $\mathrm{Nu}_{s,array}$ values of the parallel configurations are significantly greater than those of the mirrored configurations. Compared to an array without longitudinal fins, the array with the mirrored configuration consistently displays lower heat transfer; however, the majority of the parallel configurations demonstrate superior heat transfer.

For $\psi_2 > 0$, decreasing ψ_2 generally leads to a decrease in heat transfer, except at the longitudinal spacing of $S_l = 3D/2$, where reducing ψ_2 from 60° to 45° results in a slight enhancement in $\mathrm{Nu}_{s,array}$. However, in the cases where $\psi_2 < 0$, heat transfer consistently declines with decreasing ψ_2. This suggests, in general, that a lower angle between the longitudinal fin and the x-axis yields greater heat transfer compared to a greater angle.

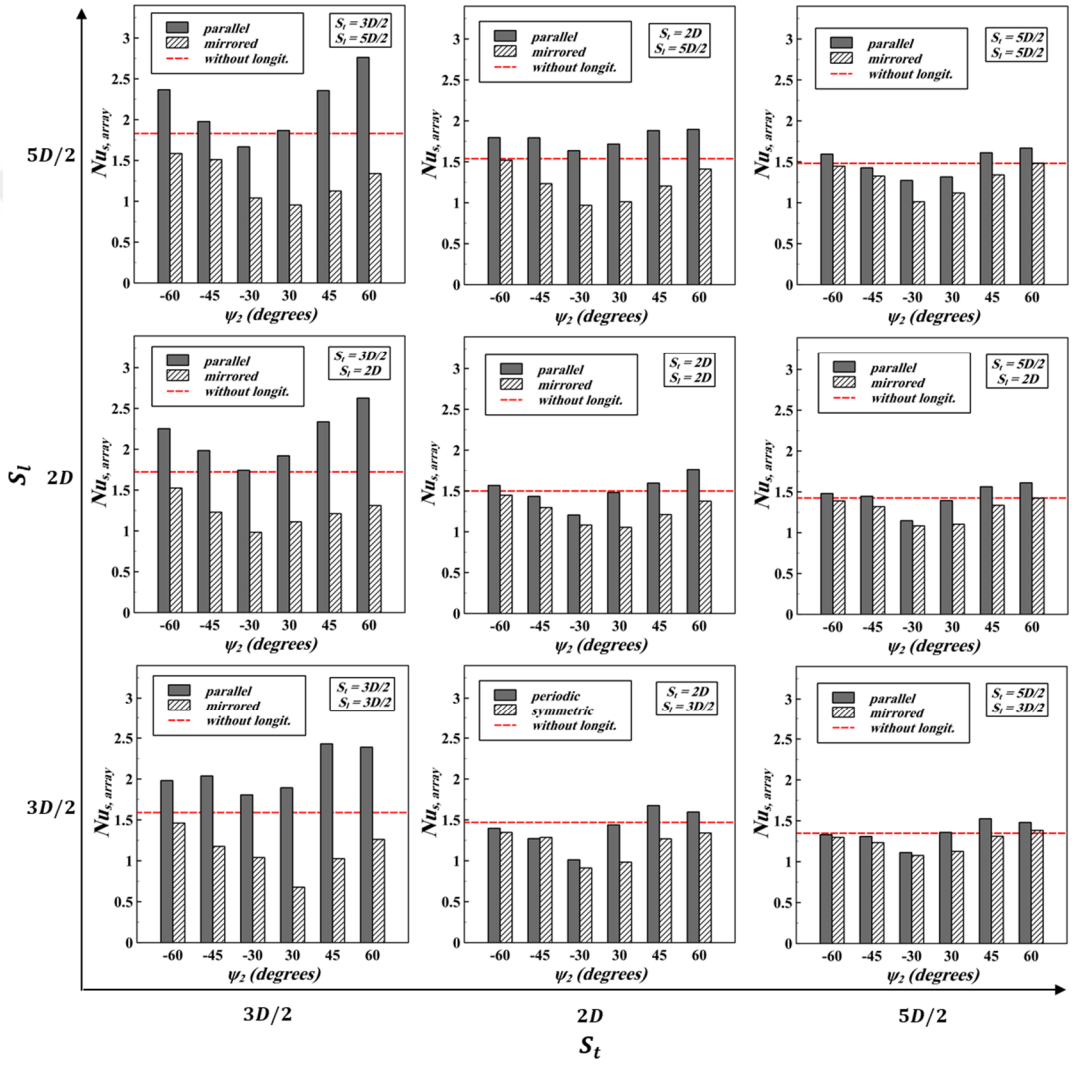


Figure 3.15. Variation of $\mathrm{Nu}_{s,array}$ for an array with two rows at parallel and mirrored configurations and different ψ_2, S_t, and S_l values

The heat transfer is significantly impacted by both the transverse and longitudinal distances between the tubes. In parallel configurations, increasing S_t diminishes heat transfer, while increasing S_l improves it. However, S_t has a greater influence on heat transfer. For instance, in the parallel configuration with $\psi_2 = 60°$ and $S_t = S_l = 3D/2$, $\mathrm{Nu}_{s,array}$ rises by 15% with S_l increasing to $5D/2$ but drops by 38% with S_t increasing to $5D/2$.

At higher S_t values, $\mathrm{Nu}_{s,array}$ exhibits less dependence on ψ_2. For instance, in the parallel configuration with $\psi_2 = 60°$, $S_t = 3D/2$ and $S_l = 5D/2$, which has the highest heat transfer among the studied cases, $\mathrm{Nu}_{s,array}$ is 32% greater than the case with $\psi_2 = 30°$ with the S_t and S_l values. However, with S_t increased to $5D/2$, this difference diminishes to 21%.

3.3.2 An Array with Several Rows

In the previous section, it was determined that for an array of fin and tube units with two rows, the parallel configuration with $\psi_2 = 60°$, $S_t = 3D/2$ and $S_l = 5D/2$, yields the highest heat transfer among the studied cases. Thus, in this section, the impact of varying the number of rows from 1 to 5 within this specific configuration is investigated to observe the evolution of heat transfer.

Figure 3.16 and Figure 3.17 depict the velocity contours embedded with streamlines, and temperature contours, respectively, for the cases without longitudinal fin. The addition of rows increases the velocity of air entering the domain, consequently, enhancing the velocity between the annular fins. However, increasing the number of rows simultaneously expands the low-velocity area behind the tubes. The streamlines follow a straightforward path in the x-direction toward the top boundary of the domain and do not extend beyond the side boundaries of the domain.

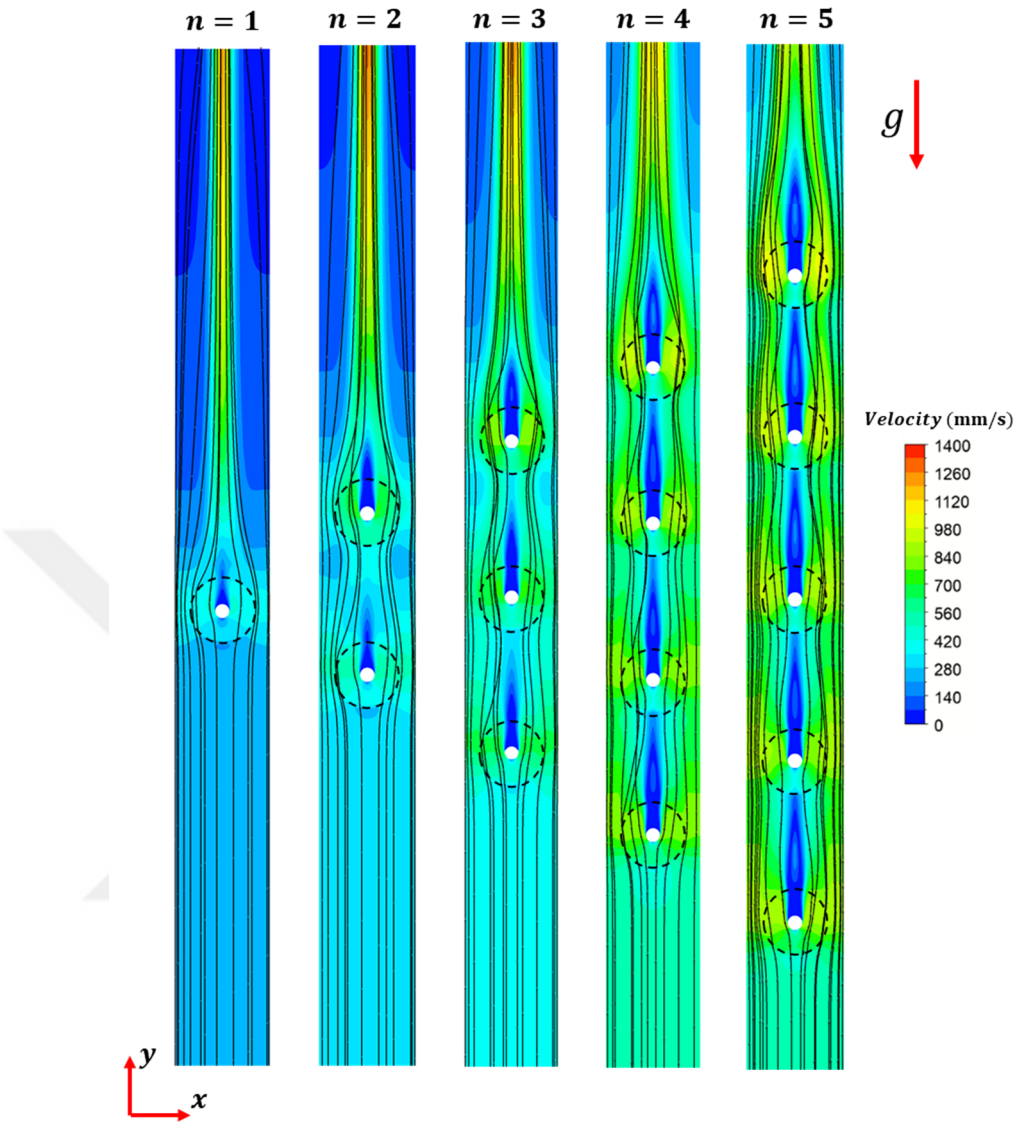


Figure 3.16. Velocity contours embedded with streamlines for the cases without longitudinal fins

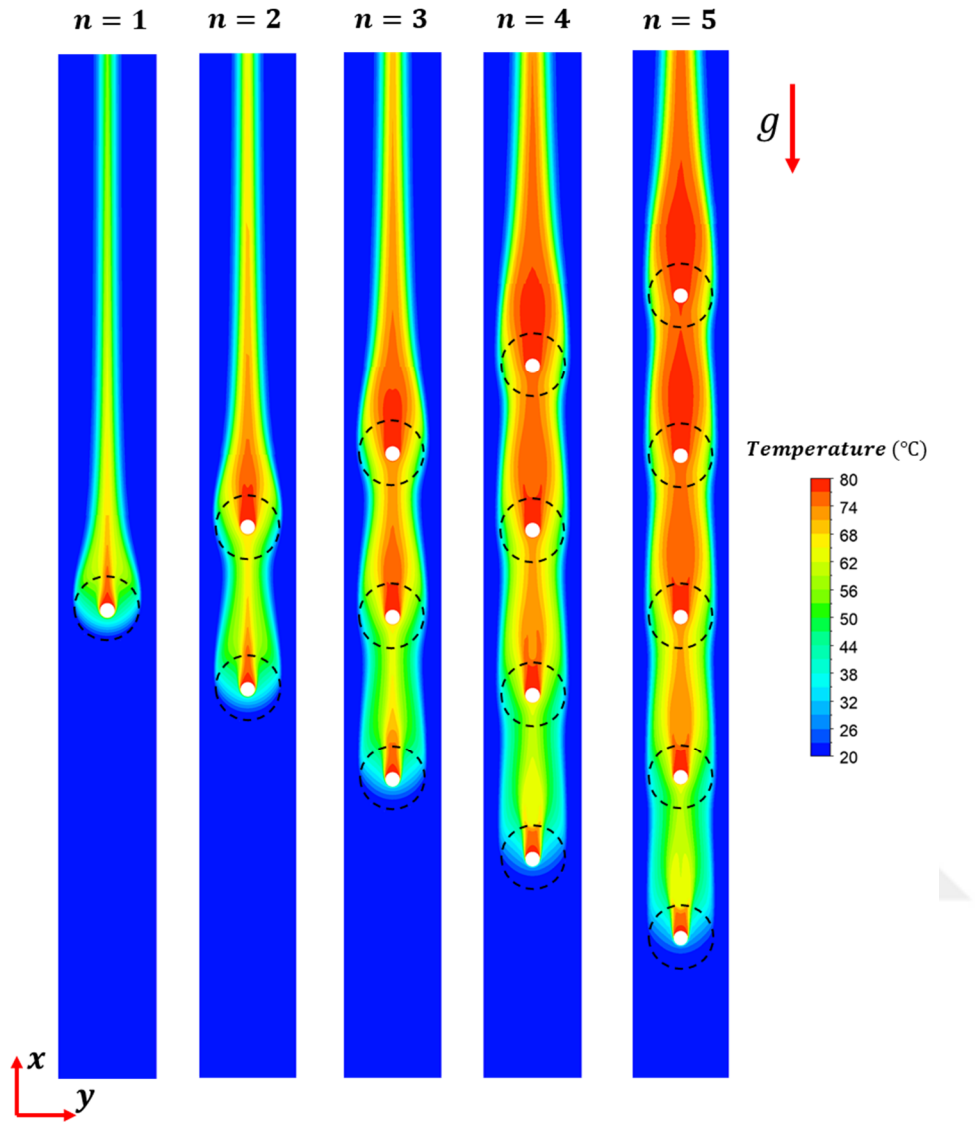


Figure 3.17. Temperature contours for the cases without longitudinal fins

The temperature contours suggest that with the addition of rows, the temperature of the plume above the fin and tube units increases significantly. This high-temperature air infiltrates the fin spacings of the above units, thereby decreasing the temperature gradient. Furthermore, ambient-temperature air is observed along the x-direction, indicating limited mixing between the high and low-temperature regions.

Figure 3.18 and Figure 3.19 demonstrate the velocity contours embedded with streamlines, and temperature contours for the cases with longitudinal fins, respectively. With a single row, the velocity of air entering the domain is approximately similar to that of the case without the longitudinal fin. However, with the addition of rows, there is a noticeable increase in the velocity of the air entering the domain, surpassing that of the case without the longitudinal fin.

When there are multiple rows, the velocity of air in the vicinity of the fin and tube units improves significantly compared to cases without longitudinal fins. The streamlines cross the side boundaries of the domain, indicating that the deflected air by the longitudinal fin influences the units in the adjacent column. Furthermore, the low-velocity areas above the tubes are deflected and do not cover the area between the annular fins of the units above.

With a single row, the temperature of the air above the fin and tube unit remains relatively unchanged compared to the unit without the longitudinal fin. However, with multiple rows, the temperature of the air above all rows, except the first one, is lower compared to the conventional design. Additionally, the ambient-temperature air at the sides of the domain mixes with the high-temperature air above the fin and tube units, indicating the high mixing potential of the longitudinal fins. As a result, in comparison to the conventional design, air with a lower temperature enters the area between the fins at the downstream units, leading to a greater heat transfer.

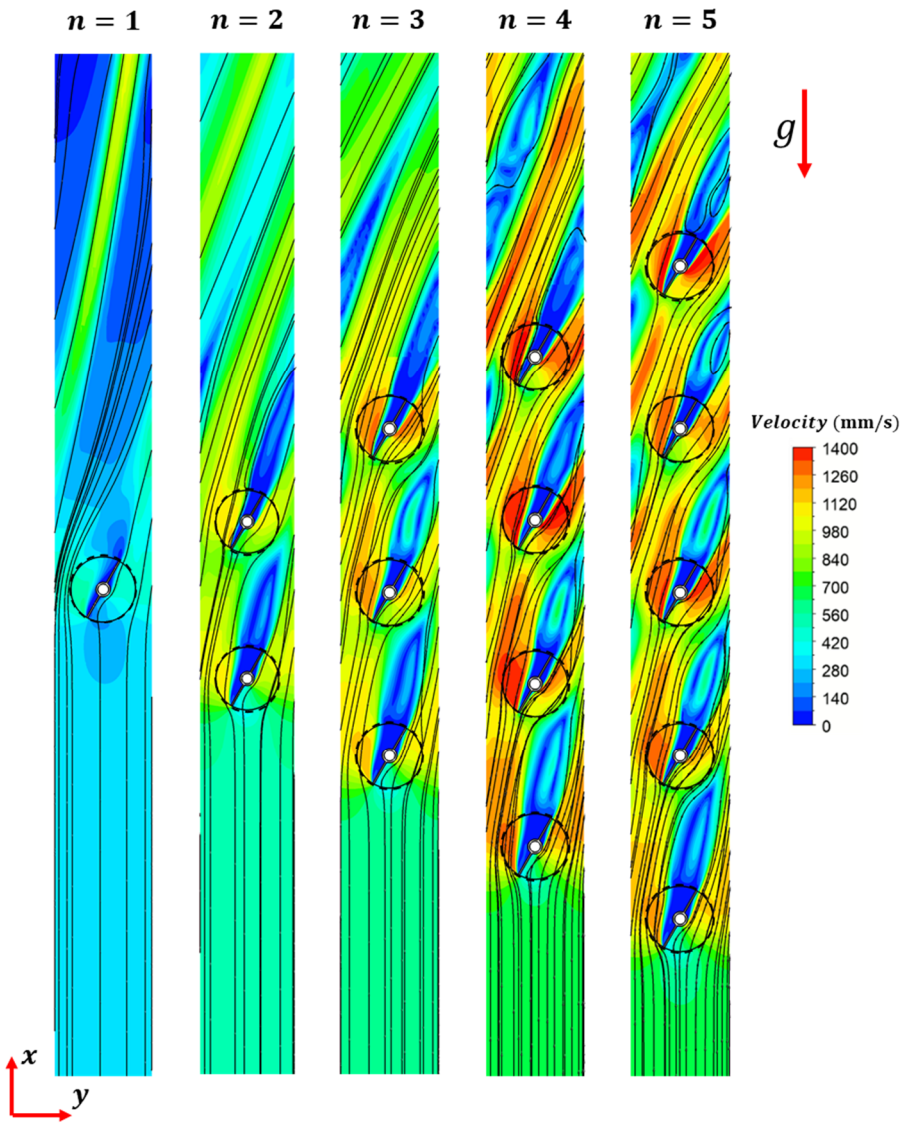


Figure 3.18. Velocity contours embedded with streamlines for the cases with longitudinal fins

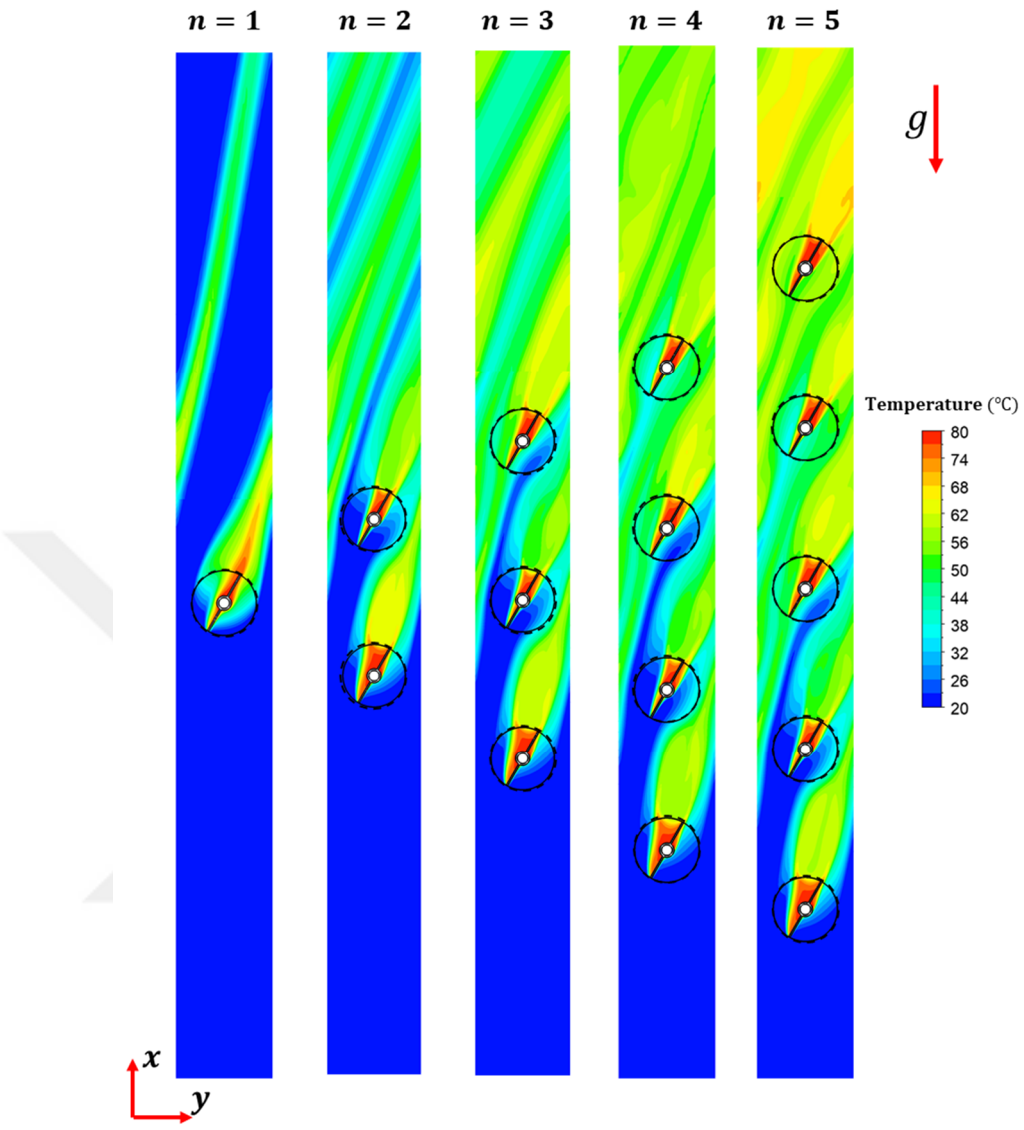


Figure 3.19. Temperature contours for the cases with longitudinal fins

Figure 3.20 represents the development of $Nu_{s,array}$ with increasing the number of rows from 1 to 5 for both designs with and without longitudinal fins. For the design without the longitudinal fins, the maximum $Nu_{s,array}$ is achieved with a single row. However, as the number of rows increases, $Nu_{s,array}$ decreases continuously.

For the design with longitudinal fins, $\mathrm{Nu}_{s,array}$ is at its minimum when there is a single row, approximately 6% lower than $\mathrm{Nu}_{s,array}$ of the design without longitudinal fins. However, with the number of rows increased to two, $\mathrm{Nu}_{s,array}$ experiences a sudden increase of about 30%, performing 49% better than the conventional design. Nevertheless, similar to the design without the longitudinal fins, a further increase in the number of rows leads to a gradual decrease in $\mathrm{Nu}_{s,array}$.

Yet, when there are multiple rows, the proposed design significantly outperforms the conventional design. The maximum difference between the $\mathrm{Nu}_{s,array}$ of the proposed and conventional designs is about 65% when the number of rows is equal to 4.

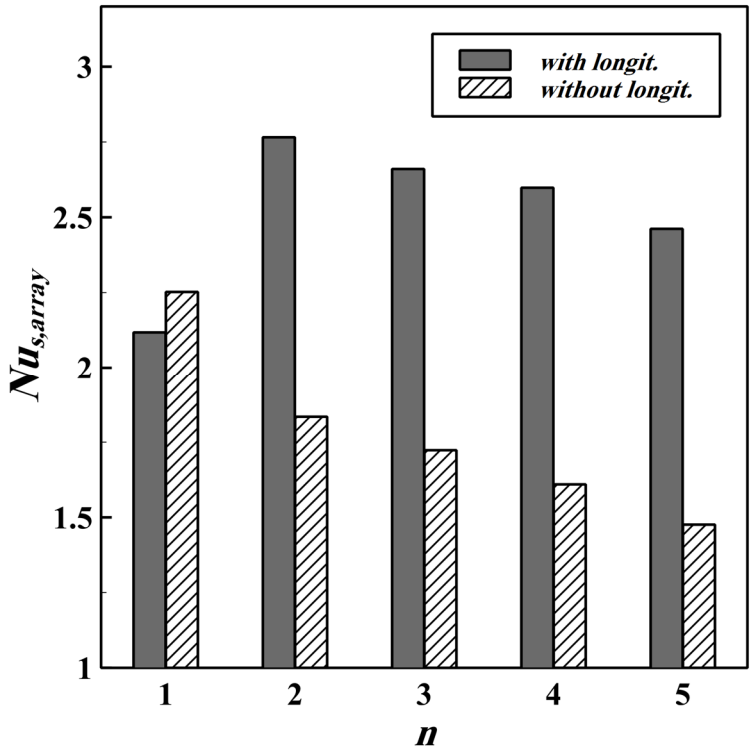


Figure 3.20. The evolution of $\mathrm{Nu}_{s,array}$ with n for the parallel case, $\psi_{\mathrm{n}} = 60°$, $S_t = 3D/2$, and $S_l = 5D/2$

CHAPTER 4

CONCLUSION

Natural convection is a popular cooling method utilized in a wide variety of industries because of its high reliability, simplicity, low energy consumption and maintenance cost, and noise-free nature. However, because of lower coolant fluid velocity in the natural convection compared to the forced convection, it has lower heat transfer. To resolve this issue and improve the performance of naturally-cooled heatsinks, researchers have proposed surface extension which increases the convective heat transfer surface area.

The extended surfaces, referred to as fins in the literature are divided into four main categories including longitudinal fins, annular fins, pin fins, and unconventional fin designs. Longitudinal and annular fins are the most common type of designs due to ease of manufacturing, cheaper cost, simplicity, rigidity, and durability. Although pin fins and unconventional fin designs provide a significant surface area and consistently interrupt the thermal boundary layer, manufacturing hardships limit their usage.

This study introduces a novel design in which the annular and longitudinal fins are combined and mounted on a heated tube. Two longitudinal plates located along the same plane are attached to the tube, dividing the annular fins into two halves. The proposed design deflects the air from its simple path, redirects the hot air plume above the fin and tube unit, and increases the local velocities. The study aims to investigate the heat transfer of the proposed design when it is used singly or in an array of fin and tube units.

To investigate the proposed design, five test pieces with different s values are manufactured from aluminum blocks using CNC machining. An experimental setup

is designed and constructed to examine the heat transfer of the manufactured test pieces in $20℃ \leq \Delta T \leq 100℃$ and $\theta = 0°$, $45°$, and $90°$.

In the experiments, the radiation heat transfer covers a considerable portion of the total heat transfer and cannot be neglected. However, the objective of the current study is to investigate convective heat transfer. A 3D numerical model, considering radiation and convection is generated for each test piece, and the experimental data is used to validate the numerical model. After the numerical simulations of the validation study, the radiation is disregarded. On top of the models of the manufactured test pieces, other s and θ values are investigated and compared with the results of the fin and tube units without longitudinal fins. The main findings for a single fin and tube unit are listed below:

- In the proposed design, similar to the conventional annular fin design, for each ΔT and θ, there exists an optimal s in which the heat transfer is maximum.
- At the optimal s, the proposed design achieves the highest heat transfer rate when $\theta = 90°$. However, its heat transfer is slightly lower than that of the conventional annular fin design.
- Increasing θ and ΔT results in the reduction of the optimal s.
- At large s values, the convective heat transfer is not significantly affected by θ however, by reducing s, the heat transfer dependence on θ increases.
- Despite that the proposed design's heat transfer is lower than the conventional design, the inclined longitudinal fin can deflect the air plume above the unit which can be a desirable characteristic when the unit is used in an array since the heat transfer from the units in the higher rows is affected by the plume exerted by the units below.

Next, the fin and tube unit with the optimal s at $\Delta T = 60℃$ is selected and its heat transfer is investigated in an array, numerically. The findings of this section of the study are as follows:

- The heat transfer of the mirrored configuration is always lower than that of the conventional design. However, in the parallel configuration, the majority of the studied cases perform superior compared to the conventional design.
- In an array with parallel configuration, when $\psi_2 = 60°$, the array achieves the highest heat transfer compared to other studied inclination angles.
- The overall heat transfer of the array increases by reducing S_t and increasing S_l.
- In the conventional design and proposed design with the mirrored configuration, the air cannot cross horizontally from a column to adjacent columns. However, in the parallel configuration, the air is deflected towards adjacent columns by the longitudinal fins, resulting in higher air velocities, mixing, and heat transfer.
- When there is a single row, the proposed design has lower heat transfer compared to the conventional design without longitudinal fins. However, by increasing the number of rows, the heat transfer of the novel design surpasses that of the conventional design. Such that, with 5 rows of fin and tube units, the proposed design exhibits 65% higher heat transfer compared to the conventional design.

For future studies, the effects of the fin-to-tube diameter ratio and the length of the longitudinal fin on heat transfer can be examined. Furthermore, an optimization can be performed for the fin and tube units in an array to find the optimal longitudinal fin inclination angle, S_t and S_l to maximize the heat transfer.

REFERENCES

[1] A. Sadeghianjahromi, and C.-C. Wang, "Heat transfer enhancement in fin-and-tube heat exchangers – A review on different mechanisms," *Renewable and Sustainable Energy Reviews,* vol. 137, 2021.

[2] S. S. Mousavi Ajarostaghi, M. Zaboli, H. Javadi, B. Badenes, and J. F. Urchueguia, "A Review of Recent Passive Heat Transfer Enhancement Methods," *Energies,* vol. 15, no. 3, 2022.

[3] T. M. Abou Elmaaty, A. E. Kabeel, and M. Mahgoub, "Corrugated plate heat exchanger review," *Renewable and Sustainable Energy Reviews,* vol. 70, pp. 852-860, 2017.

[4] T. Dixit, and I. Ghosh, "Review of micro- and mini-channel heat sinks and heat exchangers for single phase fluids," *Renewable and Sustainable Energy Reviews,* vol. 41, pp. 1298-1311, 2015.

[5] M. Pedram, and S. Nazarian, "Thermal modeling, analysis, and management in VLSI circuits: Principles and methods," *Proceedings of the IEEE,* vol. 94, no. 8, pp. 1487-1501, 2006.

[6] I. E. Ghandouri, A. E. Maakoul, S. Saadeddine, and M. Meziane, "A comprehensive review of methods used to improve the thermal performance of heat sinks in natural convection," *Heat and Mass Transfer,* vol. 59, no. 5, pp. 825-849, 2022.

[7] Siddhartha, S. Rath, and S. K. Dash, "Thermal performance of a wavy annular finned horizontal cylinder in natural convection for electronic cooling application," *International Communications in Heat and Mass Transfer,* vol. 128, 2021.

[8] S. Unger, M. Beyer, J. Thiele, and U. Hampel, "Experimental study of the natural convection heat transfer performance for finned oval tubes at different

tube tilt angles," *Experimental Thermal and Fluid Science,* vol. 105, pp. 100-108, 2019.

[9] H. Nemati, M. Moradaghay, M. A. Moghimi, and J. P. Meyer, "Natural convection heat transfer over horizontal annular elliptical finned tubes," *International Communications in Heat and Mass Transfer,* vol. 118, 2020.

[10] F. P. Incropera, D. P. DeWitt, T. L. Bergman, and A. S. Lavine, *Fundamentals of heat and mass transfer*: Wiley New York, 1996.

[11] S. M. Sohel Murshed, and C. A. Nieto de Castro, "A critical review of traditional and emerging techniques and fluids for electronics cooling," *Renewable and Sustainable Energy Reviews,* vol. 78, pp. 821-833, 2017.

[12] J. R. Senapati, S. K. Dash, and S. Roy, "Numerical investigation of natural convection heat transfer over annular finned horizontal cylinder," *International Journal of Heat and Mass Transfer,* vol. 96, pp. 330-345, 2016.

[13] A. A. Bhuiyan, and A. S. Islam, "Thermal and hydraulic performance of finned-tube heat exchangers under different flow ranges: A review on modeling and experiment," *International Journal of Heat and Mass Transfer,* vol. 101, pp. 38-59, 2016.

[14] N. Kayansayan, and R. Karabacak, "Natural convection heat transfer coefficients for a horizontal cylinder with vertically attached circular fins," *Heat Recovery Systems and CHP,* vol. 12, no. 6, pp. 457-468, 1992.

[15] S. Yildiz, and H. Yüncü, "An experimental investigation on performance of annular fins on a horizontal cylinder in free convection heat transfer," *Heat and Mass Transfer,* vol. 40, no. 3-4, pp. 239-251, 2004.

[16] H.-T. Chen, and J.-C. Chou, "Investigation of natural-convection heat transfer coefficient on a vertical square fin of finned-tube heat exchangers," *International Journal of Heat and Mass Transfer,* vol. 49, no. 17-18, pp. 3034-3044, 2006.

[17] H.-T. Chen, and W.-L. Hsu, "Estimation of heat transfer coefficient on the fin of annular-finned tube heat exchangers in natural convection for various

fin spacings," *International journal of heat and mass transfer,* vol. 50, no. 9-10, pp. 1750-1761, 2007.

[18] H.-T. Chen, Y.-S. Lin, P.-C. Chen, and J.-R. Chang, "Numerical and experimental study of natural convection heat transfer characteristics for vertical plate fin and tube heat exchangers with various tube diameters," *International Journal of Heat and Mass Transfer,* vol. 100, pp. 320-331, 2016.

[19] H.-T. Chen, Y.-J. Chiu, C.-S. Liu, and J.-R. Chang, "Numerical and experimental study of natural convection heat transfer characteristics for vertical annular finned tube heat exchanger," *International Journal of Heat and Mass Transfer,* vol. 109, pp. 378-392, 2017.

[20] H.-T. Chen, Y.-J. Chiu, H.-C. Tseng, and J.-R. Chang, "Effect of domain boundary set on natural convection heat transfer characteristics for vertical annular finned tube heat exchanger," *International Journal of Heat and Mass Transfer,* vol. 109, pp. 668-682, 2017.

[21] H.-T. Chen, H.-Y. Chou, H.-C. Tseng, and J.-R. Chang, "Numerical study on natural convection heat transfer of annular finned tube heat exchanger in chimney with experimental data," *International Journal of Heat and Mass Transfer,* vol. 127, pp. 483-496, 2018.

[22] H.-T. Chen, Y.-L. Hsieh, P.-C. Chen, Y.-F. Lin, and K.-C. Liu, "Numerical simulation of natural convection heat transfer for annular elliptical finned tube heat exchanger with experimental data," *International Journal of Heat and Mass Transfer,* vol. 127, pp. 541-554, 2018.

[23] H.-T. Chen, W.-X. Ma, and P.-Y. Lin, "Natural convection of plate finned tube heat exchangers with two horizontal tubes in a chimney: Experimental and numerical study," *International Journal of Heat and Mass Transfer,* vol. 147, 2020.

[24] A. Kumar, J. B. Joshi, A. K. Nayak, and P. K. Vijayan, "3D CFD simulations of air cooled condenser-II: Natural draft around a single finned tube kept in

a small chimney," *International Journal of Heat and Mass Transfer,* vol. 92, pp. 507-522, 2016.

[25] J. R. Senapati, S. K. Dash, and S. Roy, "3D numerical study of the effect of eccentricity on heat transfer characteristics over horizontal cylinder fitted with annular fins," *International Journal of Thermal Sciences,* vol. 108, pp. 28-39, 2016.

[26] H. C. Kang, and S.-M. Chang, "The Correlation of Heat Transfer Coefficients for the Laminar Natural Convection in a Circular Finned-Tube Heat Exchanger," *Journal of Heat Transfer,* vol. 140, no. 3, 2018.

[27] S.-C. Wong, and W.-Y. Lee, "Numerical study on the natural convection from horizontal finned tubes with small and large fin temperature variations," *International Journal of Thermal Sciences,* vol. 138, pp. 116-123, 2019.

[28] H. Nemati, M. Moradaghay, S. A. Shekoohi, M. A. Moghimi, and J. P. Meyer, "Natural convection heat transfer from horizontal annular finned tubes based on modified Rayleigh Number," *International Communications in Heat and Mass Transfer,* vol. 110, 2020.

[29] E. Sparrow, and P. Bahrami, "Experiments on natural convection heat transfer on the fins of a finned horizontal tube," *International Journal of Heat and Mass Transfer,* vol. 23, no. 11, pp. 1555-1560, 1980.

[30] D. G. Kröger, *Air-cooled heat exchangers and cooling towers*: Penwell Corporation Oklahoma, 2004.

[31] J. R. Senapati, S. K. Dash, and S. Roy, "Numerical investigation of natural convection heat transfer from vertical cylinder with annular fins," *International Journal of Thermal Sciences,* vol. 111, pp. 146-159, 2017.

[32] S. R. Pradhan, V. M. Behera, S. K. Rathore, and J. R. Senapati, "Study of combined effect of natural convection and radiation heat transfer from annular finned vertical cylinder," *Heat Transfer,* vol. 52, no. 2, pp. 1754-1777, 2022.

[33] B. Yazicioğlu, and H. Yüncü, “Optimum fin spacing of rectangular fins on a vertical base in free convection heat transfer,” *Heat and Mass Transfer,* vol. 44, no. 1, pp. 11-21, 2006.

[34] H. Yüncü, and G. Anbar, “An experimental investigation on performance of rectangular fins on a horizontal base in free convection heat transfer,” *Heat and Mass Transfer,* vol. 33, no. 5, pp. 507-514, 1998.

[35] A. Dayan, R. Kushnir, G. Mittelman, and A. Ullmann, “Laminar free convection underneath a downward facing hot fin array,” *International Journal of Heat and Mass Transfer,* vol. 47, no. 12-13, pp. 2849-2860, 2004.

[36] L. Dialameh, M. Yaghoubi, and O. Abouali, “Natural convection from an array of horizontal rectangular thick fins with short length,” *Applied Thermal Engineering,* vol. 28, no. 17-18, pp. 2371-2379, 2008.

[37] R. C. Adhikari, D. H. Wood, and M. Pahlevani, “Optimizing rectangular fins for natural convection cooling using CFD,” *Thermal Science and Engineering Progress,* vol. 17, 2020.

[38] G. Mittelman, A. Dayan, K. Dado-Turjeman, and A. Ullmann, “Laminar free convection underneath a downward facing inclined hot fin array,” *International Journal of Heat and Mass Transfer,* vol. 50, no. 13-14, pp. 2582-2589, 2007.

[39] I. Tari, and M. Mehrtash, “Natural convection heat transfer from inclined plate-fin heat sinks,” *International Journal of Heat and Mass Transfer,* vol. 56, no. 1-2, pp. 574-593, 2013.

[40] K. Roy, A. Giri, and B. Das, “A computational study on natural convection heat transfer from an inclined plate finned channel,” *Applied Thermal Engineering,* vol. 159, 2019.

[41] S. C. Haldar, “Laminar Free Convection Around a Horizontal Cylinder with External Longitudinal Fins,” *Heat Transfer Engineering,* vol. 25, no. 6, pp. 45-53, 2004.

[42] J. M. Wu, and W. Q. Tao, “Numerical Computation of Laminar Natural Convection Heat Transfer around a Horizontal Compound Tube with

External Longitudinal Fins," *Heat Transfer Engineering,* vol. 28, no. 2, pp. 93-102, 2007.

[43] H. J. Kim, B. H. An, J. Park, and D.-K. Kim, "Experimental study on natural convection heat transfer from horizontal cylinders with longitudinal plate fins," *Journal of Mechanical Science and Technology,* vol. 27, no. 2, pp. 593-599, 2013.

[44] D. Konar, M. A. Sultan, and S. Roy, "Numerical analysis of 2-D laminar natural convection heat transfer from solid horizontal cylinders with longitudinal fins," *International Journal of Thermal Sciences,* vol. 154, 2020.

[45] R. Sajedi, M. Taghilou, and M. Jafari, "Experimental and numerical study on the optimal fin numbering in an external extended finned tube heat exchanger," *Applied* Thermal *Engineering,* vol. 83, pp. 139-146, 2015.

[46] S. C. Haldar, G. S. Kochhar, K. Manohar, and R. K. Sahoo, "Numerical study of laminar free convection about a horizontal cylinder with longitudinal fins of finite thickness," *International Journal of Thermal Sciences,* vol. 46, no. 7, pp. 692-698, 2007.

[47] S. Acharya, and S. K. Dash, "Natural convection heat transfer from a hollow horizontal cylinder with external longitudinal fins: A numerical approach," *Numerical Heat Transfer, Part A: Applications,* vol. 74, no. 7, pp. 1405-1423, 2018.

[48] S. Rath, Siddhartha, and S. K. Dash, "Thermal performance of a radial heat sink with longitudinal wavy fins for electronic cooling applications under natural convection," *Journal of Thermal Analysis and Calorimetry,* vol. 147, no. 16, pp. 9119-9137, 2022.

[49] M. Lee, H. J. Kim, and D.-K. Kim, "Nusselt number correlation for natural convection from vertical cylinders with triangular fins," *Applied Thermal Engineering,* vol. 93, pp. 1238-1247, 2016.

[50] Q. Shen, D. Sun, Y. Xu, T. Jin, X. Zhao, N. Zhang, K. Wu, and Z. Huang, "Natural convection heat transfer along vertical cylinder heat sinks with

longitudinal fins," *International Journal of Thermal Sciences,* vol. 100, pp. 457-464, 2016.

[51] S. Kaushik, S. Singh, N. Kanojia, R. Naudiyal, R. Kshetri, A. Raj Paul, R. Kumari, A. Kumar, and S. Kumar, "Effect of introducing varying number of fins over LED light bulb on thermal behavior," *Materials Today: Proceedings,* vol. 46, pp. 9794-9799, 2021.

[52] A. Tolpadi, and T. Kuehn, "Experimental investigation of conjugate natural convection heat transfer from a horizontal isothermal cylinder with a nonisothermal longitudinal plate fin at various angles," *International journal of heat and mass transfer,* vol. 28, no. 1, pp. 155-163, 1985.

[53] B. A/K Abu-Hijleh, "Optimization of natural convection heat transfer from a cylinder with high conductivity fins," *Numerical Heat Transfer: Part A: Applications,* vol. 43, no. 1, pp. 65-82, 2003.

[54] D. Jang, S.-J. Park, S.-J. Yook, and K.-S. Lee, "The orientation effect for cylindrical heat sinks with application to LED light bulbs," *International Journal of Heat and Mass Transfer,* vol. 71, pp. 496-502, 2014.

[55] B. Li, and C. Byon, "Experimental and numerical study on the heat sink with radial fins and a concentric ring subject to natural convection," *Applied Thermal Engineering,* vol. 90, pp. 345-351, 2015.

[56] J. Lee, H. Kim, and D.-K. Kim, "Thermal Optimization of Horizontal Tubes with Tilted Rectangular Fins under Free Convection for the Cooling of Electronic Devices," *Applied Sciences,* vol. 7, no. 4, 2017.

[57] Y. Joo, and S. J. Kim, "Comparison of thermal performance between plate-fin and pin-fin heat sinks in natural convection," *International Journal of Heat and Mass Transfer,* vol. 83, pp. 345-356, 2015.

[58] L. Micheli, K. S. Reddy, and T. K. Mallick, "Experimental comparison of micro-scaled plate-fins and pin-fins under natural convection," *International Communications in Heat and Mass Transfer,* vol. 75, pp. 59-66, 2016.

[59] Y. J. Lee, and S. J. Kim, “Thermal optimization of the pin-fin heat sink with variable fin density cooled by natural convection,” *Applied Thermal Engineering,* vol. 190, 2021.

[60] Y. Ding, W. Zhang, B. Deng, Y. Gu, Q. Liao, Z. Long, and X. Zhu, “Experimental and numerical investigation on natural convection heat transfer characteristics of vertical 3-D externally finned tubes,” *Energy,* vol. 239, 2022.

[61] C.-H. Huang, and Y.-T. Wu, “An optimum design for a natural convection pin fin array with orientation consideration,” *Applied Thermal Engineering,* vol. 188, 2021.

[62] A. A. Sertkaya, M. Ozdemir, and E. Canli, “Effects of pin fin height, spacing and orientation to natural convection heat transfer for inline pin fin and plate heat sinks by experimental investigation,” *International Journal of Heat and Mass Transfer,* vol. 177, 2021.

[63] S. Unger, M. Beyer, L. Szalinski, and U. Hampel, “Thermal and flow performance of tilted oval tubes with novel fin designs,” *International Journal of Heat and Mass Transfer,* vol. 153, 2020.

[64] D. Kim, and D.-K. Kim, “Experimental study of natural convection from vertical cylinders with branched pin fins,” *International Journal of Heat and Mass Transfer,* vol. 177, 2021.

[65] S. Sundar, G. Song, M. Z. Zahir, J. S. Jayakumar, and S.-J. Yook, “Performance investigation of radial heat sink with circular base and perforated staggered fins,” *International Journal of Heat and Mass Transfer,* vol. 143, 2019.

[66] S.-J. Park, D. Jang, and K.-S. Lee, “Thermal performance and orientation effect of an inclined cross-cut cylindrical heat sink for LED light bulbs,” *International Journal of Heat and Mass Transfer,* vol. 103, pp. 1371-1377, 2016.

[67] A. Abbas, and C.-C. Wang, "Augmentation of natural convection heat sink via using displacement design," *International Journal of Heat and Mass Transfer,* vol. 154, 2020.

[68] M. Tiji, J. Mahdi, H. Mohammed, H. Majdi, A. Ebrahimi, R. Mahani, P. Talebizadehsardari, and W. Yaïci, "Natural Convection Effect on Solidification Enhancement in a Multi-Tube Latent Heat Storage System: Effect of Tubes' Arrangement," *Energies,* vol. 14, no. 22, 2021.

[69] K. Kitamura, A. Mitsuishi, T. Suzuki, and F. Kimura, "Fluid flow and heat transfer of natural convection induced around a vertical row of heated horizontal cylinders," *International Journal of Heat and Mass Transfer,* vol. 92, pp. 414-429, 2016.

[70] J. Kang, J. Moon, Y. Ko, S.-G. Lim, and B. Yun, "Steam condensation on tube-bundle in presence of non-condensable gas under free convection," *International Journal of Heat and Mass Transfer,* vol. 178, 2021.

[71] H. Bian, Z. Sun, X. Cheng, N. Zhang, Z. Meng, and M. Ding, "CFD evaluations on bundle effects for steam condensation in the presence of air under natural convection conditions," *International Communications in Heat and Mass Transfer,* vol. 98, pp. 200-208, 2018.

[72] A. V. Novozhilova, and Z. G. Mar'ina, "A Generalized Dependence for Convective Heat Transfer in Horizontal Bundles of Finned Tubes with Free Air Convection," *Chemical and Petroleum Engineering,* vol. 52, no. 9-10, pp. 669-674, 2017.

[73] M. Ashjaee, and T. Yousefi, "Experimental Study of Free Convection Heat Transfer from Horizontal Isothermal Cylinders Arranged in Vertical and Inclined Arrays," *Heat Transfer Engineering,* vol. 28, no. 5, pp. 460-471, 2007.

[74] G. Marsters, "Arrays of heated horizontal cylinders in natural convection," *International Journal of Heat and Mass* Transfer*,* vol. 15, no. 5, pp. 921-933, 1972.

[75] S. Unger, M. Beyer, H. Pietruske, L. Szalinski, and U. Hampel, “Natural convection heat transfer performance of additively manufactured tube bundle heat exchangers with novel fin design,” *Heat and Mass Transfer,* vol. 57, no. 7, pp. 1193-1203, 2021.

[76] E. Salamatbakhsh, and Ö. Bayer, “Hydrothermal performance of a wavy minichannel heatsink with longitudinal vortex generators,” *Thermal Science and Engineering Progress,* vol. 50, 2024.

[77] A. Fluent, “12.0 Theory Guide,” *Ansys Inc,* vol. 5, no. 5, pp. 15, 2009.

[78] R. J. Moffat, “Describing the uncertainties in experimental results,” *Experimental thermal and fluid science,* vol. 1, no. 1, pp. 3-17, 1988.

[79] V. T. Morgan, "The overall convective heat transfer from smooth circular cylinders," *Advances in heat transfer*, pp. 199-264: Elsevier, 1975.

[80] S. W. Churchill, and H. H. Chu, “Correlating equations for laminar and turbulent free convection from a horizontal cylinder,” *International journal of heat and mass transfer,* vol. 18, no. 9, pp. 1049-1053, 1975.